"No problem can be solved from the same level of consciousness that created it."

-Albert Einstein

"I regard consciousness as fundamental. I regard matter as a derivative of consciousness."

-Max Planck

University of Alberta

An Assessment of the Information Processing Capabilities of Neuronal Microtubules at Physiological Temperature

by ©

Travis John Adrian Craddock

A thesis submitted to the Faculty of Graduate Studies and Research
in partial fulfillment of the requirements for the degree of

Master of Science

Department of Physics

Edmonton, Alberta
Spring 2008

Library and
Archives Canada

Published Heritage
Branch

395 Wellington Street
Ottawa ON K1A 0N4
Canada

Bibliothèque et
Archives Canada

Direction du
Patrimoine de l'édition

395, rue Wellington
Ottawa ON K1A 0N4
Canada

Your file Votre référence
ISBN: 978-0-494-45798-6
Our file Notre référence
ISBN: 978-0-494-45798-6

NOTICE:
The author has granted a non-exclusive license allowing Library and Archives Canada to reproduce, publish, archive, preserve, conserve, communicate to the public by telecommunication or on the Internet, loan, distribute and sell theses worldwide, for commercial or non-commercial purposes, in microform, paper, electronic and/or any other formats.

The author retains copyright ownership and moral rights in this thesis. Neither the thesis nor substantial extracts from it may be printed or otherwise reproduced without the author's permission.

AVIS:
L'auteur a accordé une licence non exclusive permettant à la Bibliothèque et Archives Canada de reproduire, publier, archiver, sauvegarder, conserver, transmettre au public par télécommunication ou par l'Internet, prêter, distribuer et vendre des thèses partout dans le monde, à des fins commerciales ou autres, sur support microforme, papier, électronique et/ou autres formats.

L'auteur conserve la propriété du droit d'auteur et des droits moraux qui protège cette thèse. Ni la thèse ni des extraits substantiels de celle-ci ne doivent être imprimés ou autrement reproduits sans son autorisation.

In compliance with the Canadian Privacy Act some supporting forms may have been removed from this thesis.

While these forms may be included in the document page count, their removal does not represent any loss of content from the thesis.

Conformément à la loi canadienne sur la protection de la vie privée, quelques formulaires secondaires ont été enlevés de cette thèse.

Bien que ces formulaires aient inclus dans la pagination, il n'y aura aucun contenu manquant.

Canada

Abstract

Both direct and indirect experimental evidence have shown signaling, communication and conductivity in microtubules. Theoretical models have predicted that microtubules can be potentially used for both classical and quantum information processing in neurons, with the latter being implicated in the phenomena of consciousness, although controversies have arisen in regards to physiological temperature effects on these capabilities. The following discusses microtubule structure, known biophysical functions and theoretical predictions related to signaling, conduction and transport, all of which may contribute to pre-conscious processing at a molecular level. Major criticisms of microtubule information processing based concepts of cognitive brain function are examined, and the progress in work addressing these issues is also discussed. To examine the notion of quantum phenomena in microtubules two quantum-based models are suggested and used to investigate the effect of temperature on microtubule dynamics: a cellular automata microtubule model, and an exciton model of the microtubule

To

My Mother for convincing me that there is always something more to life, my Father for teaching me to always strive for more, and my Wife for accompanying me in this journey.

Preface

The work presented in this thesis was carried out at the University of Alberta, Edmonton, Canada in the Department of Physics. All material presented was completed under the supervision of Jack A. Tuszynksi. Much of the subject matter presented in the following report has been published as articles in various journals. The publication information of this thesis material is as follows:

Chapter 1 and 4

- T. J. A. Craddock, and J. A. Tuszynski, *On the Role of the Microtubules in Cognitive Brain Functions*, Neuroquantology, Vol. 4, No. 1, pp. 32-57, (March 2007)

Section 3.5

- J. A. Tuszynski, T. J. A Craddock, and E. J. Carpenter, *Bioferroelectricity at the Nanoscale*, submitted to the Journal of Computational and Theoretical Nanoscience as of September 2007.

Chapter 5

- T. J. A. Craddock, C. Beauchemin, and J. A. Tuszynski, *Cellular automata modeling of information processing in microtubules at physiological temperature*, submitted to Physical Review E as of June 2007, resubmitted September 2007.

The material of Chapter 6 has yet to be submitted for publication.

Acknowledgments

MITACS, NSERC, ACB, and the Allard Foundation provided funding for the research presented in this report. Professor Marshall Stoneham, Dr. Luca Turin, Dr. Nancy Woolf, Dr. Avner Priel, and Dr. Stuart Hameroff provided many useful comments and suggestions that were greatly appreciated. Eric Carpenter provided continual help and advice. Dr. Jack Tuszynski provided support, guidance, and instruction on the subject matter, and provided the opportunity to follow this line of research.

Table of Contents

Introduction 1
  References 6

1 An Introduction to the Quantum Brain 10
  1.1 A Working Definition of Consciousness 10
  1.2 Classical approach to consciousness 11
  1.3 Introduction to quantum theory 12
  1.4 Theories of quantum brain function 14
  1.5 Arguments for and against quantum brain function 16
  References 19

2 The Physics of Biology 22
  2.1 A Brief Introduction to Biophysics 22
  2.2 Mechanisms of Biological Activity 23
    2.2.1 The Importance of Signaling in Biology 23
    2.2.2 Energy Transfer in Biology 24
  2.3 Review of the Physics of Solids 26
    2.3.1 Lattice Properties of Solids 26
    2.3.2 Electrical Properties of Solids 29
    2.3.3 Collective Excitations and Energy Transfer 35
  References 41

3 The Cell Biology of the Neuronal Cytoskeleton 44
  3.1 The Archetypal Neuron and its Components 44
    3.1.1 Structure of the Archetypal Neuron 44
    3.1.2 Organelles of the Neuron 46
    3.1.3 Cytosol of the Neuron 47
    3.1.4 The Neuronal Cytoskeleton 47
  3.2 The Cytoskeleton and its Components 48
    3.2.1 Microfilaments 48
    3.2.2 Intermediate Filaments 49
    3.2.3 Microtubules 50
  3:3 The Structure of Microtubules and their related proteins 52
    3.3.1 The microtubule subunit Tubulin 52
    3.3.2 Microtubule structure 53
    3.3.3 Assembly Microtubule Associated Proteins 55

3.3.4 Motor Microtubule Associated Proteins....56
3.4 The Dynamics of Microtubules....59
3.4.1 Microtubule assembly/disassembly, polarization and dynamic instability....59
3.4.2 Microtubule Organizing Centers....61
3.4.3 Cell Division....62
3.5 Examining the Conduction Properties of Microtubules....64
References....70

4 Information Processing in Microtubules....74
4.1 An overview of Cellular Automata....74
4.1.1 History and Background....74
4.1.2 Universal Computation and Cellular Automata....76
4.2 Examples of Cellular Automata....77
4.2.1 The Ising Spin Model....77
4.2.2 Artificial Neural Net/ Hopfield Net Systems....78
4.3 Previous Computer Models of Microtubules....79
4.3.1 Original Cellular Automata Models of Microtubules....79
4.3.2 Ising Spin Based Ferroelectric Models....83
4.3.3 Hopfield Network Microtubule Model....84
4.4 Current Ideas on Dendritic Cytoskeletal Computation....85
4.4.1 C-termini based Signaling and Information Processing....85
4.4.2 Computation within the Dendritic Cytoskeleton....87
References....89

5 A Cellular Automata Model of a Microtubule at Physiological Temperature....93
5.1 Quantum Cellular Automata....93
5.2 The Cellular Automata Lattice Structure....93
5.2.1 The Microtubule Lattice....93
5.2.2 The Seven Dimer Hexagonal Neighborhood....94
5.3 The Cellular Automata Cell....95
5.3.1 The Electrostatic Properties of the Tubulin Dimer....95
5.3.2 Tubulin Dimer as a Double Potential Well....97
5.4 The Cellular Automata Dynamic Governing Rules....100
5.4.1 The Energy Dynamics of the System....100
5.4.2 The Transition Rules....102
5.5 The Cellular Automata Simulation....103
5.5.1 Simulation Conditions....103
5.5.2 Simulation Procedure and Timing....105
5.6 Results of Simulations....106

5.6.1 Typical automata pattern evolution for synchronous updating............106
5.6.2 Typical pattern evolution for asynchronous updates..........................108
5.6.3 Discussion of results..109
References..111

6 An Examination of Possible Mechanisms of Coherent Energy Transfer in Microtubules..........114
6.1 The Electron Wavefunction in a Symmetric Double Well Potential..............114
6.2 Collective Excitations in Microtubules..119
6.2.1 The Phonon System..119
6.2.2 The Exciton System..120
6.3 Discussion of Results..126
References..128

Conclusion..........130

Appendix – QCAMM Code..........135
QCAMM.C..........135
ENERCALC.C..........149
ENERDIFF.C..........150
FOR_CALC.C..........151
DISTENR6.C..........152
DISTFOR6.C..........153
PROBCALC.C..........154
RANMAR.C..........155
RANMAR.H..........158
INPUT.DAT..........158

List of Figures

Figure 2.1: The 7 crystal symmetries and corresponding 14 Bravais lattices 26

Figure 2.2: Construction of a Wigner-Seitz cell 27

Figure 2.3: Peptide group showing amide-I vibration 39

Figure 3.1: A sketch of a characteristic neuron cell body 44

Figure 3.2: Shapes and sizes of various specialized neurons 45

Figure 3.3: Sketch of a microfilament filament 49

Figure 3.4: Sketch of an arbitrary intermediate filament 50

Figure 3.5: Sketch of a microtubule 51

Figure 3.6: The tubulin heterodimer 53

Figure 3.7: Diagram of the microtubule structure 54

Figure 3.8: Tubulin monomer arrangements in microtubule lattice structures 55

Figure 3.9: Schematic representation of a neuron 62

Figure 3.11: Electroorientation time constant versus average microtubule length 66

Figure 3.12: Normalized microtubule polarization coefficient versus frequency 67

Figure 5.1: Section of the two dimensional array of tubulin dimers 94

Figure 5.2: Seven dimer tilted hexagonal neighborhood 95

Figure 5.3: Cross section of an electrostatic map of the tubulin dimer 96

Figure 5.4: A typical infinite square double well potential 98

Figure 5.5: Dimensions of a MT-13A Lattice 100

Figure 5.6: Type II evolution for synchronous updating 107

Figure 5.7: Type III evolution for synchronous updating. 107

Figure 5.8: Type IV evolution for synchronous updating. 108

Figure 5.9: Type III evolution for asynchronous updating. 108

Figure 5.10: Tubulin dielectric constant versus tubulin potential well depth 109

Figure 6.1: An infinite square double well potential 115

Figure 6.2: Plot of transcendental equation over energies 117

Figure 6.3: Diagram of tubulin neighborhood groups 122

List of Tables

Table 5.1 : Electron's total energy range, and the maximum energy difference between wells for tubulin dielectric constant values between 2 and 10....101

Introduction

The nature of brain activity has been dealt with by many disciplines such as science, religion, and philosophy, yet all the available evidence accumulated over the numerous years of investigation has yet to provide a final answer [1-4]. This may be due to the vast amount of information stemming from the different vantage points expressing their knowledge in unique manners, of which, each is based in the context of its individual discipline. While this pursuit seems to suffer as an intellectual "Tower of Babel" the problem itself is not trivial by any means. Aside from the importance of this problem in regards to the theoretical and applied aspects of the sciences and humanities, as well as its role in defining fundamental human values, the basic and practical significance for the etiology and treatment of mental disease cannot be overlooked.

In the past twenty years there has been an ever-growing increase in attempts by science to understand and describe the phenomena of the brain. This movement has mainly focused on the biological and social sciences, however there have been key additions to this discussion by the physical sciences as well. There are several approaches to understanding the cognitive functions of the brain, which is taken to include consciousness. While all scientific studies of cognition may be grouped under the umbrella of cognitive science, the underlying disciplines of this multidisciplinary field are quite diverse.

Psychology has a rich history of investigating the mind [5-8]. The specialized branch of cognitive psychology specifically studies cognition and the mental processes underlying behavior from the standpoint that mental function can be understood by quantitative, positivist scientific methods. This cognitivist viewpoint argues for the use of information processing models as a framework for understanding the mind [9-11]. From the biological viewpoint, the cognitive neurosciences, address the mind via the study of the biological mechanisms underlying cognition, with a specific focus on the neural substrates of mental processes and their behavioral manifestations. It addresses the questions of how psychological/cognitive functions are produced by the neural circuitry [12-14]. Experimentally the field uses imaging techniques to investigate the electrophysiological response of the neural system to stimuli. Theoretically the responses of neural systems to various input stimuli are understood through the computer models of neurons, and neuron systems characteristic of computational neuroscience. From a strictly computational perspective the field of artificial consciousness seeks to apply the findings of the above mentioned disciplines to the development of theoretical foundations of information and computation and implement them in computer systems to engineer conscious machines [15, 16]. This field is closely related to the idea of artificial intelligence, but requires that beyond the Turing test, which states that a machine that acts in such a way that its actions cannot be discerned from the actions of an intelligent human being is itself intelligent, the machine is also capable of experiencing a subjective self-awareness. However this form of strong artificial intelligence has been strongly argued against [3, 4, 17].

Interestingly these same arguments against strong artificial machine intelligence are used to point out the shortcomings of a classical scientific understanding of consciousness, and the confusion associated with objectively trying to investigate what appears to be a subjective phenomenon. Minsky suggested that whenever a question leads to confusion and inconsistent answers it is due to one of two reasons [15]. The first is that the question itself is ultimately meaningless or at least unanswerable. The second is that an adequate answer requires a powerful analytical apparatus. The question of consciousness cannot be meaningless as the above stated practical importance of a scientific understanding of consciousness to the understanding and treatment of mental disease shows. The long history of cognitive studies with its lack of solutions suggests that these questions may be unanswerable, however new technical and conceptual tools may provide the powerful analytic apparatus required.

The currently accepted view is that cognition emerges as a property of an ever-increasing computational complexity among neurons. This approach relies on emergence as a framework. Emergent phenomena are characterized by high levels of complexity resulting from an aggregation of basic units whose individual properties differ from those of the aggregate itself. Emergent brain phenomena are thus taken to be the result of the complexity of neuronal connections, where the neuron is the basic unit of information processing in the brain. While this appears to be the currently accepted approach to explaining cognitive functions of the brain, it may not be adequate to properly explain the richness of the neuron's biophysical state space. The classical deterministic activities of neurons, while explaining a host of neurophysiological phenomena [22-24], cannot account for several key properties of conscious experience, such as free will and the unitary sense of self. The fact that neuronal assemblies are mostly described in terms of classical behavior does not rule out the possibility that quantum effects play a role in sub-neuronal components such as proteins, DNA or neurotransmitters. The brain contains both electrical and chemical synapses. Electrical synapses allow current generated by an action potential in a presynaptic neuron to flow directly into a postsynaptic cell via the physical connection of a gap junction. Chemical synapses propagate signals via releasing a chemical transmitter (e.g., glutamate, acetylcholine) from a presynaptic terminal via exocytosis, which diffuses across the synaptic cleft and binds to receptors embedded in a postsynaptic neuron's membrane. This results in the opening of an ion channel or in the initiation of a signal transduction cascade. These steps seem to operate according to classical physics. However, it has been suggested that alternative descriptions, based on quantum processes, may be required for a quantitative understanding of exocytosis, the action by which a cell directs, and secretes soluble proteins to the extracellular environment [18, 19]. Explanations of exocytosis may aid in understanding cognition, as chemical synapses using NMDA receptors are critical to perception and consciousness because of the plasticity expressed by NMDA receptors. As well, anesthetic agents block NMDA receptors and consequently lead to a loss of consciousness [25].

Another reason to look beyond classical models is that currently accepted models of cognitive brain function are unable to properly explain the behaviour of single-celled organisms. Single-celled organisms, such as the paramecium, have no neurons or synapses, but still exhibit an apparent awareness of and responsiveness to their environment. Although the complex interactions between neurons and synapses are certain to contribute to the richness of sensory experience it can be concluded from the actions of single celled organisms that the rudiments of cognition lie someplace else. The neuronal cytoskeleton is the most ubiquitous and most basic subcellular level site thus far proposed for quantum processes in relation to brain activity [3, 20]. Microtubules are major constituents of the cytoskeleton that literally fill the interior of neurons. They are essential for axoplasmic transport among other cellular processes within neurons and regulate cell shape thus being involved in neuronal plasticity [26, 27], as well as having shown possible signaling capabilities in axons [28, 29]. Microtubules due their mesoscale size, provide an ideal bridge between the classical and quantum boundary.

Information processing at the level of microtubules within each neuron would provide an enormous increase in the brain's computing power even at a classical level. The currently accepted scientific model suggests that cognition arises as a result of computational complexity among the approximately 10^{11} neurons in the brain. There are on the order of 10^4 synapses per large neuron, which switch their states at a rate of some 10^3 switches per second, thus arriving at a number of $\approx 10^{18}$ operations per second in the brain on average. This is a truly huge number, however it may pale by comparison with the yield given by the brain if neuronal microtubules are actively involved in computational processes. Consider that at the microtubule level there are roughly 10^7 microtubule globular protein subunits, called tubulin, in each neuron that can switch their conformational states on the order of nanoseconds resulting in 10^{16} operations per second per neuron or 10^{27} operations per second in an entire brain. If each tubulin dimer functions as a quantum bit and not a classical bit processor, the computational power becomes almost unimaginably vast. It has been claimed that as few as 300 quantum bits, otherwise known as qubits, have the same computational power as a hypothetical classical computer comprised of as many processing units as there are particles in the universe [30]. While this statement is illustrative in purpose, as the total number of particles in the universe is not known, it does convey the astronomical number of classical bits required to match the computing power of a small number of qubits.

There is evidence that microtubules are computationally relevant to cognitive processes.

Evidence suggests that microtubules can propagate signals in cells [29], and interactions between microtubules and membrane activities are clearly recognized [31, 32, 33]. Other processes involved in the functioning of the brain, such as ion channels opening and closing, enzymes catalyzing, motor proteins moving cargo inside cells, and the propagation of ionic waves along filaments, may be inextricably linked to the function of microtubules [34, 35]. Neurons in the visual cortex produce massive amounts of tubulin during a critical period of visual development [36]. As well, Alzheimer's disease, a cognitive mental disease, which is accompanied by deficits in intellect, memory and consciousness, has been linked to microtubule degradation [30]. Microtubules also provide a non-selective mechanism for general anesthesia. Anesthetics, which serve to induce a lack of conscious awareness, inhibit a number of neurotransmitter receptors, but differ from receptor inhibitors by having effects on the cytoskeleton [37]. One of the suggested mechanisms of anesthesia is the inhibition of electron movement within the hydrophobic pockets of tubulin dimers caused by the presence of anesthesia [38]. Electron mobility is essential to the quantum superposition of electronic states in a material, but as suggested the presence of anesthetic gas would inhibit the electron motion that is required for protein conformational stability and quantum superposition, thus inducing a loss of consciousness. Conversely, it has been speculated that instead of inhibiting electron movement, hallucinogenic drugs, which serve to increase conscious awareness, would increase electron motion. Lysergic acid diethylamide (LSD), known to be a potent hallucinogen, appears to be a potent electron donor, thus possibly facilitating the movement of electrons and supporting the above hypothesis [39].

While the evidence suggests a possible relation between quantum behavior in microtubules and cognition, it is still far from trivial to reconcile these qualitative statements with the persistent decoherence effects dominating quantum phenomena at physiological temperatures [21]. As such, the endeavor of this thesis is as follows. Firstly, this thesis attempts to present pertinent information regarding the capabilities of microtubules to process information, and the relation of this information processing to brain functions. Secondly this thesis aims at investigating whether or not microtubules are capable of information processing at physiological temperature, and finally it attempts to answer the question of whether microtubules can maintain and support coherent quantum phenomena at physiological temperature, or not. In order to investigate and answer these questions the thesis has been laid out in the following format.

Chapter 1 of the thesis outlines the motivation for investigating information processing and quantum behavior in microtubules. In this section a working definition of consciousness is given as well as the standard classical methods of approach to this problem. The gaps in the standard methods of explanation are outlined and reasons for using a quantum-based approach are summarized. A brief introduction to quantum theory is supplied for the reader unfamiliar with the subject. As well, arguments for and against this physical method of inquiry into cognitive brain function are stated. The following Chapter 2, reviews the connections between physics and biology. Justifications for the use of condensed matter physics to explain biological phenomena are outlined, and key concepts including biological energy, dielectrics, conduction and signaling are introduced. As well, a section describing theoretical quantum phenomena giving rise to energy transfer in biological systems is discussed. The third chapter of the thesis provides a review of the literature concerning microtubules and their place within the cell and cell cytoskeleton with a heavy emphasis on their place within the neuron. The structure and dynamics of the microtubule are reviewed in detail and many key terms used in the rest of the thesis are defined. The electrical properties of the microtubule are discussed in relation to their conduction properties, as well as the difficulty in determining these properties via experiment. Chapter 4 reviews previous models of information processing within microtubules with an emphasis on cellular automata approaches. An overview of cellular automata modeling is given followed by common examples of such models. Pure cellular automata models, Ising spin models and Hopfield net models of microtubules are outlined and discussed and their conclusions regarding the information processing capabilities of microtubules are presented. As well a model describing how information processing in microtubules may affect the processes of neurons and contribute to cognitive brain function is reviewed. An adaptation of the cellular automata models described in Chapter 4 is presented in Chapter 5. The model is described in detail starting from the physical basis for the cellular automata cell, moving to reasoning behind the lattice structure, followed by the equations determining the overall dynamics of the system. Reasons for the use of varying conditions are given, and the effect of different updating methods is discussed. The results of simulations for synchronous and asynchronous updating with varying conditions are presented and are discussed with their relevance to information processing being stressed. The final chapter, Chapter 6, investigates quantum mechanisms of coherent energy transfer in microtubules. Following previous models of energy transfer via collective excitations in molecular aggregates the strength of phonon and exciton interactions, and their effects on the formation of coherent excitation domains in clusters of tubulin dimers is examined. As well, estimates of energy and time scales for excitons, phonons and their interaction in a thermal environment are presented. The chapters are followed up by a conclusion summarizing the material and main findings presented in the thesis.

References

[1] A. C. Scott, Stairway to the Mind: the controversial new science of consciousness, (Copernicus, New York, 1995)

[2] M. Velmans, The Science of Consciousness: psychological, neuropsychological and clinical reviews, (Routledge, New York, 1996)

[3] R. Penrose, Shadows of the Mind, (Oxford University Press, Oxford, New York and Melbourne, 1994)

[4] R. Penrose, The Emperor's New Mind, (Oxford University Press, Oxford, New York and Melbourne, 1989)

[5] K. S. Lashley, *The Behavioristic Interpretation of Consciousness*, Psychological Review, Vol. 30, No. 4, pp. 237-272, (September 1923)

[6] K. S. Lashley, *The Behavioristic Interpretation of Consciousness II*, Psychological Review, Vol. 30, No. 5, pp. 329-353, (July 1923)

[7] W. James, The Principles of Psychology, (Dover Publications, New York, 1950)

[8] J. M. Baldwin, *Consciousness and Evolution*, Science, New Series, Vol. 2, No. 34, pp. 219-223, (August 23, 1895)

[9] S. Franklin, and A. Graesser, *A software model of consciousness*, Consciousness and Cognition, Vol. 8, No. 3, pp. 285-301, (September 1999)

[10] G. O'Brien, and J. Opie, *Cognitive Science and Phenomenal Consciousness: A dilemma, and how to avoid it*, Philosophical Psychology, Vol. 10, No. 3, pp. 269-286, (September 1997)

[11] J. Baars, In the Theatre of Consciousness: Global Workspace Theory, A Rigorous Scientific Theory of Consciousness, Journal of Consciousness Studies, vol. 4, No. 4, pp. 292-309, (1997)

[12] F. Crick, and C. Koch, Towards a neurobiological theory of consciousness, Seminars in the Neurosciences, Vol. 2, pp. 263-275, (1990)

[13] F. Crick, and C. Koch, *Consciousness and Neuroscience*, Cerebral Cortex, Vol. 8, No. 2, pp. 97-107, (March 1998)

[14] G. Rees, G. Kreiman, and C. Koch, *Neural correlates of consciousness in humans*, Nature Reviews Neuroscience, Vol. 3, No. 4, pp. 261-270, (April 2002)

[15] M. L. Minsky, *Matter, Minds and Models*, in Semantic Information Processing, edited by M. L. Minsky, (MIT Press, Cambridge, 1968)

[16] J. McCarthy, *Making Robots Conscious of their Mental States*, in Machine Intelligence 15: Applied Machine Intelligence, edited by K. Furukawa, D. Michie, and S. Muggleton, (Oxford University Press, Oxford, 1999)

[17] J. R. Searle, *Minds, brains, and programs*, Behavioral and Brain Sciences, Vol. 3, No. 3, pp. 417-457, (1980)

[18] F. Beck, and J. C. Eccles, *Quantum Aspects of Brain Activity and the Role of Consciousness*, Proceedings of the National Academy of Science of the United States of America, Vol. 89, pp. 11357-11361, (1992)

[19] F. Beck, and J. C. Eccles, *Quantum processes in the brain: A scientific basis of consciousness*, in Advances in Consciousness Research, Vol. 49, A neural Basis of Consciousness, edited by N. Osaka, (John Benjamins Publishing Company, Philadelphia, 2003)

[20] S. Hameroff, *Quantum Computation in Brain Microtubules? The Penrose-Hameroff 'Orch OR' Model of Consciousness [and Discussion]*, Philosophical Transactions of the Royal Society of London A: Mathematical, Physical and Engineering Sciences, Vol. 356, No. 1743, Quantum Computation: Theory and Experiments, pp. 1869-1896, (Aug. 15, 1998)

[21] M. Tegmark, *Importance of quantum decoherence in brain processes*, Physical Review E, Vol. 61, p. 4194, (2000)

[22] S. Kastner, and L. G. Ungerleider, *Mechanisms of Visual Attention in the Human Cortex*, Annual Review of Neuroscience, Vol. 23, pp. 315-341, (2000)

[23] M. F. Bear, *A synaptic basis for memory storage in cerebral cortex*, Proceedings of the National Academy of Sciences of the United States of America, Vol. 93, pp. 13453-13459, (November 1996)

[24] T. Curran, *On the Neural Mechanisms of Sequence Learning*, Psyche, Vol. 2, No. 12, (August 1995)

[25] N. J. Woolf, *Microtubules in the Cerebral Cortex: Role in Memory and Consciousness*, in The Emerging Physics of Consciousness, edited by J. A.

Tuszynski, (Springer-Verlag, New York, 2006)

[26] P. Dustin, *Microtubules*, (Springer-Verlag, New York, 1978).

[27] K. Roberts, and J. S. Hyams, *Microtubules*, (Academic Press, New York, 1979).

[28] J. A. Tuszynski, S. Hameroff, M. V. Sataric, B. Trpisova, and M. L. A. Nip, *Ferroelectric Behavior in Microtubule Dipole Lattices: Implications for Information Processing, Signaling and Assembly/Disassembly*, Journal of Theoretical Biology, Vol. 174, pp. 371-380, (1995).

[29] J. A. Brown, and J. A. Tuszynski, *Dipole Interactions in Axonal Microtubules as a Mechanism of Signal Propagation*, Physical Review E, Vol. 56, pp. 5834-5840, (1997).

[30] A. M. Steane, and E. G. Rieffel, *Beyond Bits: The Future of Quantum Information Processing*, Computer, Vol. 33, No. 1, pp. 38-45, (January 2000)

[31] G. G. Gundersen, and T. A. Cook, *Microtubules and signal transduction*, Current Opinion in Cell Biology, Vol. 11, pp. 81-94, (1999)

[32] J. Glanz, *Cell Biology: Force-Carrying Web Pervades Living Cell*, Science, Vol. 276, pp. 678-679, (May 1997)

[33] A. J. Manitois, C. S. Chen, and D. E. Ingber, Demonstration of mechanical connections between integrins, cytoskeletal filaments, and nucleoplasm that stabilize nuclear structure, Proceedings of the National Academy of Sciences of the United States of America, Vol. 94, No. 3, pp. 849-854, (February 4, 1997)

[34] A. Priel, J. A. Tuszynski, and N. J. Woolf, Transitions in microtubule C-termini conformations as possible dendritic signaling phenomenon, European Biophysics Journal, Vol. 35, pp. 40-52, (2005)

[35] A. Priel, J. A. Tuszynski, and H. F. Cantiello, *The dendritic cytoskeleton as a computational device: An hypothesis*, in The Emerging Physics of Consciousness, edited by J. A. Tuszynski, (Springer-Verlag, New York, 2006)

[36] J. Cronly-Dillon, and G. W. Perry, *Effect of Visual Experience on Tubulin During a critical Period of Visual Cortex Development in the Hooded Rat*, The Journal of Physiology, Vol. 293, pp. 469-484, (1979)

[37] K. Bjornstrom, and C. Eintrei, *The Difference Between Sleep and Anaesthesia is in the Intracellular Signal*, Acta Anaesthesiologica Scandinavica, Vol. 47, pp. 157-

164, (2003)

[38] S. Hameroff, *Anesthesia, consciousness and hydrophobic pockets – a unitary quantum hypothesis of anesthetic action*, Toxicology Letters, Vol. 23, pp. 31-39, (1998b)

[39] S. H. Snyder, and C. R. Merril, *A relationship between the hallucinogenic activity of drugs and their electronic configuration*, Proceedings of the National Academy of Sciences of the United States of America, Vol. 54, pp. 258-266, (1965)

Chapter 1

An Introduction to the Quantum Brain

1.1 A Working Definition of Consciousness

Consciousness is an elusive and enigmatic problem for science. It remains a hotly debated topic in psychology and neuroscience, yet for most of the last century the issue has been approached hesitantly by the physical and life sciences [1]. This lack of exploration has, in part, been due to the Cartesian view that consciousness, as well as other mental phenomena, are inherently non-material, and therefore outside the scope of science. However, in the past two decades numerous studies on both conscious and unconscious processes have appeared in the literature of the psychological and brain sciences, including several theories based on physical frameworks [2, 3, 4].

The word consciousness is derived from the Latin *conscienta*, meaning to know with, or to know together, and originally was used in the sense of moral conscience. The modern definitions of consciousness however have quite different meanings. There are a considerable number of definitions for consciousness stemming from the various philosophical, scientific, and even spiritual approaches to understanding the phenomena. Some of the definitions agree across disciplines despite the differences in the method of investigation, while others are at complete odds with one another. In general, however, it is accepted that consciousness is the "condition of being aware of one's surroundings and one's own existence or self-awareness" [5].

From a scientific viewpoint it is agreed that consciousness is a function of the brain [6, 7]. Since the brain is a material entity, consciousness is subject to the study of science. Currently there are a number of physical theories of consciousness in existence, some of which are based on classical physics [2, 4] while others require the use of quantum theory [3, 8, 9]. These theories of consciousness and their basis in classical and quantum physics are discussed in the following sections of this chapter.

1.2 Classical approach to consciousness

The brain is the control center for the central nervous system in higher animals. It is composed of brain cells, known as neurons and glia. Glia cells are believed to perform supporting functions in the brain, while neurons are electrically active cells that process information. Neurons are composed of a cell body, or soma, short branching cellular extensions, called dendrites, and a long cable-like extension, known as an axon. Neurons communicate with one another via connections among axons, dendrites and somas called synapses.

The majority of biophysical researchs on cognitive processes, including studies on consciousness, models the brain as a neural network. A neural network is a system of interconnecting neurons that work together via electrical signals and other mechanisms that follow the laws of classical physics to produce an output function [10]. This method of investigation assumes neurons, and synapses, to be the fundamental units of information processing within the brain. Neurons in the system are assumed to be in one of two different states, comprising what is known as a binary point artificial neural network. When the neuron is sending a signal it is considered in the "on" state, and when it is at rest it is considered to be in the "off" state. The progress made in modeling memory, learning and other cognitive processes [11, 12] via artificial neural networks has led to the conjecture that consciousness arises from increasing computational complexity among neurons in the brain [5, 6]. It is believed that when a critical level of complexity among neurons is reached, interacting neurons form a conscious experience. This approach marks consciousness as a highly non-linear, emergent property arising from neuronal features of the brain that is fully compatible with the laws of classical physics.

The world of classical physics is envisioned as a simple aggregate of logically independent, local, functional objects, which only interact with their close neighbors to form larger objects or systems [13]. In the case of a neural network the brain is the simple aggregate composed of independent neurons. This view of the brain leaves several properties of consciousness unexplainable. The unsolved problems arising from these enigmatic features are as follows [3, 5, 14, and 15]:

1) What is the nature of subjective experience and how do the sensations of a conscious experience arise from the combined actions of neurons and their associated cellular, synaptic, and molecular processes?

2) How do spatially distributed brain activities bind together to produce a unity of conscious perception, such as seeing unitary objects in vision? (This is known as the Binding Problem)

3) What is the critical level of complexity required by a system to move from a pre-conscious processing system to a conscious processing system?

4) How can a system based on the deterministic laws of classical physics account for non-computable processes such as consciousness?

5) How can a system based on the deterministic laws of classical physics account for concepts such as free will?

6) How can a description of consciousness based on the interactions of neurons explain the rudimentary consciousness observed in single-celled organisms?

The classical description of consciousness as an emergent property addresses these problems with the explanation that non-linear and deterministic chaotic behavior can be described fully via classical physics and can lead to non-computable results. Thus, while consciousness is fully compatible with classical physics it is not easy to predict its properties from highly non-linear phenomena [16, 17]. This classically based approach to consciousness leaves many of these questions largely unanswered. As a result it has been suggested that the physics of quantum theory may provide an answer.

1.3 Introduction to quantum theory [18]

It has been suggested that the new insights into the behavior of matter given by the rules of quantum mechanics can aid in solving the mystery of consciousness. Quantum theory is the most fundamental theory of matter known at this point in time, and is responsible for much of the technological advancements of the 20th century. Since the brain is a material entity, and it is an accepted assumption that the brain gives rise to higher cognition and consciousness, studying the brain at the quantum level to find a physical description of brain functions is a valid pursuit.

Quantum theory is a theory of physics in which many of the variables taken as continuous by classical physics take on discrete values. Initially the term quantum, (or plural quanta), was used to denote a discrete packet of electromagnetic radiation, hence the origin of the name quantum theory. The three main categories of quantum theory are determined by the extent to which the continuous variables of classical physics are converted to discrete variables, otherwise known as quantization. Quantum mechanics is a first-quantized or semi-classical theory of physics in which particle properties are discrete but field properties and interactions are not. Quantum field theory is a second-quantized theory in which all particle properties, field properties, and interactions are discrete except for those due to gravity. Quantum gravity is an incomplete third-quantized theory in which gravity is also made discrete.

There are several key differences between quantum physics and traditional classical physics that are of importance. In quantum theories physical entities possess both a wave aspect and a particle aspect. This view of the physical world is known as the principle of wave-particle duality, or complementarity. It is possible to observe either wave-like properties or particle-like properties of an entity depending on the circumstances, but never both at the same time. According to the Copenhagen interpretation of quantum mechanics, all the information about a particle or system can thus be described in a wave-like manner that is denoted mathematically by a wave function. The wave function of a particle describes the probability of finding a particle in space, thus information about the particle is described probabilistically rather than deterministically. However, wave functions behave like waves and can diffract, and interfere together forming superpositions. This implies that the wave function describes quantum particles as existing in multiple spatial locations or states simultaneously. When a measurement is made one of the multiple states is chosen and the quantum superposition of states ends leaving a classical state. The process of moving from a quantum state to a classical state is known as the collapse of the wavefunction, however, the mechanism by which the wave function collapses is still under debate giving rise to what is known as the measurement problem in quantum theory.

Another aspect of quantum theory is that when two consecutive measurements are made on certain pairs of variables, called complementary variables, there is a fundamental limitation on the precision of the two measurements. Thus, there is no state in which both complementary variables can be defined simultaneously with arbitrary accuracy. This phenomenon is known as the Heisenberg uncertainty principle. This is at odds with the classical notion that measurement of a system does not affect the results.

In certain instances a system of many particles cannot be separated into individual wave functions for each particle, rather the system is described by a single wave function. This physical property is called quantum coherence and is the result of individual particles losing their separate identities such that the entire system acts as a whole. Particles that were once unified in a common quantum state remain physically connected even at a distance. Measurements made on one particle cause the collapse of the entire wave function for the system, resulting in an instantaneous effect for all particles no matter where they are spatially located. This interaction over distance is referred to as non-local quantum entanglement. Decoherence occurs when such a system interacts with its environment in an irreversible thermodynamic way resulting in different particles in the quantum superposition no longer being able to interfere with one another.

The unique properties of quantum theory are made all the more evident when applied to information processing. Classical computation consists of manipulating a register or series of fundamental units of information processing, called bits, via logic gates. Bits are discrete units and can take on one of two values (i.e. 0 or 1). In quantum computation the fundamental units are known as quantum bits, or qubits. Qubits are quantum superposition states representing two values simultaneously with an arbitrary amplitude (i.e. 0 and 1 together). Quantum computation involves allowing qubits to interact with each other then collapsing them to a particular set of measurable states. As a consequence of this, the number of classical states contained within a quantum register grows exponentially, resulting in a faster computation time and thus greater computing power.

These unique properties of quantum theory have led some theorists to suggest that the enigmatic features of consciousness can be explained via macroscopic quantum phenomena in the brain. The notion of non-local quantum entanglement, and the probabilistic nature of quantum theory alone have been used as explanations for the binding problem and the deterministic problems [14, 15]. As well, it can be understood that since quantum theory deals with the fundamental level of matter, the notion of rudimentary consciousness can be explained via quantum descriptions of brain function. However, other theorists still contend that the special properties associated with quantum physics are not relevant in structures such as neurons and the brain, and that classical physics is better suited to the study of such large objects. Yet the boundary between quantum and classical regimes is still under debate. The next section discusses some of the quantum-based theories of brain function followed by the major objections to such theories.

1.4 Theories of quantum brain function

Almost since the inception of the quantum theory of matter in the early part of the last century the notion of quantum properties playing an important role in life processes has been debated [19]. Perhaps the first attempt to describe the brain using the terminology of quantum physics was made by Ricciardi and Umezawa [20]. Based on experimental observations of brain activity they proposed that the brain could be conceived of as a spatially distributed system placed into particular quantum states by stimuli from the external environment. Thus, information can be thought of as being coded into the brain in the form of metastable excited states representative of short-term memory. This code would then be later on transferred to the ground state of the system by means of a condensation to the ground state in the manner of Bose-Einstein condensation accounting for learning and long-term memory. This model proposes that brain functions are manifestations of spontaneous symmetry breaking in the dynamics of the brain regulated by long-range correlations. The model put forth by Ricciardi and Umezawa relating macroscopic quantum states to brain function, memory specifically, was later extended proposing that the brain is a mixed physical system [21]. In this model the brain is considered to consist of two distinct interacting parts, the first part consisting of the classical electrochemical interactions of the neurons of the brain, and the second being the macroscopic quantum state responsible for the creation and maintenance of memory.

This idea of large quantum states in biological systems is more generally illustrated in Fröhlich's notion of biological coherence. Biological coherence is a high state of order that occurs in a biological system when the thermal energy supplied to the system reaches a certain threshold causing the coupled molecules to vibrate in unison [22]. The quantum properties exhibited by such systems have been used to explain the synchronization of biological rhythms such as sleep cycles, and heart rhythms. This idea is further expanded upon in Section 2.3.3.

Inspired by the application of quantum theoretical methods to the study of the brain and other biological structures scientists began to study brain functioning from the microscopic level of quantum physics. Several groups focused specifically on protein polymers located within individual cells known as the cytoskeleton [23, 24]. Anesthesiologist Stuart Hameroff investigated many of these relationships between molecular biology, computers and future ideas of nanotechnology in a book dealing with the co-evolution of consciousness and technology [25]. Specifically it highlights the cytoskeletal structure of living cells to act as a cellular nervous system via computations in the cytoskeleton, and gives numerous arguments based on theory and experimental observation. Using physical models including models based on previous theoretical notions of holography, biological coherence and solitary waves, known as solitons, acting in microtubules [26] the computations of the cytoskeleton are shown to provide explanations of the mechanisms observed in brain cells, and in turn their relation to the functioning of the brain including consciousness. In general Hameroff indicates two main concepts to the understanding of cytoskeletal brain activity from the viewpoint of modern physics. The first is that microtubules act as dielectric waveguides for electromagnetic energy, or photons, creating coherent excitations within microtubules via Fröhlich's theory. The second is that via interference of coherent electromagnetic waves, or photons, through the interaction of microtubules, a network of microtubules acts as a holographic information-processing device.

Physicist Roger Penrose examined the relationship between consciousness and modern physics in a summary exposition of Turing machines, Gödel's theorem, chaos, classical and quantum mechanics, thermodynamics, relativity, cosmology, quantum gravity, quasi-crystals, and brain neurophysiology [14]. In this investigation Penrose introduced mathematics as a bridge from the artificial world of computers to the natural world of physics and argued via Gödel's incompleteness theorem that human consciousness is non-algorithmic, and thus that physical theories of brain function are incomplete due to their dependence on computable algorithmic laws. He further hypothesized that quantum effects play a fundamental role in the understanding of human consciousness by enabling the brain to perform non-computable computations. In his explanation of the new physics required to explain the mind and consciousness he examined the division between classical and quantum physics, specifically the measurement problem, and related the collapse of the wavefunction to conscious events using the notion of Objective Reduction [15]. This led to the suggestion that microtubules within neurons provide the brain with structures capable of orchestrating the collapse of the wavefuntion via quantum computations. This union of Penrose and Hameroff's theories has become known as the Penrose-Hameroff Orchestrated Objective Reduction (Orch OR) theory.

The Penrose-Hameroff Orchestrated Objective Reduction theory of consciousness is perhaps the most well known theory describing brain function based on quantum principles. Objective Reduction is a solution to the measurement problem in quantum theory, which considers the superposition of quantum states as a separation in underlying reality at its most basic level, the Planck scale. The solution involves a description of loop quantum gravity, which identifies superpositions as curvatures of opposite direction in space-time, and thus a separation in fundamental space-time geometry. These separations are considered unstable and reduce to a single space-time curvature once an objective threshold is reached [3]. The theory considers a conscious event as a quantum computation concluding via objective state reduction. Quantum computation within the brain was considered to occur within neuronal microtubules. The individual molecules of tubulin that compose a microtubule were taken as biological qubits. Tubulin molecules are proposed to interact and compute with other tubulin molecules in microtubules via entanglement. The biological conditions in the brain, including synaptic activity, are considered to influence the quantum computations thus orchestrating the collapse of the qubits and giving rise to a conscious event.

However, the Penrose-Hameroff theory of consciousness is not the only theory to relate brain function to microtubules. Based on the pioneering work of Umezawa, Jibu and Yasue give a systematic account of advanced brain functions including consciousness and memory, based on the fundamental principles of quantum theory known as Quantum Brain Dynamics (QBD) [27]. In their theory the QBD system, consisting of the rotational field of water in the brain interacting with the electromagnetic field, exchanges energy directly with what is termed as the external system. The external system surrounding the QBD system includes the microscopic protein filament system of the cytoskeleton, including microtubules, as well as the macroscopic systems of dendritic and neural networks. Hameroff in conjunction with Jibu, Yasue and others predict that microtubules play the role of nonlinear coherent optical devices that take advantage of the ordering of water molecules and the quantized electromagnetic field confined inside the hollow microtubule core to produce signaling free of thermal noise and loss, through the transformation of incoherent, disordered energy into coherent photons within its hollow core, a process termed 'superradiance' [28]. The optical computing proposed to occur in networks of microtubules and other cytoskeletal structures as a basis for cognitive brain functions again implicates information processing within microtubules as playing a key role.

1.5 Arguments for and against quantum brain function

Quantum theories of brain function assert that brain processes are governed by the rules of quantum theory. These theories have met with many objections and criticisms based on both philosophical and scientific grounds [29, 30, 31, 32, and 33]. The main concerns of these remarks however can be broadly separated into the following three categories.

1) The empirical evidence linking how the activity of a single synapse enters into the dynamics of neural assemblies is lacking thus the relevance of quantum processes in mental phenomena is merely a claim [31].

2) There appears to be no special quantum mechanical properties needed to explain psychological and neurological phenomena. The relevance of quantum effects to the structure and function of the brain does not necessitate their involvement in explaining consciousness. Such systems that are expected to behave classically will behave classically. [32, 33]

3) Structures such as microtubules and neurons are large, high temperature systems from the quantum mechanical point of view. As such it is not possible for them to remain in states of linear superposition capable of coherently interfering with one another, thus decoherence eliminates any possibility of quantum effects playing a role in brain processes [29, 30].

There have been many debates concerning whether the quantum description of the brain is valid, realistic or needed. However, only recently have advances in nanotechnology allowing for serious empirical investigation into the biophysical workings of subcellular structures been made. As such, the lack of evidence in support of quantum brain theories should not be taken as proof against such theories, but rather as an area in need of scientific investigation. The several enigmatic features of consciousness mentioned previously are still, for the most part, left unexplained by classical theories. The apparent ability of quantum theories to answer these questions may provide new avenues of investigation into the study of consciousness. It is known that phenomena such as superconductivity, superfluidity and laser action exist and that these phenomena cannot be explained via classical means, but rather require the idea of macroscopic quantum coherence. As such, it can be stated that not all phenomena observed in large-scale systems can be expected to behave classically. Thus, while the first two arguments against quantum brain function represent a general resistance to the idea the third is an argument of worthwhile concern.

Macroscopic quantum phenomena such as superconductivity, and superfluidity require high isolation from their environment in order to avoid the effects of decoherence. In order for such phenomena to exist in the brain nature would need to provide mechanisms to isolate against decoherence. The subject of decoherence in relation to quantum computation in microtubules particularly has been widely discussed and strong arguments have been made on both sides of the discussion.

Tegmark makes a major objection specifically to the Orch-OR theory, and the notion of a quantum brain in general, based on calculations of neural decoherence rates for both regular neuron firings and for kink-like polarization excitations in microtubules, that the degrees of freedom in the human brain should be considered classical rather than quantum [29]. Tegmark found decoherence time-scales for superpositions of solitons moving along a microtubule of approximately $10\text{-}^{-13}\text{-}10^{-11}$ s, which are much shorter when compared with the relevant time-scale of $10^{-3}\text{-}10^{-1}$ s. Thus, it was concluded that quantum coherence within the brain is not feasible. However, Hagan et. al. [34], point out that Tegmark's calculations are based on an incorrect model of the Orch-OR process. Accounting for this discrepancy, as well as effects that screen thermal fluctuations, such as layers of ordered water and actin gel states surrounding microtubules, Hagan et. al. found new decoherence rates of 10^{-5}–10^{-4} s that are in line with relevant dynamical times of biological phenomena. These arguments are both refuted by Rosa et. al. [35] who find, based on decoherence calculations, that the Orch-OR model based on gravitational collapse is incompatible with decoherence, but that the notion of quantum phenomena in the brain is still feasible if decoherence is taken as the collapse mechanism rather than gravity. Thus, investigations into the quantum nature of microtubules and the effects of decoherence on the system may elicit some new information on quantum based cognitive processes in the brain.

References

[1] B. Baars, W. P. Banks, and J. B. Newman, Essential Sources in the Scientific Study of Consciousness, (MIT Press, Cambridge, Massachusetts, 2003)

[2] F. Crick, and C. Koch, *Towards a Neurobiological Theory of Consciousness*, Seminars in the Neurosciences, Vol. 2, pp. 263-275, (1990)

[3] S. Hameroff, *Quantum Computation in Brain Microtubules? The Penrose-Hameroff 'Orch OR' Model of Consciousness [and Discussion]*, Philosophical Transactions of the Royal Society of London A: Mathematical, Physical and Engineering Sciences, Vol. 356, No. 1743, Quantum Computation: Theory and Experiments, pp. 1869-1896, (Aug. 15, 1998)

[4] J. McFadden, *Synchronous firing and its influence on the brain's electromagnetic field: Evidence for an electromagnetic field theory of consciousness*, Journal of Consciousness Studies, Vol. 9, pp. 23-50, (2002)

[5] J. A. Tuszynski and N. Woolf, *The Path Ahead*, in The Emerging Physics of Consciousness, edited by J. A. Tuszynski, (Springer-Verlag, New York, 2006)

[6] C. Koch, The Quest for Consciousness, (Roberts and Company Publishers, Englewood, Colorado, 2004)

[7] E. H. Walker, *The Nature of Consciousness*, in Mathematical Biosciences 7, pp. 131-178, (1970)

[8] F. Beck, and J. C. Eccles, *Quantum Aspects of Brain Activity and the Role of Consciousness*, Proceedings of the National Academy of Science of the United States of America, Vol. 89, pp. 11357-11361, (1992)

[9] F. Beck, and J. C. Eccles, *Quantum processes in the brain: A scientific basis of consciousness*, in Advances in Consciousness Research, Vol. 49, A neural Basis of Consciousness, edited by N. Osaka, (John Benjamins Publishing Company, Philadelphia, 2003)

[10] A. C. C. Coolen, R. Kuhn and P. Sollich, Theory of Neural Information Processing Systems, (Oxford University Press, New York, 2005)

[11] F. H. Eeckman, and J. M. Bower, Computation and Neural Systems, (Kluwer Academic Publishers, Boston, 1993)

[12] D. R. McMillen, G. M. T. D'Eleuterio, and J. R. P. Halperin, *Simple central pattern generator model using phasic analog neurons*, Physical Review E, Vol. 59, No. 6, pp. 6994-6999, (June 1999)

[13] H. Stapp, *Why Classical Mechanics Cannot Naturally Accommodate Consciousness but Quantum Mechanics Can*, Psyche, Vol. 2, No. 5, (May 1995)

[14] R. Penrose, The Emperor's New Mind, (Oxford University Press, Oxford, New York and Melbourne, 1989)

[15] R. Penrose, Shadows of the Mind, (Oxford University Press, Oxford, New York and Melbourne, 1994)

[16] C. Koch, *Introduction to Chapter X Consciousness*, in Cognitive Neurosciences III, edited by M. S. Gazzaniga, (MIT Press, Cambridge, Massachusetts, 2004)

[17] A. C. Scott, Stairway to the Mind: The Controversial New Science of Consciousness, (Springer-Verlag, New York, 1995)

[18] J. Evans, and A. S. Thorndike, Quantum mechanics at the crossroads: New perspectives from history, philosophy and physics, (Springer-Verlag, Berlin, 2007)

[19] E. Schrödinger, What is Life?, (Cambridge University Press, Cambridge, UK, 1944)

[20] L. M. Ricciardi, and H. Umezawa, *Brain and Physics of Many-Body Problems*, Kybernetik, Vol. 4, No. 2, pp. 44-48, (July 3, 1967)

[21] C. I. J. M. Stuart, Y. Takahashi, and H. Umezawa, *On the Stability and Non-local Properties of Memory*, Journal of Theoretical Biology, Vol. 71, pp. 605-618, (1978)

[22] H. Fröhlich, *Long Range Coherence and Energy Storage in Biological Systems*, International Journal of Quantum Chemistry, Vol. 2, pp. 641-649, (1968)

[23] S. R. Hameroff, and R. C. Watt, *Information Processing in Microtubules*, Journal of Theoretical Biology, Vol. 98, pp. 549-561, (1982)

[24] E. Del Giudice, S. Doglia, M. Milani, and G. Vitello, *Electromagnetic field and spontaneous symmetry breaking in biological matter*, Nuclear Physics B, Vol. 275, No. 2, pp. 185-199, (1986)

[25] S. Hameroff, Ultimate Computing, (North Holland, Amsterdam, 1987)

[26] S. R. Hameroff, *Ch'i: A Neural Hologram? Microtubules, Bioholography, and Acupuncture*, American Journal of Chinese Medicine, Vol. 2, No. 2, pp. 163-170, (1974)

[27] M. Jibu, and K. Yasue, Advances in Consciousness Research Vol. 3, Quantum brain dynamics and consciousness: An introduction, (John Benjamins Publishing Company, Philadelphia, 1995)

[28] M. Jibu, S. Hagan, S. R. Hameroff, K. H. Pribram, and K. Yasue, *Quantum optical coherence in cytoskeletal microtubules: implications for brain function*, Biosystems, Vol. 32, pp. 195-209, (1994)

[29] M. Tegmark, *Importance of quantum decoherence in brain processes*, Physical Review E, Vol. 61, p. 4194, (2000)

[30] C. Seife, *Cold Numbers Unmake the Quantum Mind*, Science Vol. 287, No. 5454, p.791, (February 4, 2000)

[31] C. Koch, and K. Hepp, *Quantum mechanics in the brain*, Nature 440, p. 611, (March 30, 2006)

[32] A. Litt, C. Eliasmith, F. W. Kroon, S. Weinstein and P. Thagard, *Is the Brain a Quantum Computer?*, Cognitive Science, Vol. 30, pp. 593-603, (2006)

[33] R. Grush, and P. S. Churchland,. *Gaps in Penrose's toilings*, Journal of Consciousness Studies, Vol. 2, pp. 10-29, (1995)

[34] S. Hagan, S. R. Hameroff, and J. A. Tuszynski, *Quantum computation in brain microtubules: Decoherence and biological feasibility*, Physical Review E, Vol. 65, p. 061901, (2002)

[35] L. P. Rosa, and J. Faber, *Quantum models of the mind: Are they compatible with environment decoherence?* Physical Review E, Vol. 70, p. 031902, (2004)

Chapter 2

The Physics of Biology

2.1 A Brief Introduction to Biophysics

Biophysics attempts to understand physiological processes of living systems from a fundamental level. The difference between living and inanimate matter stems from the ability of organisms to reproduce, adapt and control biological actions such as biochemical reactions, protein assembly/ folding, and biological signaling, all of which are governed by molecular events. Biomolecules are comparatively large and complex. Proteins, for example, have a diverse array of functions and molecular masses ranging from thousands to millions of Daltons (D). However, the chemical constituents of biomolecules are not nearly as complex. There are 20 proteinogenic (protein-building) amino acids that act as the building blocks of all proteins. The diversity of such molecules is thus the result of the many combinations of such constituents. The specific organization of these complex molecular systems provides the specific molecular functions all of which are governed by physical laws. Biophysics seeks to understand these biophysical systems through intramolecular and intermolecular interactions and the resulting electronic and structural conformational changes including the transfer of electrons, protons, ions and energy within the system. Condensed matter physics investigates such problems via methods of quantum mechanics, statistical physics and thermodynamics. Since biological systems are not isolated from their environments these descriptions can become quite complicated due to the openness and far-from-equilibrium nature of living systems. In terms of physics, biological systems exhibit the following properties [1]:

1) They are relatively stable while far from equilibrium requiring that various excitations are stable thus indicating the existence of metastable states.

2) They exhibit a non-trivial order requiring a motional organization whose generalization leads to biological coherence (see Section 2.3.3).

3) They exhibit extraordinary dielectric properties arising from high electric fields maintained in membranes, on the order of 10^7 Volts/meter (V/m), that are sensitive to very low fields.

Investigations into the physical properties of rigid matter and solids are generally classified as condensed matter physics and involve not only the study of a material's mechanical properties, but its electronic structure and ability for electronic transport as well. Semiconductors are solids with an electrical conductivity that can be controlled permanently or dynamically over a wide range, while superconductors are solids with no electrical resistance. Certain biological systems, including parts of the living cell, also fall into the category of condensed matter materials, and thus the electronic structure and ability of these materials to conduct electrical signals is of great importance to their function.

2.2 Mechanisms of Biological Activity

2.2.1 The Importance of Signaling in Biology [18]

The regulation of the complex behavior of living systems is performed through various mechanisms of biological signaling. Signaling within a single cell is part of a complex system of communication that governs basic cellular activities and coordinates cell actions. Single cell signaling is limited to intracellular signals between the cell's various organelles and other constituents. Within larger more complex organisms this includes not only the intracellular signals within individual cells but also the transmission and reception of extracellular signals between cells.

Extracellular signaling is understood mainly in terms of chemical signals between cells. Most signaling molecules are secreted from the transmitting cell via exocytosis, the remainder of the signaling molecules being released by diffusion through the cell membrane. These transmitter molecules can be carried far distances to act on distant target cells, or act as local mediators that affect cells in the immediate vicinity of the signaling cell. Target cells respond to the transmitter molecules through specified proteins in the cell membrane, called receptors, which bind specific signaling molecules that in turn initiate a specified response within the target cell.

There are various methods for extracellular signaling. Paracrine signaling is used to locally mediate groups of cells by secreting transmitter molecules that are quickly taken up by surrounding target cells, thus initiating responses in target cells located close to the signaling cell. Autocrine signaling works in a similar manner. Whereas in paracrine signaling the signaling cell, and target cell are of different varieties, the cells in autocrine signaling are of the same type. Thus, not only can the transmitter molecules from the signaling cell bind to other target cells, they can also bind to the receptors of the signaling cell itself. Synaptic signaling is a highly specified fast form of paracrine signaling in which specialized cells, namely nerve cells, signal amongst one another across widely separate parts of an organism. When activated, a nerve cell initiates an electrical response sending an electrical impulse, known as an action potential, along long cellular extensions known as axons. This signal stimulates the release of chemical transmitter molecules, known as neurotransmitters, from the terminal end of the axon. These nerve terminals are in contact with specialized junctions on the target cell called chemical synapses. These junctions provide close contact between the signaling and target cell allowing for quick and direct signaling. Current opinion suggests that neurotransmitters diffuse across the synaptic cleft, which is the gap between the signaling and target cell at the synapse [19]. However, it has been suggested that the process may involve quantum tunneling of the transmitter molecules across the synaptic cleft [20], although experimental evidence to support this hypothesis remains to be found.

Another method of signaling used by nerve cells is signaling through gap junctions. A gap junction is a specialized cell-to-cell connection that forms between two adjacent cell membranes. At the junction the cells connect directly through small openings in the cell membrane joined by narrow water-filled channels, thus directly linking the interiors of the two cells. These junctions allow the transport of small intracellular signaling molecules, such as charged ions, but not large macromolecules such as proteins. This allows the two cells to communicate directly via the electrical flow of ions without dealing with the cell membrane barrier.

Intracellular signaling includes all signaling mechanisms that coordinate and orchestrate the inner working of a single cell. This includes the signaling required to organize the interior structures of the cell. However, unlike extracellular signaling these mechanisms are not yet fully understood. As such, research to investigate these mechanisms remains active. Traditional work in biology has focused on studying individual parts of cell signaling pathways. This systems biology approach works to understand the underlying structure of cell signaling networks and how changes in these networks can affect the transmission of information.

2.2.2 Energy Transfer in Biology

In the life sciences, the biochemical paradigm is prevalent implying that essential biological processes occur at the molecular level and above. This view focuses on molecular structures and the molecular mechanisms involved in energy transfer. However, the activity of biological systems does not simply follow from the structure of its constituent molecules. Biological activity is frequently turned on and off. From the view of physics these activities can be expressed in terms of non-linear excitations. To establish and maintain these excitations and to compensate for the effects of entropy, biological systems require a supply of energy, as the majority of biophysical processes are endothermic. Biological processes receive a supply of energy by coupling to exothermic processes, namely the hydrolysis of adenosine triphosphate (ATP) or guanosine triphosphate (GTP), as GTP is readily converted to ATP. Energy is packed into these important biological molecules and transferred to the sites where needed. The hydrolysis of ATP is given as,

$$ATP + H_2O \Leftrightarrow ADP + P_i \tag{2.1}$$

where H_2O is water, ADP is adenosine diphosphate and P_i is an inorganic phosphate. The free energy released from the removal of a single phosphate from ATP when all reactants and products are in standard concentrations is approximately 30 kilojoules/mol (kJ/mol), whereas at typical cellular concentrations this value is closer to 57 kJ/mol.

In eukaryotic cells the mitochondria organelles produce ATP via a process called the mitochondrial electron transport chain. Energy sources, such as glucose, are initially metabolized in the cytoplasm with the products being taken up by the mitochondria. In brief, the mitochondrial electron transport chain then removes electrons from an electron donor and passes them to a terminal electron acceptor via a series of redox reactions. These reactions create a proton gradient across the mitochondrial inner membrane of the mitochondria resulting in a trans-membrane proton gradient that is used to make ATP via the enzyme ATP synthase. Sub-molecular transportation of particles through biological structures, such as the mitochondrial electron transport chain, has been discovered in modern organisms and is a rapidly growing area of research.

The term bioenergetics, originally coined by Szent-Györgyi in 1957 to refer to energy not confined within biomolecules but emitted or absorbed directly by tissue, is used in modern biology to refer to the transfer and conversion of biological energy [10]. From this viewpoint energy production and transport is a conversion of energy from one form to another. Many biological processes may be understood as energy conversion, for example vision (light energy → electrical energy), nerve impulses (chemical energy → electrical energy), or muscle contraction (chemical energy → mechanical energy).

In regards to biophysical explanations of biological signaling and energy transfer, it has been hypothesized that these processes are electromagnetic in nature, where interactions of biomolecules produce chemical reactions and thus elicit electrical signals via charged ions in order to transfer energy throughout the system. The electromagnetic regulation of these processes would have the advantage of signaling occurring at a relatively rapid rate when compared to extracellular signals.

2.3 Review of the Physics of Solids [26, 27, 28]

2.3.1 Lattice Properties of Solids

A solid is any material in a state characterized by resistance to deformation and changes of volume. At the microscopic scale a solid has atoms or molecules that are packed closely together. These elements have fixed positions in space relative to each other thus accounting for the rigidity of the solid. Unless a sufficient force is applied to permanently deform the material, the solid maintains is shape and volume. When there is a unique arrangement of atoms in the solid, such that the structure is composed of a set of atoms or molecules arranged in a periodically repeating three-dimensional lattice, the material is known as a crystal. The spacing in various directions between primitive unit cells, the particular arrangement of atoms/ molecules that is periodically repeated in a crystal, is called a crystal's lattice vector. A Bravais lattice is the simplest type of crystal, and is characterized by the vector distance $\vec{R}$ as given by,

$$\vec{R} = A\vec{l}_1 + B\vec{l}_2 + C\vec{l}_3 \tag{2.1}$$

where A, B and C are integers and $\vec{l}_i$ are the basis vectors of the lattice. There are 14 possible Bravais lattice configurations that fill three-dimensional space based on the 7 crystal symmetries (see Figure 2.1). Primitive unit cells may take any shape as long as they fulfill the requirement stated above, thus resulting in primitive cells of equal volume, but without unique orientation around a given lattice point. Primitive cells that are invariant under all symmetry operations around a given lattice point are known as Wigner-Séitz cells. The Wigner-Seitz cell of a crystal lattice is defined as the volume around a single lattice point that is closer to that lattice point than to any of the other lattice points. It is found by taking the surfaces at the midway point between one lattice point and its nearest neighbors, otherwise known as Bragg planes (see Figure 2.2).

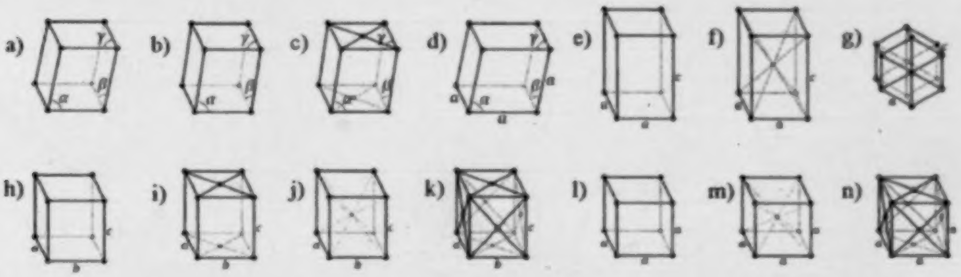

Figure 2.1: The 7 crystal symmetries and corresponding 14 Bravais lattices: Triclinic (α, β, γ ≠ 90°) a) simple, Monoclinic (α ≠ 90°, β, γ = 90°) b) simple, and c) base-centered, Trigonal (α, β, γ ≠ 90°) d) simple, Tetragonal (a ≠ c) e) simple and f) centered, Hexagonal (a ≠ c) g) simple, Orthorhombic (a ≠ b ≠ c) h) simple, i) base, j) body-centered, and k) face-centered, and Cubic l) simple, m) body-centered, and n) face-centered.

Another way to define the crystal is via the reciprocal lattice of any given Bravais lattice. The reciprocal lattice is the set of all wave vectors $\vec{K}$ that give plane waves with the periodicity of a given Bravais lattice. That is, the reciprocal lattice is the set of wave vectors $\vec{K}$ that satisfy,

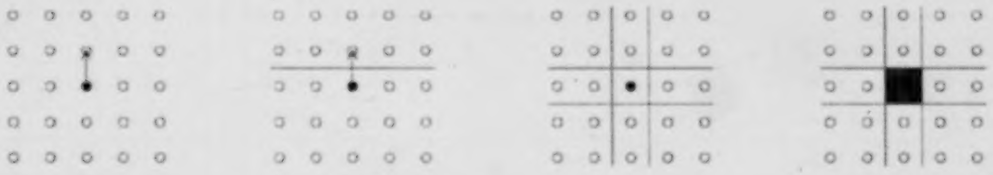
(A) (B) (C) (D)

Figure 2.2: Construction of a Wigner-Seitz cell. From a single lattice site (A) draw a line to a nearest neighbor lattice site, (B) create a Bragg plane by bisecting this line, (C) repeat for remaining nearest neighbors, and (D) the enclosed area represents the Wigner-Seitz cell.

$$e^{i\vec{K}\cdot\vec{R}} = 1 \tag{2.2}$$

where,

$$\vec{K} = D\vec{q}_1 + E\vec{q}_2 + F\vec{q}_3 \tag{2.3}$$

and D, E, and F are integers. The basis vectors in k-space $\vec{q}_i$ are defined in terms of the Bravais lattice basis vectors as given by,

$$\begin{aligned}
\vec{q}_1 &= 2\pi\frac{\bar{l}_2\times\bar{l}_3}{\bar{l}_1\cdot(\bar{l}_2\times\bar{l}_3)}\\
\vec{q}_2 &= 2\pi\frac{\bar{l}_3\times\bar{l}_1}{\bar{l}_1\cdot(\bar{l}_2\times\bar{l}_3)}\\
\vec{q}_3 &= 2\pi\frac{\bar{l}_1\times\bar{l}_2}{\bar{l}_1\cdot(\bar{l}_2\times\bar{l}_3)}
\end{aligned} \tag{2.4}$$

The uniquely defined primitive cell of the reciprocal lattice in k-space is called the first Brillouin zone, and is found by the same method as for the Wigner-Seitz cell in the Bravais lattice. If the volume of the Wigner-Seitz cell for a given Bravais lattice is V, then the volume of the primitive cell for the reciprocal lattice is given by $(2\pi)^3/V$. Note that although the Wigner-Seitz cell and the first Brillouin zone refer to the same geometrical shape, the term Brillouin zone applies only to cells in *k*-space.

A crystal's structure and symmetry play a role in determining many of its properties, such as electronic and optical properties. Thus, by knowing a materials crystal structure many of its physical properties can be determined. Proteins, the fundamental chemical constituent of most biomolecules, like many other molecules, can be prompted to form crystals when subjected to the appropriate conditions. Proteins crystallize when the purified protein form undergoes a slow precipitation from an aqueous solution. As a result, individual protein molecules align themselves in repeating series of unit cells by adopting a consistent orientation. Protein crystallization serves as the basis for X-ray and electron crystallography, wherein X-ray or electron diffraction from a crystallized protein is used to determine the protein's three-dimensional structure. This method determines the three-dimensional density distribution of electrons in the crystallized protein from which the coordinates of the proteins constituent atoms may be inferred down to a certain resolution. By determining the three-dimensional structure of proteins it becomes possible to understand the functions of proteins at a molecular level. This is the basis for the field of structural biology.

However, a static crystal lattice does not capture the reality of a material such as a protein polymer, as the constituent atoms/molecules are not expected to remain stationary. The simplest way to consider the movement of the lattice is to regard the atoms/molecules as simple harmonic oscillators of equal masses *M*, connected by springs of force constant *K*. Considering a one-dimensional lattice of identical atoms/molecules as a group of coupled harmonic oscillators the Hamiltonian in position space for the system is then given by,

$$H = \sum_n \frac{p_n^2}{2M} + \sum_n \frac{1}{2} M\omega^2 (x_n - x_{n+1})^2 \tag{2.5}$$

where *n* denotes an individual atom/molecule of the *N* atoms/molecules in the system, x_n is the operator of n^{th} atom/molecule defining its displacement from its equilibrium position *A*, $\omega^2 = K/M$, and the second sum is taken only over nearest neighbors in the system. To obtain the Hamiltonian in *k*-space the Fourier transforms of the momentum and position are taken such that,

$$\begin{aligned} p_n &= \frac{1}{\sqrt{N}} \sum_k (p_k e^{iknA} + p_k^{\dagger} e^{-iknA}) \\ x_n &= \frac{1}{\sqrt{N}} \sum_k (x_k e^{iknA} + x_k^{\dagger} e^{-iknA}) \end{aligned} \tag{2.6}$$

such that,

$$H=\sum_k\left(\frac{p_k^\dagger p_k}{2M}+\frac{1}{2}M\omega_k^2 x_k^\dagger x_k\right) \tag{2.7}$$

where $\omega_k = 2\omega\sin(\frac{kA}{2})$ gives the frequencies of the oscillations, otherwise known as phonons.

By defining creation and annihilation operators for phonons as,

$$\begin{aligned} b_k^\dagger &= \sqrt{\frac{M\omega_k}{2\hbar}}\left(x_k^\dagger - \frac{i}{M\omega_k}p_k\right) \\ b_k &= \sqrt{\frac{M\omega_k}{2\hbar}}\left(x_k + \frac{i}{M\omega_k}p_k^\dagger\right) \end{aligned} \tag{2.8}$$

where $[b_k, b_k^\dagger]=1$. The phonon Hamiltonian may be given in the second quantized form as,

$$\begin{aligned} H_{ph} &= \sum_k \frac{\hbar\omega_k}{2}(b_k b_k^\dagger + b_k^\dagger b_k) \\ &= \sum_k \hbar\omega_k\left(N_k+\frac{1}{2}\right) \end{aligned} \tag{2.9}$$

with the number operator $N_k = b_k^\dagger b_k$.

2.3.2 Electrical Properties of Solids

The previous section described the shape and certain properties of a periodic crystal lattice structure. In order to understand the electrical properties of a solid the interaction of electrons with the lattice potential must be taken into account. An electron in such a periodic potential is known as a Bloch electron. Bloch's theorem states that the wavefunction for an electron in a periodic potential, $V(\vec{r}+\vec{R})=V(\vec{r})$ may be written as,

$$\psi_{\vec{k}}(\vec{r}) = e^{i\vec{k}\cdot\vec{r}}u_{\vec{k}}(\vec{r}) \tag{2.10}$$

with u possessing the same periodicity as the potential, i.e. $u(\vec{r}+\vec{R})=u(\vec{r})$ or likewise $\psi(\vec{r}+\vec{R})=\psi(\vec{r})e^{i\vec{k}\cdot\vec{R}}$. For any given value of the Bloch wavevector $\vec{k}$ and periodic potential $V(\vec{r})$ there are a number of energy eigenvalue solutions to the Schrödinger equation, indexed by n, such that,

$$H_{eff}\psi_{n\bar{k}}(\bar{r}) = \varepsilon_{n\bar{k}}\psi_{n\bar{k}}(\bar{r}) \tag{2.11}$$

where the effective Hamiltonian H_{eff} is given by,

$$H_{eff} = -\frac{\hbar^2}{2m}(\bar{\nabla} + i\bar{k})^2 + \hat{V}(\bar{r}) \tag{2.12}$$

The Bloch wavevector is free to adopt a wide range of values, but must obey restrictions arising from the finite size of the crystal in which the Bloch wave lies. Any two $\bar{k}$ values that differ by the reciprocal lattice vector $\bar{K}$ share the same wavefunction, and thus the same eigenvalue according to (2.2), and therefore the two $\bar{k}$ values can be considered physically identical. Thus, only those wavevector values inside the first Brillouin zone need be considered. The density of energy eigenfunction states in the n^{th} index is given by,

$$D_n(\varepsilon) = \frac{2}{V}\sum_{\bar{k}}\delta(\varepsilon - \varepsilon_{n\bar{k}}) \tag{2.13}$$

For each $\bar{k}$ the energy eigenstates are separated in energy by a finite spacing. In some cases there are ranges over which there are no states leading to bands of allowed energies, thus giving rise to a band structure for the solid where the solutions $\varepsilon_{n\bar{k}}$ are called the band energies, and n denotes the band index. Allowed bands may overlap giving rise to a single large band. In theory, any solid has an infinite number of bands, however all but a select few reside at extremely high energies so that electrons with the required energy to reach these high energy levels would possess enough energy to escape the solid. These high-energy bands are usually not considered. Energy bands contain a wealth of information regarding a solid's electrical properties. Their slopes give electron velocities, thus predicting electron transport properties, and from their shape it is possible to calculate minimum energy crystal structures and even magnetic properties. Overall band widths and shapes are determined by the properties of the atomic or molecular orbitals constituting the crystal, however the material required to calculate band structure goes beyond the scope of the material presented here.

If a given crystal contains N atoms then each Brillouin zone contains N allowed $\bar{k}$ values. Since the Pauli exclusion principle forbids multiple occupations of the same state, and an electron has two allowed spin eigenstates each Brillouin zone may contain $2N$ electrons. For the lowest energy state, or ground state, of the system the electrons provided by the atoms/ molecules will then fill all the states up to a given energy known as the Fermi energy ε_f or Fermi level, which denotes the energy of the most energetic electron in the crystal at absolute zero, or for non-zero temperature the energy at which the probability of occupation falls below 0.5. For any given lattice, there will be a set of filled bands, with a full complement of electrons and unfilled bands which have no electrons. The highest occupied band is known as the valence band, derived from the chemists' term "valence electrons" for electrons on the outermost shell of an atom. The lowest unoccupied band is known as the conduction band, as electrons that enter the conduction band are free to move about the lattice and conduct current. The energy of separation between the valence band and the conduction band is known as the band gap.

Cases in which the Fermi level lies within an energy band may be understood as the conduction band and the valence band overlapping or the valence band being only partially filled, both with the Fermi energy somewhere inside. This means that the material always has electrons that can move freely. In the presence of an electric field these electrons move giving the electron population a net momentum thus carrying current. This behavior is characteristic of metals and materials of this sort are classified as conductors.

For cases in which the Fermi level lies between energy bands, in a band gap, the states in the valence band, below the Fermi energy, are fully occupied, while those in the conduction band are empty. In order for such a material to allow electron conduction the electrons in the material must gain enough energy to jump the band gap. For materials in which the band gap is large (greater than 3 eV) the probability for electrons to bridge the band gap is very low even with extra energy provided by heat, incident light or high electric field. Materials of this sort are thus poor conductors and are classified as insulators. In the case where the band gap is less than 2 eV however, thermal energy, incident light and high electric fields can provide enough energy to increase the probability of jumping the band gap creating a substantial population of conduction electrons giving the material a limited conductivity. These materials are designated as semiconductors.

The conductivity, σ, of a material is a measure of a material's ability to conduct an electric current and is defined as:

$$\vec{j} = \sigma\vec{E} \tag{2.15}$$

where $\vec{j}$ is the current density in the material, and $\vec{E}$ is the electric field strength within the material. The current density is defined as,

$$\vec{j} = \frac{1}{V}\sum_{s,\vec{k}} N_{s,\vec{k}} e\vec{v}_{\vec{k}} \tag{2.16}$$

The drift velocity, otherwise known as the group velocity, of electrons in the *nth* band with wave number $\bar{k}$ is given as,

$$\bar{v}_{n\bar{k}} = \frac{1}{\hbar}\bar{\nabla}_{\bar{k}}\varepsilon_{n\bar{k}} \tag{2.17}$$

where n is taken as the conduction band of the material.

Conductors, which readily conduct electric currents, typically possess conductivity values greater than $10^4\ \Omega^{-1}\text{cm}^{-1}$. The extreme of this regime, when conductivity approaches an infinite value, gives rise to the special case of superconductors in which there is no resistance to the flow of current. However, this involves more complex interactions of the electrons with the crystal lattice, which will not be discussed here. Insulators, with their lack of conduction electrons and their ability to resist the flow of current, are characterized by conductivities below $10^{-10}\ \Omega^{-1}\text{cm}^{-1}$, while semiconductor conductivities fall in the intermediate range of $10^{-9}\ \Omega^{-1}\text{cm}^{-1} - 10^{3}\ \Omega^{-1}\text{cm}^{-1}$.

Knowing these conduction properties of solids gives a clearer understanding of other solid electric properties. Dielectrics are substances that act as electrical insulators, thus highly resisting electrical current. Electrons in a dielectric material are strongly bound to the atoms composing the material and therefore are not free to move throughout the material when under the influence of an applied electric field as discussed. However, the electrons can move small distances relative to their nuclei. When an electric field is applied to a dielectric, the material concentrates the field within itself through redistribution of charges within its atoms or molecules altering the shape of the field both inside and near the substance. In biology, cells and many of the relevant large molecules exhibit dielectric properties, for example cell membranes maintain a very strong dipolar layer.

Zaky and Hawley present a thorough introduction to dielectric solids, including the phenomena of ferroelectricity, piezoelectricity and pyroelectricity, in [11] which is the basis of the following discussion of the subject. Dielectrics can be largely subdivided into non-polar and polar dielectrics. Dielectric materials composed of non-polar molecules can be considered to have a positively charged nuclei symmetrically surrounded by a negatively charged cloud of electrons. When there is no external electric field applied the charges cancel. However, in the presence of an external electric field the positive and negative charges experience an electric force and are displaced by a very small distance (approximately 10^{-10}-10^{-11}m). This results in polarization of the non-polar molecules such that each molecule possesses a dipole moment, and induce an overall electric polarization in the material. When the field is removed the molecular dipoles and polarization disappear.

Polar dielectrics are composed of molecules that possess intrinsic dipole moments in the absence of external electric fields due to their intrinsic asymmetric distribution of charge.

When no external field is applied these molecular dipoles may orient themselves randomly due to the thermal agitation of the environment. This is known as the paraelectric phase and results in a zero or very small overall spontaneous polarization. When a field is applied the molecules tend to align themselves in the direction of the electric field resulting in polarization of the material. Some polar dielectrics exhibit a spontaneous dielectric polarization in the absence of an applied field. These materials are known as ferroelectrics. A material exhibiting a ferroelectric phase can make a phase transition to the paraelectric phase if the temperature of the material is raised beyond a transition temperature known as the ferroelectric Curie temperature.

In certain cases when a dielectric is placed in an electric field the small displacement of charge proportionally changes the mechanical dimensions of the material through elongation in the direction of the field. Such materials are called piezoelectric. The piezoelectric effect results from a lack of a centre of symmetry in the crystal structure of the material. Conversely, when a mechanical stress is applied to a piezoelectric material it results in an overall polarization. Piezoelectric materials are usually also pyroelectric. The pyroelectric effect generates an electric potential when a temperature gradient is applied to a pyroelectric material. Experimental evidence predicting the piezoelectric and pyroelectric properties of biological structures has been found [12, 13]. Biological piezoelectricity has been observed directly in bone, DNA, ribonucleic acid (RNA), myosin and collagen, and pyroelectricity has been directly observed in bone, tendon and nerve cells [2]. As well, several of the amino acids, the basic building blocks of proteins, have been shown to exhibit piezoelectric and pyroelectric properties [14].

The transfer of electrons, however, is not the only form of biological conductance discussed. Proton transfer reactions are also important in maintaining cellular life, they are part of the metabolic processes taking place in the cell including in the synthesis of cellular energy stored in ATP, as discussed in section 2.2.2. ATP synthesis in particular is discussed as proton transport in a membrane-spanning proton semiconductor. The movement of ions or charged particles is another form of biological conductance considered. Ion condensation on biopolymers is discussed as a method of intracellular signaling, in particular the condensation/ decondensation of calcium ions and its relation to coherent patterns of protein phosphorylation.

In dielectrics electrical conduction can be mediated via three different types of charge carrier: molecular ions, electrolytes and electrons. The first mechanism uses molecular ions, or clusters of ionized molecules, and is related to the phenomena of electrophoresis. Molecular ionic conduction is most commonly encountered in amorphous or liquid dielectric systems. The second mechanism uses electrolytes, otherwise referred to as ions, or charged atoms. Conduction occurs through the movement of ions, originating in the material or from impurities, or through the motion of ion vacancies. Proton conduction is a specific example of ionic conduction, protons being hydrogen ions. The final mechanism is understood in terms of the flow of electrons or electron holes and is most commonly referred to as electronic conduction.

In order for insulators and semiconductors to conduct any form of current, electrons in the valence band must be excited into the conduction band. For systems in which the electrons are non-interacting an electron excitation such as this could be understood in terms of the occupation number $N_{s,\vec{k}}$. For a single excitation, by interaction with an incident quantum of energy or photon, $N_{s,\vec{k}}$ would differ from the ground state in that one $\vec{k}$ value below the Fermi level would become empty, and one above it would become occupied. In order to return to the ground state, the excited electron would need to reoccupy the empty state, thus as a system tends to its lowest energy state the electron can be considered attracted to the empty "hole" state. The hole can be thought of as possessing an opposite electric charge to that of the electron, and thus the two attract one another via the Coulomb interaction. This results in a bound electron-hole pair quasiparticle known as an exciton. The excited system can then be considered as the ground state system plus an excitation composed of an exciton having a well-defined energy above the ground energy. Since the exciton results from the binding of the electron and hole, it has slightly less energy than the unbound electron and hole. In the case where the binding is considered sufficiently weak, the electron and hole orbit one another at large distances. This limiting case is known as a Mott-Wanier exciton. In the opposite extreme, when the binding is considered very tight, the electron and hole separation can be regarded as negligible. This second case is known as a Frenkel exciton.

If the energy difference between the ground state configuration and the configuration containing one exciton is defined as $\hbar\Omega$ then the Hamiltonian for a single exciton system may be described in second quantized form as $H_{ex} = \hbar\Omega a^\dagger a$, where $a^\dagger$ and a are the exciton creation and annihilation operators, respectively. If the interaction energy between two excitons is defined as J, then the one-dimensional exciton Hamiltonian for a chain of n identical atoms/molecules with can be defined as,

$$H_{ex} = \sum_n [\hbar\Omega a_n^\dagger a_n + J(a_n^\dagger a_{n-1} + a_n^\dagger a_{n+1})] \tag{2.18}$$

where only interaction between nearest neighbors are taken into account. A dispersion relation in one-dimension can be determined,

$$\varepsilon_k = \hbar\Omega + 2J\cos(kA) \tag{2.19}$$

when k-space creation and annihilation operators,

$$\begin{aligned} a_k^\dagger &= \frac{1}{\sqrt{2\pi}} \sum_n e^{-iknA} a_n^\dagger \\ a_k &= \frac{1}{\sqrt{2\pi}} \sum_n e^{-iknA} a_n \end{aligned} \tag{2.20}$$

are entered into Equation 2.18 to yield,

$$H_{ex} = \sum_k \varepsilon_k a_k^\dagger a_k \qquad (2.21)$$

as the *k*-space exciton Hamiltonian.

2.3.3 Collective Excitations and Energy Transfer

Szent-Györgyi provided a new approach to the mechanism of biological reactions involving energy transfer over large distances by suggesting that biological macromolecules, with their size and symmetry, possess conduction bands similar to those which emerge from the collective electron models of metals. In 1941 Szent-Györgyi hypothesized that the phenomena of electronic conduction may be crucial to understanding the fundamental workings of biological systems [15, 16], and further supported this hypothesis in 1946 with the finding of photoconductive effects in protein films [17]. This gave rise to the description of conduction within organic solids in terms of semiconductors. The term organic semiconductor is used to describe organic compounds that display properties that are inconsistent with electrical insulators.

In his 1975 review paper on the application of solid-state physics concepts to biological systems Cope identifies several solid-state physical phenomena in components of living cells [2]. The review connected rate-limiting processes in the enzyme cytochrome oxidase to the semiconduction of electrons across enzyme particles, semiconductor junction conduction electrons to the function of the eye as well as the process of photosynthesis, superconduction to the growth of nerves, phonons and polarons to mitochondrial phosphorylation, piezoelectricity and pyroelectricity to the growth of nerves and bone structure, infrared electromagnetic waves to the transmission of energy in lipid bilayers of nerve cells and mitochondria, sodium and potassium ions in structured cell water to valence band electrons in semiconductors, and free cations to conduction electrons.

Experiments and computer simulations involving enzymes, proteins that catalyze biochemical reactions in the cell, have yielded an atomic-level explanation of an enzyme catalyzed chemical reaction in terms of proton tunneling [4]. These results explicitly indicate the existence of quantum tunneling effects in these biomolecules. Another experiment has shown optical control of photoactive processes in bacteriorhodopsin, a bacterial counterpart of the protein visual sensor in the human eye, thus indicating that biological processes can be manipulated at the quantum-mechanical level [5]. Fourier transform spectroscopy performed on the bacteriochlorophyll Fenna-Matthews-Olsen antenna complex has revealed "quantum beat" variations in signal intensity that persist for hundreds of femtoseconds indicating that electronic quantum coherence plays an important role in the energy transfer process of photosynthetic systems [6]. From the theoretical standpoint an investigation into the physical mechanism of scent detection has used quantum properties to describe selective atomic-scale processes that are initiated when scent molecules interact with receptors in the nose. This method attributes phonon assisted electron tunneling to be a physically viable detection method that is consistent with observed features of the sense of smell [7].

Quantum mechanical explanations of the effect of anesthetics on the brain are of particular interest, as not only do they affect biological processes, but consciousness itself. While the exact molecular mechanisms of general anesthetics remains largely unknown it is suggested that anesthetic gas molecules occupy the hydrophobic pockets of neuronal proteins by forming London force interactions with non-polar amino acid groups [8]. London forces are not chemical bonds but rather weak quantum interactions. This implies that the quantum nature of London forces may be a key component in brain functioning and consciousness. Endogenous London forces acting in hydrophobic pockets regulate protein conformational states. It has been suggested that consciousness may involve collective fields governed by long-range dipole correlations among these forces, and that anesthetic gases prevent consciousness by weakening these forces when forming exogenous London forces in protein hydrophobic pockets [9].

However, conductance measurements made on biopolymers are difficult due to the structural variety of polymers, the liquid state of samples and the dependence of biological systems on environmental factors such as pH, temperature and ion concentration. Despite these difficulties attempts have been made to measure biopolymer resistance values, including attempts made specifically on microtubules. In a review of electronic and ionic conductivities of microtubules and actin filaments Tuszynski et. al. briefly survey the current standing of conduction in biology [3]. Due to the relative importance of deoxyribonucleic acid (DNA) in living systems it is noted that much of the work in biological conductivity has been done to investigate DNA's conduction capability. In the paper it is reported that experimental findings point to insulating, semiconducting and even superconducting properties in DNA depending on the method of investigation, and type of molecules used, and that DNA may be semiconducting, insulating and metallic simultaneously depending on the arrangement of the molecules in the structure. Yet, despite these discrepancies it is believed that the pathway for electrical transport runs through the bases in the centre of the DNA double helix, and that the dominant transport mechanism is the coherent hopping of electrons.

In Frenkel's two-part paper on the transformation of heat and light in solids [30, 31], he identified three important insights into the behavior of electronic excitations in solids as pointed out in reference [32]. The first is that the excitation can be delocalized, thus extending over several adjacent atoms, and as a result, be described by a series of Bloch wave functions depending on the crystal structure. Secondly, due to the delocalized nature of the excitation, the superposition of several of the wave configurations will result in a localized wave packet that moves through the lattice with a group velocity determined by the exciton dispersion and the extent of the exciton-lattice interaction. Third, since the exciton is coupled to the crystal lattice, the attraction of the exciton to the lattice of charged ions, thus creates a lattice distortion that travels with the electronic excitation. Thus, the phonons regulate the intermolecular interactions that are responsible for determining the mixing, or superposition of the delocalized wave states for the crystal. The result of this is a partial localization of the electron excitation allowing the excitation to propagate coherently as a wavepacket. This is allowed provided that the superposition of the *k*-states remains unchanged over times exceeding the time associated with the nearest neighbor electronic intermolecular exchange. The average frequency at which the superposition of *k*-states changes relative to the intermolecular interaction time determines the primary mechanism for electronic energy transfer in solids regardless of the temperature.

The root cause of the exciton-phonon coupling is the distance dependence of the exciton parameters Ω and J. The simplest way to write the Hamiltonian for an interaction of this type in position space is,

$$H_{ex-ph} = \chi_1 \sum_n (x_{n+1} - x_{n-1}) a_n^\dagger a_n + \chi_2 \sum_n (x_{n+1} - x_n)(a_{n+1}^\dagger a_n + a_n^\dagger a_{n+1}) \tag{2.22}$$

with χ_1 and χ_2 defining the coupling strength between excitons and phonons. Thus the total Hamiltonian in position space may be written as,

$$H = H_{ex} + H_{ph} + H_{ex-ph} \tag{2.23}$$

where the terms are given by Equations 2.18, 2.5 and 2.22 respectively.

When the positive and negative regions of a molecule vibrate against one another they form an oscillating electric dipole. In dielectric substances these oscillations are capable of extending over the entire material in the form of longitudinal electric oscillations. These longitudinal oscillations are a direct result of electro-dynamic interactions between the molecular dipoles of the system. When energy is fed locally to a particular dipolar oscillation, such as in certain processes of living systems, the long-range electric interaction causes this energy to be shared with the other dipoles.

In 1968 British-German physicist Herbert Fröhlich showed that when the energy supply is sufficiently large in comparison with the energy loss of the system the dipoles tend to oscillate in a coherent manner [21]. With increased energy supply from an external source, such as thermal fluctuations, deformations of the system caused by non-linear effects reduce the energy loss moving the system into a metastable stationary state such that the energy of the electric oscillations is larger than that in thermal equilibrium. Provided that the energy supply exceeds a critical value the excess energy of the system is channeled into a single longitudinal oscillation. The random energy supply is therefore not converted wholly into thermal energy, but is used to maintain a coherent electric wave in the material. This occurrence in biomolecules is referred to as biological coherence. Thus, Fröhlich indicated that the channeling of randomly supplied energy into a single oscillation in biological systems is a special case of long-range quantum mechanical phase correlation, or coherence, such as in a Bose-Einstein condensate. The notion of biological coherence implies that energy in biological systems is transmitted in coherent waves that propagate without thermal loss [22].

This analysis by Fröhlich was based on rate equations. It wasn't until 1977 that Wu and Austin provided a microscopic approach to Fröhlich's theory of Bose condensation in biological systems. Supposing that a biological system consisted of oscillating segments of giant dipoles occurring along macromolecules with the remainder forming a heat bath, and an external energy source coupled to the oscillating units, Wu and Austin formed the Hamiltonian for Fröhlich's theory in second quantized form as [29]

$$\begin{aligned} H = \sum_i \hbar\omega_i a_i^\dagger a_i + \sum_k \hbar\Omega_k b_k^\dagger b_k + \sum_p \hbar\Omega'_p P_p^\dagger P_p + \sum_{i,k}(\lambda b_k^\dagger a_i + \lambda^* b_k a_i^\dagger) + \\ \frac{1}{2}\hbar\sum_{i,j,k}(\chi a_i^\dagger a_j b_k^\dagger + \chi^* a_j a_i^\dagger b_k) + \hbar\sum_{p,i}(\xi P_p a_i^\dagger + \xi^* P_p^\dagger a_i) \end{aligned} \tag{2.4}$$

where the interaction between oscillating units produces a narrow band of frequencies, ω_i, representing the normal electromagnetic modes with $a^\dagger{}_i$ and a_i the related creation and annihilation operators, Ω_κ are the vibrational modes with $b^\dagger{}_i$ and b_i the related creation and annihilation operators, Ω'_p are the external energy source frequencies with $P^\dagger{}_i$ and P_i the related creation and annihilation and λ, χ, and ζ are the coupling constants for the one quantum process, two quantum process and the energy supply to the oscillating constituents respectively.

In 1973 Davydov suggested a dynamic method to explain how energy is transduced and transported in biological systems [23]. Using simplified models he showed that proteins could self-focus, or trap, energy in stable pulse-like waves known as solitons. Originally Davydov suggested the soliton model to explain the role of myosin in the conversion of chemical energy to mechanical energy in muscle contraction [23], only later generalizing the model to explain energy transfer along protein molecules [24], and DNA.

The energy released by the hydrolysis of molecules such as ATP or GTP is insufficient to excite the electronic states of molecules indicating the importance of vibration excitations of groups of atoms within protein molecules. Polymerization of amino acids in proteins results in a compound containing a peptide group characterized by a carbon-oxygen double bond linked to a nitrogen hydrogen bond.

Stretching and contraction of the carbon oxygen double bond is one type of vibration that may occur in proteins and are denoted as amide I vibrations (see Figure 2.3). Furthermore, hydrogen bonds formed between oxygen and hydrogen atoms of peptide groups form polypeptide chains of amino acids that may fold into secondary protein structures such as α-helices.

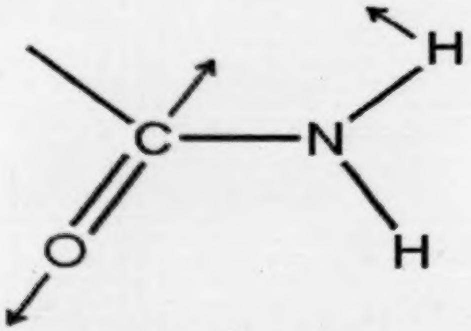

Figure 2.3: Peptide group showing amide-I vibration. The major contribution to the amide-I vibration comes from the stretching vibration of the C=O bond, although relatively small contributions come from both the C-N in-plane stretching and N-H in-plane bending vibrations.

In Davydov's [23, 24] model the amide I vibrations are allowed to interact with the hydrogen bonds that stabilize the α-helical structure. Due to the regular spacing of the peptide groups, amide I vibrations correspond to electric dipole oscillations. The electric dipole oscillations of one peptide group interact with the dipoles of neighboring peptide groups in a resonant manner. Considering only amide I vibrations the energy would dissipate through the system as disordered heat motion. However, due to the amide I vibrations the peptide groups will move from their equilibrium positions causing local deformations in the hydrogen bonds around the area of excitation. These two effects are coupled by a non-linear interaction. The amide I vibrations create local deformations which in turn change the energy of the amide I vibrations due to the change in distance between peptide groups. The result is that the local deformations create a potential well that traps the amide I vibrations preventing its dispersion. Coupled together the amide I vibration and local deformation can travel along an α-helical chain in the form of a stable solitary excitation, or soliton, with no energy loss.

The Hamiltonian for the Davydov model of a one dimensional protein chain coupling the high-frequency amide I vibrations to longitudinal-acoustic phonons was formulated by Davydov in 1982 as [25],

$$\begin{aligned} H = \sum_n E_0 B_n^\dagger B_n - J\sum_n (B_n^\dagger B_{n+1} + B_n^\dagger B_{n-1}) + \sum_n [\frac{p_n^2}{2m} + \frac{1}{2} w(u_n - u_{n-1})^2] + \\ \chi \sum_n (u_{n+1} - u_{n-1}) B_n^\dagger B_n \end{aligned} \tag{2.5}$$

where n denotes the lattice site along the protein chain, $B^\dagger{}_n$ and B_n are the creation and annihilation operators for quanta of the intramolecular vibrations with energy E_0, the u_n and p_n are the molecular displacement and momentum operators, m is the molecular mass, w is the intermolecular force constant, and J is the intersite transfer energy produced by the interaction of dipoles.

References

[1] H. Fröhlich, *Theoretical physics and biology*, in Biological coherence and response to external stimuli, edited by H. Fröhlich, (Springer-Verlag, New York, 1988)

[2] F. W. Cope, *A Review of the applications of solid state physics concepts to biological systems*, Journal of Biological Physics, Vol. 3, No. 1, pp. 1-41, (1975)

[3] J. A. Tuszynski, A. Priel, J. A. Brown, H. F. Cantiello, and J. M. Dixon, *Electronic and Ionic Conductivities of Microtubules and Actin Filaments and Their Consequences for Cell Signaling*, (unpublished), (August 17, 2006)

[4] L. Masgrau, A. Roujeinikova, L. O. Johannissen, P. Hothi, J. Basran, K. E. Ranaghan, A. J. Mulholland, M. J. Sutcliffe, N. S. Scrutton, and D. Leys, *Atomic Description of an Enzyme Reaction Dominated by Proton Tunneling*, Science, Vol. 14, pp. 237-241, (April 2006)

[5] V. I. Prokhorenko, A. M. Nagy, S. A. Waschuk, L. S. Brown, R. R. Birge and R. J. D. Miller, *Coherent Control of Retinal Isomerization in Bacteriorhodopsin*, Science, Vol. 313, pp. 1257-1261, (September 1, 2006)

[6] G. S. Engel, T. R. Calhoun, E. L. Read, T. Ahn, T. Manacal, Y. Cheng, R. E. Blankenship, and G. R. Fleming, *Evidence for wavelike energy transfer through quantum coherence in photosynthetic systems*, Nature, Vol. 446, pp. 782-786, (April 2007)

[7] J. C. Brookes, F. Hartoutsiou, A. P. Horsfield, and A. M. Stoneham, *Could humans recognize odor by phonon assisted tunneling?*, (unpublished), (November 22, 2006)

[8] R. G. Eckenhoff, and J. S Johansson, *Molecular interactions between inhaled anesthetics and proteins*, Pharmacological Reviews, Vol. 49, No. 4, pp. 343-368, (December 1997)

[9] S. R. Hameroff, *The entwined mysteries of anesthesia and consciousness: Is there a common underlying mechanism?*, Anesthesiology, Vol. 105, No. 2, pp. 400-412, (August 2006)

[10] A. Szent-Györgyi, Bioenergetics, (Academic Press, New York, 1957)

[11] A. A. Zaky, R. Hawley, Dielectric Solids, (Dover Publications Inc., New York, 1970)

[12] H. Athenstaedt, *Pyroelectric and piezoelectric properties of vertebrates*, Annals of the New York Academy of Sciences, Vol. 238, No. 1, pp. 68-94, (1974)

[13] L. Margulis, L. To, and D. Chase, *Microtubules in prokaryotes*, Science, Vol. 200, No. 4346, pp. 1118-1124, (June 9, 1978)

[14] V. V. Lemanov, *Piezoelectric and pyroelectric properties of protein amino acids as basic materials of soft state physics*, Ferroelectrics, Vol. 238, pp. 211-218, (2000)

[15] A. Szent-Györgyi, *Study of energy levels in biochemistry*, Nature, Vol. 148, pp. 157-159, (1941)

[16] A. Szent-Györgyi, *Towards a new biochemistry*, Science, Vol. 93, p. 609, (1941)

[17] A. Szent-Györgyi, *Internal photoelectric effect and band spectra in proteins*, Nature, Vol. 157, p. 875, (1946)

[18] W. M. Becker, L. J. Lewis, and J. Hardin, The World of the Cell, 5th Edition, (Pearson Benjamin Cummings, San Fransisco, 2003)

[19] G. Liu, *Presynaptic control of quantal size: kinetic mechanisms and implications for synaptic transmission and plasticity*, Current Opinion in Neurobiology, Vol. 13, pp. 324-331, (2003)

[20] F. Beck, and J. C. Eccles, *Quantum Aspects of Brain Activity and the Role of Consciousness*, Proceedings of the National Academy of Science of the United States of America, Vol. 89, pp. 11357-11361, (1992)

[21] H. Fröhlich, *Bose Condensation of Strongly Excited Longitudinal Electric Modes*, Physics Letters A, Vol. 26, No. 9, pp. 402-403, (1968)

[22] H. Fröhlich, *Long-Range Coherence and Energy Storage in Biological Systems*, International Journal of Quantum Chemistry, Vol. 2, pp. 641-649, (1968)

[23] A. S. Davydov, *The theory of contraction of proteins under their excitation*, Journal of Theoretical Biology, Vol. 38, pp.559-569, (1973)

[24] A. S. Davydov, *Solitons and Energy Transfer Along Protein Molecules*, Journal of Theoretical Biology, Vol. 66, pp. 379-387, (1977)

[25] A. S. Davydov, *Solitons in quasi-one-dimensional molecular structures*, Soviet Physics - Uspekhi, Vol. 25, pp. 898-918, (1982)

[26] M. P. Marder, Condensed Matter Physics, (John Wiley and Sons, Inc., New York, 2000)

[27] P. L. Taylor, and O. Heinonen, A Quantum Approach to Condensed Matter Physics, (Cambridge University Press, New York, 2002)

[28] N. W. Ashcroft, and N. D. Mermin, Solid State Physics (Holt, Reinhart and Winston, New York, 1976)

[29] T. M. Wu, and S. J. Austin, *Bose condensation in biosystems*, Physics Letters A, Vol. 64, No. 1, pp. 151-151, (November 28, 1977)

[30] J. Frenkel, *On the Transformation of Light into Heat in Solids I*, Physical Review, Vol. 37, pp. 17-44, (January 1, 1931)

[31] J. Frenkel, *On the Transformation of Light into Heat in Solids II*, Physical Review, Vol. 37, pp. 1276-1294, (May 15, 1931)

[32] C. B. Harris, and D. A. Zwemer, *Coherent Energy Transfer in Solids*, Annual Review of Physical Chemistry, Vol. 29, pp. 473-495, (1978)

Chapter 3

The Cell Biology of the Neuronal Cytoskeleton [1]

3.1 The Archetypal Neuron and its Components [2]

3.1.1 Structure of the Archetypal Neuron

The cell is the basic unit of structure and function in a living entity. Each cell is composed of a cytoplasm enclosed by a cell membrane. The cytoplasm consists of specialized discrete functioning structures called cell organelles, a solution of water, molecules and ions designated as the cytosol, and a network of filamentous proteins known as the cytoskeleton. The way in which genetic material is housed within the cytoplasm designates the two classes of cells. Eukaryotic cells possess a membrane bound organelle containing genetic material known as the cell nucleus, while prokaryotic cells lack such nuclei. Prokaryotic cells most always form single-celled organisms such as bacteria, while eukaryotic cells form multicellular organisms such as plants and higher animals.

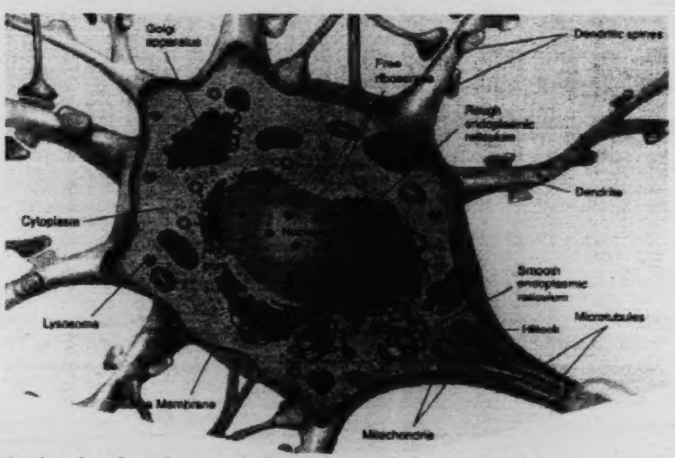
Golgi apparatus
Dendritic spines
Free ribosomes
Rough endoplasmic reticulum
Dendrite
Cytoplasm
Nucleus
Smooth endoplasmic reticulum
Microtubules
Hillock
Lysosome
Membrane
Mitochondria

Figure 3.1: A sketch of a characteristic neuron cell body showing the most prominent cell organelles. Figure obtained from reference [44] in chapter 3

Neurons, or nerve cells, are specialized eukaryotic cells found in the nervous system of higher animals. In vertebrates, neurons are found in the brain, the spinal cord and in the nerves and ganglia of the peripheral nervous system. Their main function is to process and transmit information.

The neuron is composed of a cell body, called a soma, and protrusions, otherwise called neurites, of varying sizes, known as axons and dendrites, which emanate from the cell body. The typical neuronal soma ranges in diameter from 4 to 100 micrometers. Neurons are encased in a double layer of phospholipid molecules known as the plasma membrane. The membrane acts as a barrier segregating the cytoplasm from the extracellular fluid and contains the organelles housed within the soma. Organelles of the neuron, including the cell nucleus, are discussed in greater detail in Section 3.1.2.

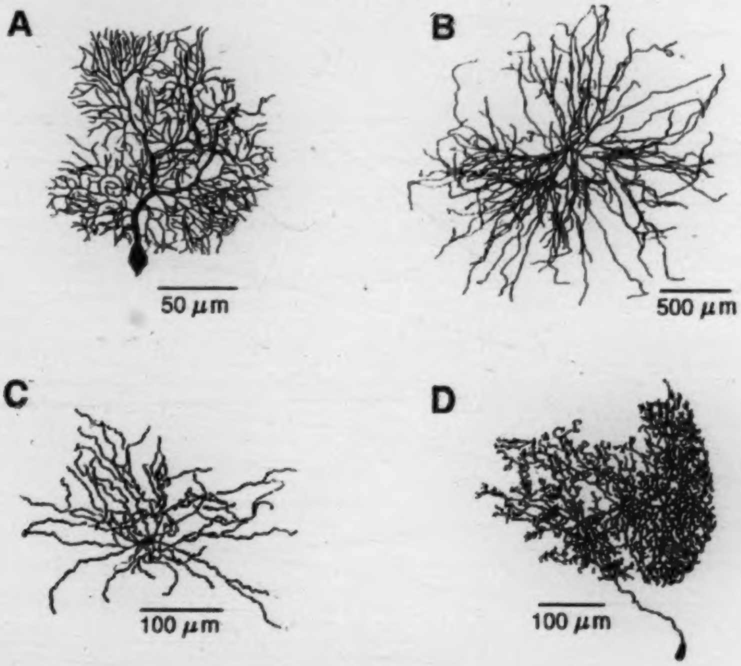

Figure 3.2: Shapes and sizes of various specialized neurons showing the soma, axons and dendrites. (A) Cerebellar Purkinje cell from a guinea pig, (B) Alpha-motorneuron from a cat, (C) Neostriatal spiny neuron from a rat, and (D) Axonless interneuron from a locust. Taken from reference [41] in chapter 3.

Axons are long thin tube-like processes that extend from the soma with distances ranging from micrometers to meters. They originate from the soma at a cone-shaped thickening denoted as the axon hillock, and end in a budding formation called the synaptic terminal. In certain instances the axon branches before it terminates, but this is not always the case.

The synaptic terminal is responsible for forming connections with other nerve cells in order to transmit information. The diameter of the axon remains relatively constant throughout its length. The formation and maintenance of the axon is attributed to the properties of the cytoskeleton found in these structures.

Dendrites are neuronal extensions with a relatively high degree of branching, often giving rise to a dense network known as the dendritic tree. Dendrites are shorter than their axon counterparts. They most often originate from the soma, but in some cases they emerge from the proximal regions of the axon. Small finger-like projections and thickenings from the main shaft of the dendrite have been observed and termed dendritic spines. These spines serve at the synaptic site where information is received from other cells. Like axons dendrites are formed and maintained via the cell's cytoskeleton.

3.1.2 Organelles of the Neuron

Cell organelles are highly specialized structures within a cell analogous to an organ in higher animals, and are responsible for a variety of functions, all of which are required by the cell for normal operation. Approximately half of the volume of a cell is comprised of organelles. Organelles vary across cell type and even within the same organism. They are responsible for capture and synthesis of energy, cell protection, nutrient transport and storage, toxin elimination as well as a host of other functions.

Neurons possess most all of the organelles present in the typical eukaryotic cell. However, due to some of the unique properties of neurons, there exist some minor differences. Neurons possess a cell nucleus, mitochondria, ribosomes, rough and smooth endoplasmic reticulum, Golgi complex, secretory vesicles, and lysosomes (see Figure 3.1).

In neurons, as in all eukaryotic cells, the most prominent organelle is the cell nucleus. The nucleus serves as the repository of the majority of the cell's genetic information, DNA, and acts as the control center for the information's expression. Due to the large amount of energy required for neuronal signaling neurons tend to possess a relatively large density of mitochondria. Mitochondria house the chemical reactions involved in converting cellular fuel or food into the high-energy compound ATP. Ribosomes are present as free-floating particles throughout the cytoplasm, inside mitochondria, and the nucleus, and line the rough endoplasmic reticulum. They are the focal point of protein synthesis within the cell. The rough and smooth endoplasmic reticulum, and the Golgi complex are part of the network of internal membranes of the cell known as the endomembrane system. The rough endoplasmic reticulum is responsible for folding and transporting membrane and secretory proteins, such as ion channels and peptide neurotransmitters, respectively, manufactured by its associated ribosomes, whereas the smooth endoplasmic reticulum synthesizes lipids and steroids for the cell. In neurons the rough endoplasmic reticulum forms in a noticeably dense pattern near the cell nucleus giving rise to a structural feature called the Nissl substance. The Golgi complex performs the role of post-translational processing membrane and secretory proteins, and sorting them within secretory vesicles, the vesicles being small lipid bilayer compartments. Lysosomes store enzymes for the digestion of specific biological macromolecules such as proteins, carbohydrates and fats.

3.1.3 Cytosol of the Neuron

The cytosol is the internal fluid of a cell, and is the region where most of the cells metabolic processes occur. On the molecular level the cytosol is highly organized. The concentrations of soluble molecules in the cell are regulated via osmotic gradients and molecular pumps within the cell membrane. The cytosol is composed mainly of water with the remainder consisting of dissolved ions, such as those involved in regulating the electrical excitability of neurons (e.g. Ca^{2+}, Na^{+}, K^{+}, Cl^{-} etc.), small molecules and large water-soluble proteins required for cell functioning. The proteins within the cytosol are involved in regulating cell metabolism via signal transduction pathways, glycolysis, intracellular receptors and transcription factors.

3.1.4 The Neuronal Cytoskeleton

The cytoskeleton provides the support framework for the cell, and is responsible for maintaining cell shape, providing cell motion, and plays an integral role in intra-cellular transport and cell division. The neuronal cytoskeleton is composed of three main protein filaments: microfilaments, intermediate filaments and microtubules.

In addition to providing structural support microfilaments in neurons are particularly important in the growth of axons. Microfilaments in the growing tip of an axon, known as the growth cone, regulate membrane movement. It is also believed that microfilaments play a vital role in changing the form and shape of dendritic spines.

The intermediate filaments typically found in neurons are neurofilaments and peripherins. Neurofilaments are found in the axons of vertebrate neurons and play a role in regulating axon strength and determining axon size. Peripherins are found in sensory neurons of the peripheral nervous system. The functions of these intermediate filaments in neuron activity are poorly understood at this time.

Microtubules in neurons provide structural support to the neuron and can be found in the soma, axons and dendrites. They maintain axon shape, and transport cellular material along the axon via axonal transport and throughout the rest of the cell. In dendrites and axons microtubule associated proteins (MAPs) specific to neurons alter the dynamics of microtubules. In recent years it has also been proposed that microtubules play a role in information processing and signaling at a sub-neuronal level.

3.2 The Cytoskeleton and its Components [3]

The neuronal cytoskeleton plays a significant role in the activities of the cell. It is responsible for maintaining the shape and form of the cell including the unique formations of the axons and dendrites. It is also responsible for transporting vital cell materials required for cell function and intercellular communication. The sections of this chapter describe in brief the structure and function of each of the three main cytoskeletal components (microfilaments, intermediate filaments and microtubules), and the role played by the associative proteins in the overall workings of the cytoskeleton.

3.2.1 Microfilaments

Microfilaments are double stranded helical polymers of the globular protein actin, and are the smallest of the cytoskeletal components averaging 7-8 nanometers (nm) in diameter and 0.2-17 micrometers (μm) in length. In vitro studies [4] have revealed microfilaments to be dynamic structures. It has been seen that actin monomers are added to one end of a filament while they are released from the opposite end. The rates of addition and release are normally the same resulting in the net length of the filament remaining constant. This unique behavior, called treadmilling, plays an important role in the dynamic movement of the microfilament network

Rarely occurring as isolated strands microfilaments instead prefer to form networks or bundles of interlinked fibers. The gel-like network of microfilaments that forms beneath the plasma membrane is called the cell cortex. The cell cortex, in conjunction with various forms of the motor protein myosin, one of the actin associated proteins, is responsible for moving the cell surface. Such movements result in the formation of lamellipodia and microspikes, flat and narrow projections of the cell, respectively. It is via this same process that neurites grow and extend from the cell body. The microfilament network also forms the contractile ring that separates the cell during cell division, which occurs in most cells, but is uncommon in neurons.

There are a large variety of microfilament-associated proteins that greatly modify the properties of purified actin. Actin-binding associated proteins, such as spectrin and α-actinin, transform microfilaments from a relatively invariant structure into a variety of forms ranging from highly ordered bundles to random gels. Assembly-controlling associated proteins, such as vinculin and gelsolin, modify filament formation by aiding or discouraging actin polymerization, or by severing existing filaments. Membrane-attachment proteins directly or indirectly link actin with cellular membranes, while force-

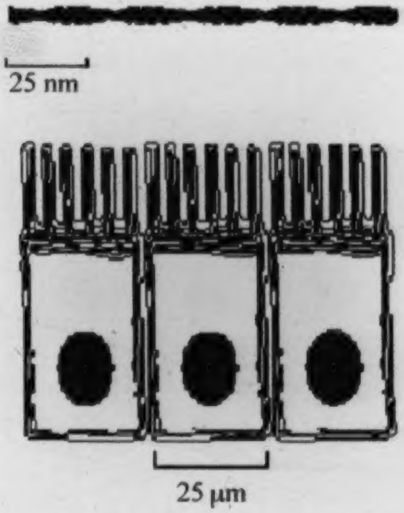

Figure 3.3: Sketch of a microfilament filament showing relative structure, size and orientation within a cell.

producing proteins, such as myosin, are able to generate sliding motility among filaments. At any given time in a cell there are dozens of proteins interacting with actin and determining the state of the cell's microfilaments and thus the cell's structure.

3.2.2 Intermediate Filaments

Intermediate filaments are tubular polymers of highly elongated protein molecules. The constituent protein of an intermediate filament depends on the type of cell in which the filament is formed. There are five types of intermediate filaments due to the diversity of the globular proteins involved in their formation. Type I and II filaments are formed of acidic and basic keratins and are typically found in epithelial cells. Type III filaments are expressed in leukocytes, blood vessel endothelial cells, some epithelial cells, and mesenchymal cells and are formed from four proteins - vimentin, desmin, glial fibrillary acidic protein (GFAP), and peripherin. Neurofilament proteins form Type IV intermediate filaments and are found in the axons of neurons. Type V intermediate filaments are formed of proteins called nuclear lamins and are found strictly in the nuclear membrane of cell nuclei.

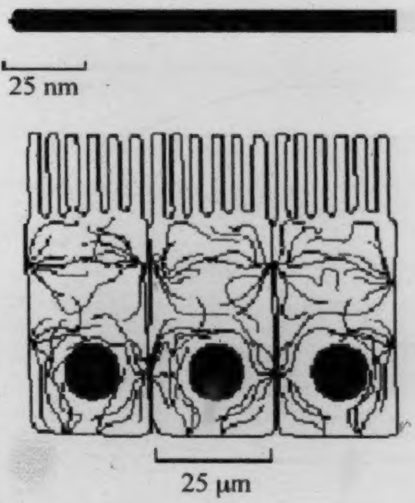

Figure 3.4: Sketch of an arbitrary intermediate filament showing relative structure, size and orientation within a cell.

Intermediate filaments are usually interconnected in a network that covers the entire cytoplasm, surrounding the nucleus and reaching to the cell membrane. Since intermediate filaments are firm inflexible fibers they are able to sustain mechanical stresses and are thus responsible for maintaining cell shape and form. On the inside of the nuclear membrane the filaments form a structure called the nuclear lamina. During cell division the nuclear lamina disassembles only to reassemble after the division takes place. Neurofilaments found in the axons of neurons are responsible for providing the axon with tensile strength and controlling the axonal caliber.

Intermediate Filament Associated Proteins are responsible for cross-linking intermediate filaments into networks and bundles. There is a diverse array of intermediate filament associated proteins that depend on the type of filaments being cross-linked. For example Filaggrin is responsible for linking keratin filaments, plectin joins vimentin fibers, and paranemin and synemin are large polypeptides associated with filaments composed of desmin. There are a host of other proteins that have been isolated and identified as intermediate filament associated proteins, but little is known about their properties and functions at this time.

3.2.3 Microtubules

Microtubules are tubular polymers of the protein tubulin and are the largest of the cytoskeletal components. Tubulin dimers form long fibers called protofilaments that wrap to form a microtubule. In vitro studies have shown microtubules to be dynamic assemblies [5]. Tubulin dimers have been observed to add to one end of a microtubule while they are removed from the opposite end. The rates of addition and removal are not equal or constant therefore resulting in the perpetual growth and shrinkage of a microtubule. This behavior is known as dynamic instability and is discussed further in Section 3.4.1.

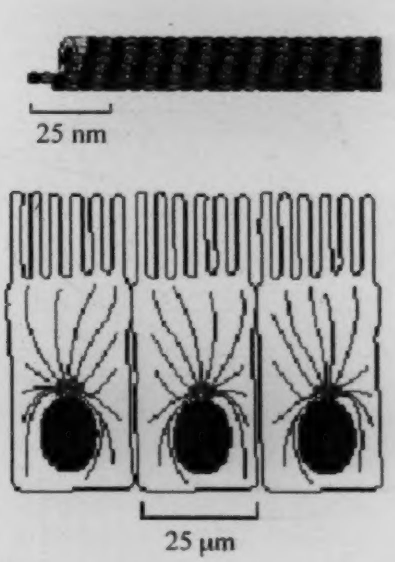

Figure 3.5: Sketch of a microtubule showing relative structure, size and orientation within a cell.

Microtubules cross link among themselves via the connecting microtubule associated proteins. Such connections form tracks along which organelles and other structures are transported around the cell via motor proteins, such as in the transport of neuronal vesicles from the cell body to the synapse in nerve cells. Microtubules are key components of the cell motility structures known as cilia and flagella that extend from the cell surface, and thus play a key role in cell motility. During cell division microtubules are responsible for chromosome separation. Microtubules are discussed in further detail in Sections 3.3 and 3.4.

There is an assortment of proteins that interact with and modulate microtubule structure. These microtubule-associated proteins are separated into two main groups. The first group, known as non-motor microtubule associated proteins, which includes such proteins as tau, regulate the polymer state and control microtubule organization in the cell. Motor microtubule associated proteins, such as kinesin and dynein, make up the second group and are responsible for generating sliding between microtubules and drive the transport of vesicles and organelles throughout the cell. Microtubule associated proteins are discussed in greater detail in Sections 3.3.3 and 3.3.4.

3.3 The Structure of Microtubules and their related proteins [6, 7]

Microtubules are cylindrical macromolecular structures composed of assemblies of the protein tubulin. They are found in the cytoplasm of nearly all eukaryotic cells and are the main component of the cell cytoskeleton. The proteins denoted as microtubule-associated proteins are involved in cross-linking microtubules to one another and to the cellular membrane, and transporting cellular material throughout the cell. The following sections discuss from a molecular view the structure of microtubules and the microtubule subunits tubulin, as well as the structure of the assembly and motor microtubule-associated proteins.

3.3.1 The microtubule subunit Tubulin

The protein tubulin is a globular structural protein that polymerizes to form microtubules. Tubulin is actually a family of similar polypeptides that can be divided into several subgroups (α, β, γ, δ, ε, ζ and η) based upon structure [8, 9]. The α, β and γ subgroups have all been widely studied and implicated in the formation of microtubules. The microtubule structure is composed of α-tubulin and β-tubulin alone while γ-tubulin is involved in structures known as microtubule organizing centers, which are discussed further in Section 3.4.2. The remaining groups have only recently been discovered and their roles in the functioning of the cytoskeleton have yet to be determined.

The basic subunit of a microtubule is a heterodimer composed of α-tubulin and β-tubulin monomers. The α-tubulin and β-tubulin monomers are highly homologous proteins with an average weight of 50-55 kilodaltons (kD) each. Each monomer is composed of approximately 450 amino acids, or about 7000 atoms [10]. Each monomer is composed of a double β-sheet core encircled by α-helices. The monomer structure can be separated into three functional domains. The amino-terminal domain contains the nucleotide-binding region, the intermediate domain contains the binding site for the drugs taxol and colchicine, and the carboxy-terminal domain which has been suggested as the binding region for motor proteins [10]. The average αβ-heterodimer has dimensions of 4 x 8 x 5 nm, or in atomic units 46 x 80 x 65 Angstroms (Å), and is a polar molecule with its positive end near the β subunit [9]. Both of the α-tubulin and β-tubulin monomers can bind a molecule of GTP. The molecule of GTP that binds to α-tubulin does not hydrolyze, while that bound to the β-tubulin will hydrolyze to GDP under certain conditions. Tubulin is known to exist in at least two different conformational states that depend on the hydrolysis of GTP [12]. When the β-tubulin bound GTP hydrolyzes the heterodimer undergoes a conformational change resulting in a 27° angle between the original centre-to-centre line joining the α and β monomers and the new configuration's centre line, and a release of 0.42 electron-volts (eV) per molecule [13]. Henceforth, unless it is otherwise stated, 'tubulin' will be used to refer to the αβ-heterodimer.

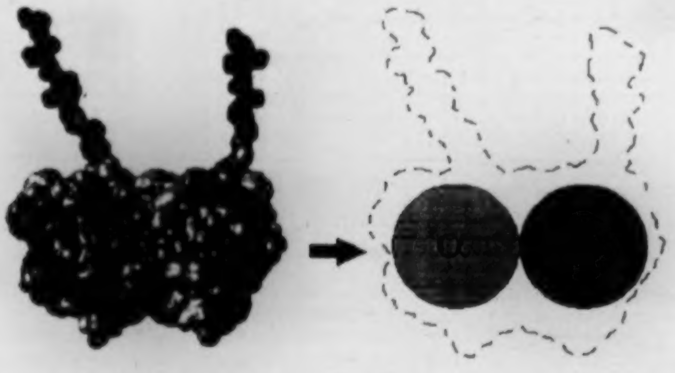

Figure 3.6: The tubulin heterodimer. Left: An electrostatic potential map of the surface of the tubulin dimer showing C-termini tails. Right: A cartoon representation of the tubulin dimer showing positions of α and β tubulin.

The electrical properties of the tubulin dimer are still actively under investigation. Currently most information has been gained from data based on the crystal structure of tubulin. Computer simulations and experimental tests based on data from the crystal structure have yielded an electric dipole moment of 1740 D, a refractive index of 2.90, a high frequency dielectric constant of 8.41 and a high frequency polarizability of $2.1\text{x}10^{-33}$ Coulomb-meters^2/Volts (Cm^2/V) [11]. The values obtained for these properties of tubulin are consistent with predictions made by theory and support the notion of information processing in microtubules. It has also been shown via a map of the electrostatic potential of the crystal structure of tubulin that the interior of a tubulin molecule contains a symmetric double well structure in the hydrophobic region of the protein providing a double well structure for a mobile electron in tubulin [10]. This aspect of the tubulin dimer is discussed in greater detail in Section 5.3.1.

3.3.2 Microtubule structure

Microtubules are hollow cylindrical protein structures comprised of tubulin. The inner and outer dimensions of an average microtubule cylinder are 15 nm and 25 nm, respectively, while there length typically varies from less than 200 nm to several micrometers, or more.

Tubulin monomers bind together end-to-end (i.e. α to β) in string like structures known as protofilaments. Microtubules in human cells typically have 13 protofilaments although structures with 7, 9, 12, or 15 protofilaments have been noted as exceptions. Protofilaments arrange themselves side by side and wrap to form a cylinder. Along protofilaments there is a slight shift such that following a row of monomers across protofilaments would result in spiraling up the microtubule in a left-handed helix.

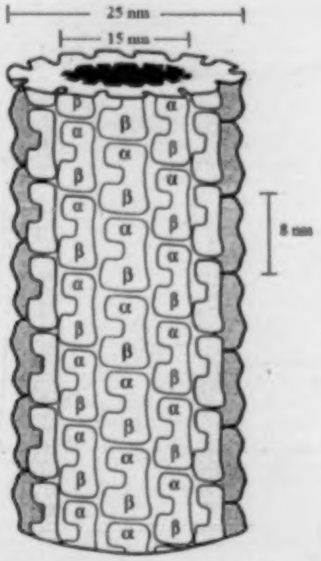

Figure 3.7: Diagram of the microtubule structure giving dimensions and showing the arrangement of α and β tubulin dimers. Figure obtained from reference [10] in chapter 3.

From the monomer point of view microtubules consist of three left handed helices, each individual helix being a 3-start helix. The microtubule can also be viewed in terms of 5-start, 8-start and 13-start helices, but these are not discussed here. The shift in position of the helices as they wrap around to form a microtubule can give rise to two types of lattice structures shown in Figure 3.8. A-lattice structures (MT-13A) consist of helices with alternating monomer types (i.e. α, β, α, β, α etc.). This pattern continues for the entire length of the helix resulting in a microtubule with rotational symmetry and continuous wrapping, and a shift of 3.1 nm between identical monomers on neighboring protofilaments. B-lattice structures (MT-13B) consist of helices with identical monomer types that change after one complete turn (i.e. 13 α monomers, 13 β monomers, 13 α monomers etc.). This pattern results in a shift of 0.9 nm between like monomers on adjacent protofilaments and a physical discontinuity running the length of the microtubule between protofilaments 1 and 13 known as a seam. Experimental evidence strongly suggests that cytoplasmic microtubules possess the B-lattice structure [14].

From the arrangement of the dimers in the A and B lattices four possible nearest-neighbor configurations for left-handed, three-start helical microtubules can be conceived. Assuming protofilaments are arranged in parallel or in anti-parallel orientations it can be seen that individual tubulin dimers can have either six (MT-13A-6, MT-13B-6) or eight (MT-13A-8, MT-13B-8) nearest neighbors. However as it has been shown that in general microtubules possess parallel protofilaments the nearest-neighbor configurations are limited to MT-13A-6 and MT-13B-8 [14].

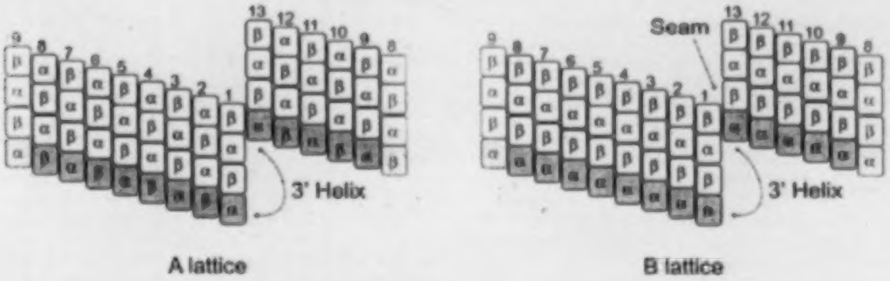

Figure 3.8: Tubulin monomer arrangements in microtubule lattice structures. Left: A-type microtubule lattice. Right: B-type microtubule lattice showing seam. Figure obtained from reference [15] in chapter 3.

3.3.3 Assembly Microtubule Associated Proteins [16]

Assembly microtubule associated proteins are those proteins that have been found to copurify with tubulin through several cycles of microtubule assembly and disassembly, promote microtubule assembly, and bind to microtubules in a relatively constant ratio. The role of these proteins is to control microtubule organization within the cytoplasm of the cell by creating crossbridges and regulating microtubule spacing. The proteins can bind either to individual tubulin dimers, or to tubulin polymerized into microtubules. The assembly proteins are high molecular weight proteins with a molecular mass ranging from 200-420 kD with the exception of the protein tau that possess a mass of 50-70 kD. The main assembly proteins that have been identified and studied at this point in time are termed MAP1A, MAP1B, MAP2, MAP4 and tau

MAP1A is a 350 kD polypeptide found in the dendrites and axons of nerve cells. It has been proposed that MAP1A has a bipolar helical structure and that the protein utilizes charge interactions to bind to microtubules. The protein has been observed to arrange itself along the microtubule wall forming projections of 20 nm length. MAP1A is responsible for inducing tubulin polymerization and controlling spacing between microtubules.

MAP1B, also known as MAP5, is found in nerve dendrites and axons. It is a high molecular weight protein with a molecular mass of 320 kD, and shares a partial sequence homology with MAP1A. It has been observed to induce the elongation of neuronal projections called neurites, and is the major microtubule associated protein in developing embryonic neurons.

MAP2 is one of the two most studied microtubule associated proteins, the other being tau. MAP2 represents a family of protein molecules that differ from one another by a small fraction of amino acids. All the isoforms of the MAP2 family are found in the dendrites of nerve cells. The carboxy-terminal domain of these proteins interacts with tubulin and strongly binds the associated proteins to microtubules. Once bound the result is a projection from the microtubule up to 90 nm long. While the carboxy-terminals of MAP2 proteins bind to microtubules, the amine-terminals bind to other parts of the cytoskeleton or the cell membrane. The mass of MAP2 has been estimated from its mobility on sodium dodecyl sulphate (SDS) gels as 280-300 kD, yet the sequence data gives a value of 199 kD. On SDS gels MAP2 can be resolved into two bands denoted as MAP2A and MAP2B. While the function of MAP2B is unknown at this time, MAP2A has been observed to promote the in vitro polymerization of tubulin [17]. MAP2C is a lower molecular weight version of MAP2, with a mass of 70 kD, and is produced by splicing the MAP2A gene to express a more juvenile form. It is more widely distributed than MAP2A and occurs in the embryonic brain. It is responsible for bundling, and increasing the stability and stiffness of microtubules.

MAP4 is a 200 kD polypeptide that has been observed to interact with microtubules at all stages of the cell cycle. It is not localized to neuronal dendrites and axons but rather is located in various types of eukaryotic cells. It contains a domain homologous to the microtubule-binding domains of MAP2, and interacts with microtubules in the same manner. The wide distribution of MAP4 makes it likely that the protein is involved in several cell functions including inducing polymerization of tubulin, cell motility and cellular transport. Experimental evidence indicates that MAP4 plays an important role as a regulator of microtubule behavior during the start of cell division. Phosphorylation of MAP4 occurs at the beginning of cell division and it is proposed that this may be an important factor in the activity and arrangement of microtubules during cell division.

Tau is a group of proteins localized in the axons of nerve cells. The typical masses range between 37 and 46 kD. Tau is responsible for inducing tubulin polymerization and for linking microtubules into tightly packed arrangements called bundles. Like MAP2 and MAP4, tau possesses a conserved carboxy-terminal microtubule-binding domain and variable amine-terminal domains that project outwards from a microtubule up to 35 nm. Tau has been observed to increase the rate of microtubule polymerization and decrease the rate of depolymerization thus making tau the most effective promoter of microtubule assembly among all the microtubule associated proteins. Experiments in which tau has been introduced into non-neuronal cell lines have resulted in the normally rounded cells expressing single long processes resembling nerve axons [18]. This suggests that neurites grow as a consequence of microtubule polymerization promoted by tau.

3.3.4 Motor Microtubule Associated Proteins [16]

While microtubules provide a system of rigid tracks that facilitate the transport of vesicles and organelles throughout the cell, they do not directly generate the forces required for movement. Motor microtubule associated proteins are proteins which attach to vesicles and organelles and use adenosine triphosphate (ATP) to provide the needed energy for mechanical work to move along microtubule tracks. These motor proteins have been shown to recognize a polarity in microtubules, thus each specific protein exhibits a preferred direction of travel. At present there are two known families of motor microtubule associated proteins: kinesins and dyneins.

Kinesins are a family of proteins with varying structure and function. They are extended molecules with a molecular weight of approximately 200 kD. Most kinesin molecules move toward the plus end of the microtubule, and are therefore responsible for transport from the cell body to the cell periphery. The first kinesins were originally discovered in the axons of giant squids and were characterized by a motor domain region comprised of two globular heads responsible for attaching the protein to microtubules and binding to and hydrolyzing ATP, a coiled helical region acting as a stalk and a light-chain region responsible for attaching to vesicles and organelles. Movement of the protein involves one of the globular heads detaching from the microtubule and moving a distance of approximately 4nm where it reattaches to a new β-tubulin subunit, followed by the other globular head detaching moving and reattaching. This movement is a result of the exchange of ATP and adenosine diphosphate (ADP) at specific sites within the heads. Other members of the kinesin family share a similar motor domain but it is located in different areas in different molecules.

The kinesin molecules have been shown to be responsible for moving and localizing substances within the cell, and they localize to mitotic/meiotic spindles or kinetochores. The dynein family of motor proteins can be segregated into two subgroups: cytoplasmic dynein, and axonemal dynein. Cytoplasmic dynein travels towards the minus end of microtubules making it responsible for transport of cell cargo from the cell membrane to the cell interior. It has a molecular weight of 1.2 MD and consists of two heavy chains that attach the protein to the microtubule, and bind and hydrolyze ATP, three intermediate chains and four light chains. Unlike kinesin, cytoplasmic dynein cannot attach to cell cargo on its own. It is believed that the protein complex dynactin, made up of the actin related protein Arp1 and the protein p150^{Glued} which are thought to be linked by dynamitin, helps link cytoplasmic dynein and cell cargo.

Axonemal dynein is associated with microtubules forming cilia and flagella, and thus is involved in cell motility. It is more complex and larger than cytoplasmic dynein with a molecular weight of 2 MD. It is consists of two to three heavy chains, and approximately ten light chains. The heavy chain heads, as well as the light chain stem each bind to separate microtubules that compose cilia and flagella. The head region hydrolyzes ATP to produce sliding between these axonemal microtubules, which results in the bending of cilia and flagella and thus cell motility.

Jülicher, Adjari, and Prost, based at the Laboratoire de Physico-Chimie Théorique in France, provide a fine review of isothermal ratchet models of motor protein behaviour [30]. Three classes of such models are discussed. The first is a fluctuating force model in which a point-like particle is placed within an asymmetric periodic potential *W(x)* and subjected to a fluctuating force not satisfying the fluctuation-dissipation theorem. The equation of motion for such a particle is given by the Langevin equation,

$$\xi \frac{dx}{dt} = \partial_x W(x) + F(t) \tag{3.1}$$

where ξ is a constant friction coefficient, x is the position of the particle, t is time, W is the potential energy the particle experiences, and F is a fluctuating force that has a zero averaged value but richer correlations than white noise reflecting the energy source, namely the kinetics of ATP binding.

The second class is given by fluctuating potentials. In this case a point-like particle is placed within a time-dependent asymmetric periodic potential $W(x,t)$ yielding,

$$\xi \frac{dx}{dt} = \partial_x W(x,t) + f(t) \tag{3.2}$$

as the equation of motion, where x, t, ξ, and W have the same meaning as above. In this case the energy source is implicit in the time dependence of the potential W. The final term f is a Gaussian white noise term that satisfies the fluctuation-dissipation theorem implying a zero averaged value and correlations defined as,

$$< f(t)f(t') >= 2\xi T\delta(t - t') \tag{3.3}$$

where T is the temperature of the system.

The final class is a generalized model given as a particle fluctuating between states. States are taken to denote local thermodynamic equilibrium of the motor system that is reached on small time scales compared to the exchange rate between states. The equation of motion then depends on the state i such that,

$$\xi_i \frac{dx}{dt} = \partial_x W_i(x,t) + f_i(t) \tag{3.4}$$

where all variables hold the same meaning as previously stated, yet depend on the considered state. In this case the Gaussian noise term f_i still satisfies the fluctuation-dissipation theorem via the time average equaling zero and,

$$< f_i(t)f_j(t') >= 2\xi T\delta(t - t')\delta_{ij} \tag{3.5}$$

When compared to experimental data these models reasonably represent the gross features of the observed motor protein behavior [39].

3.4 The Dynamics of Microtubules [6, 7]

3.4.1 Microtubule assembly/disassembly, polarization and dynamic instability

An in vitro solution containing a sufficient concentration of tubulin dimers, guanosine triphosphate (GTP) and magnesium ions (Mg^{2+}) when warmed to 37°C will begin polymerization of tubulin into microtubules. Initially there exists a lag phase where no microtubules are formed. Tubulin dimers aggregate into clusters of oligomers during this lag phase. These oligomers act as nuclei or nucleation sites from which new microtubules can form. Once a microtubule has been nucleated it begins growth through the addition of subunits at either end. This process is known as elongation, and is relatively fast compared with the lag phase.

Within microtubules all of the tubulin dimers are arranged in the same direction resulting in all of the α-tubulin subunits facing one end of the microtubule, the β-tubulin subunits facing the other. Since the tubulin heterodimer is a polar molecule the microtubule possesses an overall polarity, and thus two chemically different ends. The microtubule end baring more α-monomers is referred to as the minus end, while the end with a majority of exposed β-monomers is the named the plus end.

Microtubules in vitro elongate when tubulin concentration is high and begin depolymerization when tubulin concentration is low. When the concentration of free tubulin dimers in solution reaches a limiting value microtubule elongation stops. This is known as the plateau phase where microtubule assembly is balanced by disassembly. The concentration of free tubulin during the plateau phase is known as the critical concentration. When the concentration of free tubulin is higher than the critical value tubulin assembles into microtubules, and when the free tubulin concentration is lower than the critical value microtubules disassemble into free tubulin.

In vitro both of the microtubule ends can assemble new tubulin units but one end grows more rapidly than the other. The rapid growing end of the microtubule is labeled as the plus end. Since the two ends have different elongation rates the critical concentration of free tubulin is different for each end, the plus end having a lower value. When the concentration of free tubulin is higher than the critical concentration for the plus end, but lower than the critical concentration for the minus end tubulin dimers are assembled at the plus end and disassembled from the minus end. This results in the phenomenon known as treadmilling. Treadmilling has been demonstrated in vitro but it is uncertain whether this property plays any role within the cell. It has been shown that treadmilling of brain microtubules in vitro is suppressed by the microtubule associated protein tau [19].

Dynamic instability is a model of microtubule growth that explains how events of microtubule assembly and disassembly occur simultaneously [23]. The model explains the events in terms of GTP hydrolysis. Tubulin can bind two molecules of GTP, which readily converts to ATP. One of the molecules binds irreversibly to the α-tubulin subunit. The other GTP molecule is bound by the β-tubulin subunit and can be hydrolyzed into guanosine diphosphate (GDP) in much the same way as ATP is converted to ADP. Microtubules that have GTP bound to the plus end tubulins elongate, while disassembling microtubules have GDP molecules bound instead. It is believed that this is due to the fact that GTP bound tubulin molecules have a greater attraction among themselves rather than that between GDP bound tubulins.

A group of GTP-bound tubulin molecules at the plus end of a microtubule forms what is known as a GTP cap. This cap provides a stable microtubule tip upon which new dimers can be added. When concentrations of GTP-bound tubulin are high GTP-bound tubulin is rapidly added to the microtubule creating a large GTP cap and thus a very stable microtubule tip. However, when there is a sufficiently low concentration of GTP-bound tubulin the rate of hydrolysis of GTP on the β-subunit exceeds the rate of addition of new GTP-bound tubulin to the microtubule tip. The loss of the GTP cap results in an unstable microtubule tip that quickly depolymerizes, as the loss of GDP-bound tubulin from the microtubule is favored. The event in which a microtubule switches from growth to depolymerization is known as microtubule catastrophe, a name that implies the rapid rate at which the structure shrinks. Microtubule catastrophe can result in disassembly of the entire microtubule or the microtubule can revert back to a phase of growth depending on the concentration levels of GTP-bound tubulin. This event where the microtubule reverts back to a phase of growth is referred to as microtubule rescue.

David Sept, while at the University of Alberta, provided a simple model of microtubule growth and collapse in his doctoral dissertation [40]. Supposing that the microtubule length is given by x at any given time t, then the addition of a tubulin subunit of length a may be given as,

$$x_{t+1} = x_t + a \tag{3.6}$$

Instants of catastrophe are modeled as a collapse of the microtubule structure to a percentage γ of the original length as represented by,

$$x_{t+1} = \gamma x_t \tag{3.7}$$

Tubulin subunits are added to the microtubule with probability p such that,

$$x_{t+1} = r(x_n + a) + (1 - r)\gamma x_n \tag{3.8}$$

where,

$$\begin{aligned} r &= 0 \quad \mathit{if} \quad s > p \\ &= 1 \quad \mathit{if} \quad s \le p \end{aligned} \tag{3.9}$$

and s is a random number between 0 and 1. While this model cannot predict individual collapse events, due to its random nature, it does give the basic dynamics of microtubule assembly and dynamic instability.

3.4.2 Microtubule Organizing Centers

Within the majority of cells microtubules originate from organelles called microtubule-organizing centers (MTOC). These specialized structures consist of an array of microtubules that anchor newly forming microtubules thus allowing microtubule assembly to initiate. The two most common MTOCs in animal cells are known as centrosomes and basal bodies. A centrosome is usually positioned near the cell nucleus and is composed of two perpendicular cylindrical structures formed by nine pairs of triplet microtubules called centrioles which are surrounded by a scattered granular material called the pericentriolar material, thus the microtubules of most common cells radiate out from the centrosome forming an aster around the cell's nucleus as in Figure 3.5. Basal bodies are structurally similar to centrioles and are responsible for anchoring cilia and flagella. Microtubules originate from the pericentriolar material through the use of large ring shaped protein complexes composed of γ-tubulin that have been observed in the centrosome [20]. These γ-tubulin ring complexes serve as nucleation sites for the assembly of new microtubules [21]. The γ-tubulin ring complex acts as a cap for the minus end of the microtubule stabilizing the minus end of the microtubule and anchoring it to the MTOC. The plus end of the microtubule extends out into the cell forming a microtubule tip that continuously grows away from the organizing center.

Neurons, unlike the common cell, possess a highly organized arrangement of microtubules (see Figure 3.9). This is due to a high number of specialized non-motor MAPs within nerve cells. Four of the five main assembly MAPs identified and studied at this point in time (MAP1A, MAP1B, MAP2, MAP4 and tau) are localized within the axons and dendrites of neurons, MAP4 being the only protein found in other eukaryotic cell types. The specialized assembly MAPs in neurons link neuronal microtubules into organized networks. Unlike the radial aster that forms in other eukaryotic cells, microtubules within axons and dendrites form parallel bundles. Within the axons of neurons microtubules align with uniform polarity resulting in the plus end of all axonal microtubules being directed distally, while it has been found that microtubules in dendrites align themselves equally with both plus and minus ends directed distally. It has been suggested that the different microtubule organizations within axons and dendrites may play a role in neuronal signaling.

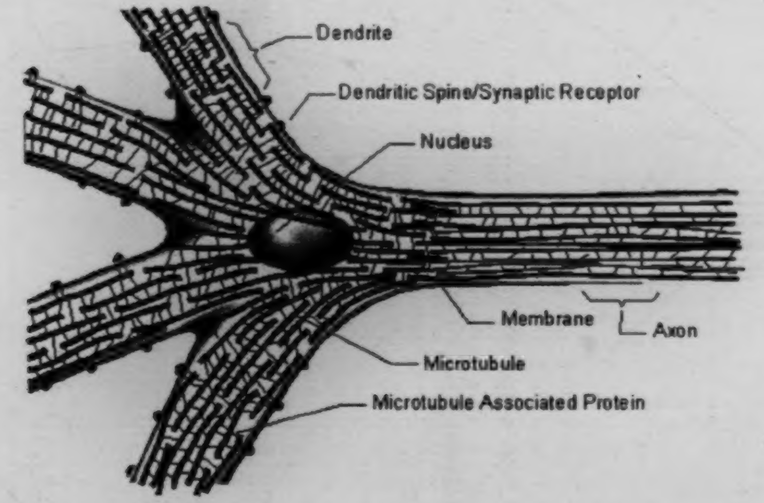
Dendrite
Dendritic Spine/Synaptic Receptor
Nucleus
Membrane
Axon
Microtubule
Microtubule Associated Protein

Figure 3.9: Schematic representation of a neuron showing the arrangement of microtubules and microtubule associated proteins. Figure obtained from reference [42] in chapter 3.

While current biophysical explanations for the organization of microtubules within cells focuses on their electromagnetic properties no coherent explanation is yet available. Other factors acting on the cell, such as gravity, have been suggested to play a role in microtubule organization. As such it should be noted that experiment has shown that microtubules assembled in microgravity conditions possessed no self-organization and were disordered locally, thus suggesting a dependence between microtubule organization and gravity [22].

3.4.3 Cell Division

The cell division cycle is the process by which cells reproduce. In general cell division does not occur in neurons but is a significant process in the lifetime of most other eukaryotic cells. The cell division cycle is separated into two main phases: interphase, a long period phase in which the cell prepares for division by producing organelles, proteins and duplicating proteins, including DNA, and the mitotic phase, a relatively short period phase in which the cell divides. Microtubules play an integral role in the mitotic phase, the process by which the parent cell is divided into two equivalent daughter cells.

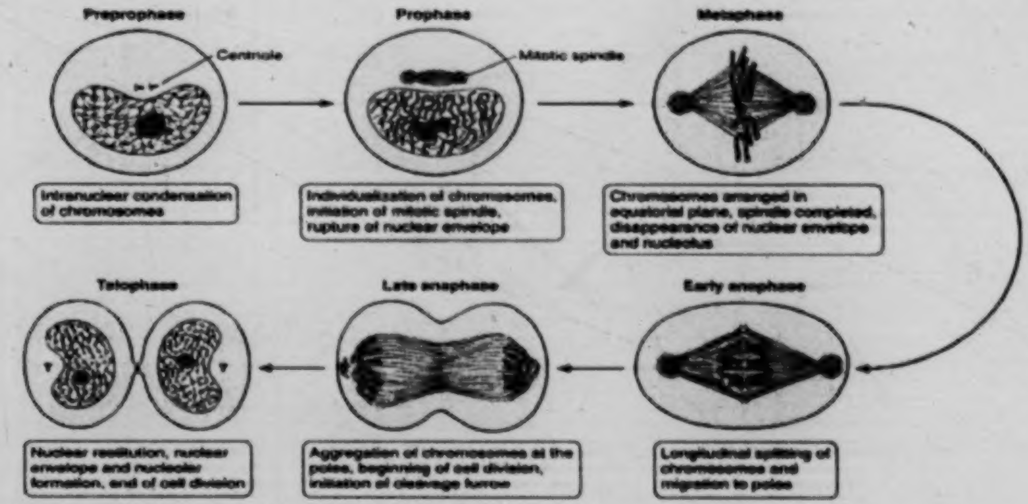
Preprophase
Centriole
Prophase
Mitotic spindle
Metaphase
Intranuclear condensation of chromosomes
Individualization of chromosomes, initiation of mitotic spindle, rupture of nuclear envelope
Chromosomes arranged in equatorial plane, spindle completed, disappearance of nuclear envelope and nucleolus
Telophase
Late anaphase
Early anaphase
Nuclear restitution, nuclear envelope and nucleolar formation, end of cell division
Aggregation of chromosomes at the poles, beginning of cell division, initiation of cleavage furrow
Longitudinal splitting of chromosomes and migration to poles

Figure 3.10: Mitosis, phases of the cell division cycle. Figure obtained from reference [43] in chapter 3.

The mitotic phase involves the process of mitosis, which is separated into five sub-phases (prophase, prometaphase, metaphase, anaphase, and telophase) followed by cytokinesis. In prophase two centrosomes outside the cell nucleus sprout microtubules, through the polymerization of free tubulin, which cause the centrosomes to move to opposite ends of the cell via repulsive interactions between the microtubules. The network of microtubules is the beginning of the formation of the mitotic spindle. In prometaphase, a phase commonly included as part of prophase, the nuclear envelope surrounding the cells DNA, in the form of chromosomes made up of two sister chromatids, dissolves and microtubules from the mitotic spindle invade the nuclear space. Microtubules that attach themselves to kinetochore structures on chromosomes are known as kinetochore microtubules, whereas those microtubules that interact with microtubules from the opposite mitotic spindle are referred to as nonkinetochore microtubules. When a microtubule connects with a kinetochore an unknown molecular motor activates and uses energy in the form of ATP to move up the microtubule toward the originating centrosome. During metaphase the center of the chromosomes convenes along an imaginary line that is equidistant from the two centrosome-poles via counterbalancing forces generated by the opposing movement of the kinetochores. The process of anaphase consists of the separation of the chromosome into two sister chromatids that are pulled apart by the shortening of kinetochore microtubules that move towards their respective centrosomes. The nonkinetochore microtubules then elongate to push the centrosomes, and chromatids to opposite ends of the cell.

At telophase the nonkinetochore microtubules continue to lengthen and elongate the cell and a new nuclear envelope forms around each set of genetic material thus ending the process of mitosis. Cytokinesis in animal cells involves microfilaments and myosin forming a contractile ring that is responsible for constricting the cell membrane creating a cleavage furrow and eventually pinching the cell into two daughter cells. As this occurs nonkinetochore microtubules reorganize and disappear into a new cytoskeleton as the cell cycle returns to interphase.

The process of meiosis where parent cells divide into four daughter cells with different genetic material is related to the process of mitosis. In meiosis, microtubules function in the same manner as in mitosis. Therefore, the specifics of microtubule dynamics in meiosis will not be discussed in detail here.

3.5 Examining the Conduction Properties of Microtubules

The electric properties of biomolecules and biomolecular structures, such as tubulin and microtubules, are of importance to a biophysical understanding of cellular processes. Microtubule electric properties may involve both intrinsic effects of the protein and ionic contributions from counter-ions attracted and concentrated near the microtubule by its electric field. Vassilev et al. observed aligned microtubules assembled *in vitro* with pulsed electric fields on the order of 10 V/cm in strength [36]. Kirson et al. [37] have demonstrated that 100–300 kHz AC electric fields at ~2 V/cm used over 24 hours can have pronounced mitotic effects in several cancerous cells lines.

In addition, nanotechnological uses of biomolecules are of interest and the microtubule is a candidate for use in nanoscale devices. Unfortunately, making conductance measurements on biopolymers is difficult due to the structural variety of polymers, the liquid state of samples and the dependence of biological systems on environmental factors such as pH, temperature and ion concentration. However recent advances in nanoscale technologies are improving experimental conditions allowing for serious investigations to take place. Thus, despite the inherent difficulties, a number of experiments have investigated either the intrinsic [24, 26, 27, 31] or ionic [26, 34] conductivities of microtubules. Comparisons of the different conductivity and resistivity measurements are provided later in this section.

In the work by Minoura and Muto an attempt was made to measure the conductivity and dielectric constant of microtubules using an electroorientation method [28]. While microtubules exhibit Brownian motion in the absence of an electric field, in fields with frequencies below 10 kHz they flow due to ionic convection. To avoid convection, a frequency of 1 MHz with a field strength sufficient to orient microtubules was used. The Minoura and Muto orientation occurs for field strengths above 50 kV/m and frequencies in the range 10 kHz–5 MHz, overlapping with the Kirson et al. range. For example, a 90 kV/m field at 1 MHz aligns microtubules in a few seconds. This orientation by AC fields depends on an induced dipole moment and not the permanent dipole moment of tubulin.

This work by Minoura and Muto is of special significance especially in regards to the manipulation of microtubules for use in nanoscale technologies. However, while this work is of great interest, there are some questions concerning the model, experimental procedures, and results that should be addressed. In the described experiment, the electric field was applied via 1500 Å thick electrodes separated by 100 µm on the surface of a glass slide. To account for viscous effects, and to avoid edge/wall effects, a region 15 µm above the slide and more than 30 µm from both electrodes was observed. Minoura and Muto do not discuss how the electric field is obtained, or if the field can be considered uniform in this region. The 15 µm-distance from the surface is about 100 times the electrode thickness. It is expected that if this analysis site were between electrodes thick in comparison to the site, then a uniform field would exist in the experiment volume. However, the electrodes described by Minoura and Muto are relatively thin, and significantly out of the relevant plane, thus it is questionable how the field strength is known, whether it is uniform, and whether field gradient effects on microtubule electroorientation merit further investigation?

Minoura and Muto analyzed microtubule electroorientation with a dielectric ellipsoid model. In the model a torque from rotation in the viscous medium counters the torque of the electric field on the microtubule. The viscous counter-torque, T_v, experienced by the ellipsoid calculated by Minoura and Muto is $4.97 \times 10^{-19}\, d\theta/dt$, where $d\theta/dt$ is the rotational velocity. Yet it is unclear why the microtubule is modeled as an ellipsoid rather than as a cylinder, the usual geometry for a microtubule model. Even considering the counter-ion layer, microtubule geometry is cylindrical rather than ellipsoidal. By taking several parameters from Minoura and Muto [28], including the 10^{-3} Pa s viscosity value η, the ellipsoid radius r, being the sum of the microtubule radius (12.5 nm) and the Debye length in the buffer (9.1 nm), and an average microtubule length l of 14 ± 0.4 µm as described in the microtubule polymerization technique used by Minoura and Muto [35], the viscous torque T_v was recalculated via,

$$T_v = \frac{4\pi\eta l}{\ln(\frac{l}{2r}) - 0.66}\frac{d\theta}{dt} \tag{3.10}$$

as obtained from [38]. A value of $T_v = 5.07 \times 10^{-19}\, d\theta/dt$ was yielded, giving a trivial change of about 2 %.

Minoura and Muto present a quantitative analysis of microtubule electroorientation as shown in Figure 3.11. Selections of the experimental data are presented as representative of the analysis. Figure 3.11 shows the electroorientation time constant, τ, as a function of microtubule length, l. It is stated by Minoura and Muto that when τ was calculated, it appears to be proportional to l^2, as illustrated by the best-fit line in Figure 3.11, $\tau = 4.1 \times 10^9\, l^{2.0}$. This is taken to show consistency with the model given a homogenous dielectric along the microtubule length. Taking the data points from this figure and using ordinary least-square fitting with equal weight for all points, and residuals in τ, the curve fitting was repeated for the relation between τ and l to estimate uncertainties for the coefficients. When a first direct fit failed, with numeric convergence problems in the routine, the log transformed relation, $\ln \tau = c_1 + c_2 \ln l$, was used instead to obtain a time constant value of $\tau = 10^{(9\pm1)} \times l^{(1.9\pm0.2)}$. Then, with an alternative routine a direct fit of the data yielded a value of $\tau = (4\pm10) \times 10^7\ l^{(1.6\pm0.2)}$.

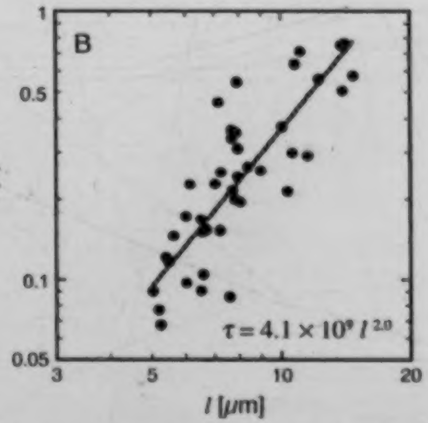

Figure 3.11: Electroorientation time constant versus average microtubule length for the Minoura and Muto microtubule electrooreintation experiment. Figure obtained from reference [28] in chapter 3.

In general, it seems that the multiplicative prefactor can vary over several orders of magnitude, with changes in the exponential coefficient compensating to produce nearly equally good fits to the data. Alternatively, to account for the inconsistency in the power of l, τ was constrained to be proportional to l^2. A first regression then yielded a time constant $\tau = (3.1 \pm 0.4) \times 10^9\ l^2 + (0.06\pm0.03)$. Again, the multiplicative coefficient was inconsistent, differing by 76 % with the Minoura and Muto result [28], and yielding an intercept comparable with the lower range τ values. When the intercept was constrained to zero, the regression gave $\tau = (3.6 \pm 0.2) \times 10^9\ l^2$, still inconsistent, at only 88 % of the Minoura and Muto value. The coefficient is very important since the relation between it and the electric field is used to determine the microtubule effective polarization and thus the microtubule conductivity and dielectric constant. It can be seen that this last fit is the most consistent with Minoura and Muto. However, when τ is constrained to be proportional to l^2, a non-negligible intercept is found suggesting that the time constants are affected by factors not in the experimental model. Minoura and Muto conclude that the effective polarization coefficient is reliably obtained, however the above analysis questions these findings.

Minoura and Muto also present a least-squares fit of the effective polarization coefficient normalized by microtubule length as a function of the field frequency (see Figure 3.12). Comparing the data in Figure 2.12 part A to those in parts B and C reveals a data point, at 10 kHz and high polarization, omitted after the first graph. Minoura and Muto note a large deviation in the data for this point, but there is no mention of omitting it from the fits. Again, taking data points from the published figure, a least-square fits with equal weight for all points was performed. A microtubule conductivity estimate of (150 ± 6) mS/m was obtained when the point was omitted, and (157 ± 7) mS/m when it was included. While this difference is small, even negligible, as it falls within the error range given by Minoura and Muto [28], the evidence favors the point being omitted. The question of whether this is the case and what the impact is on the accuracy of the results, still remains.

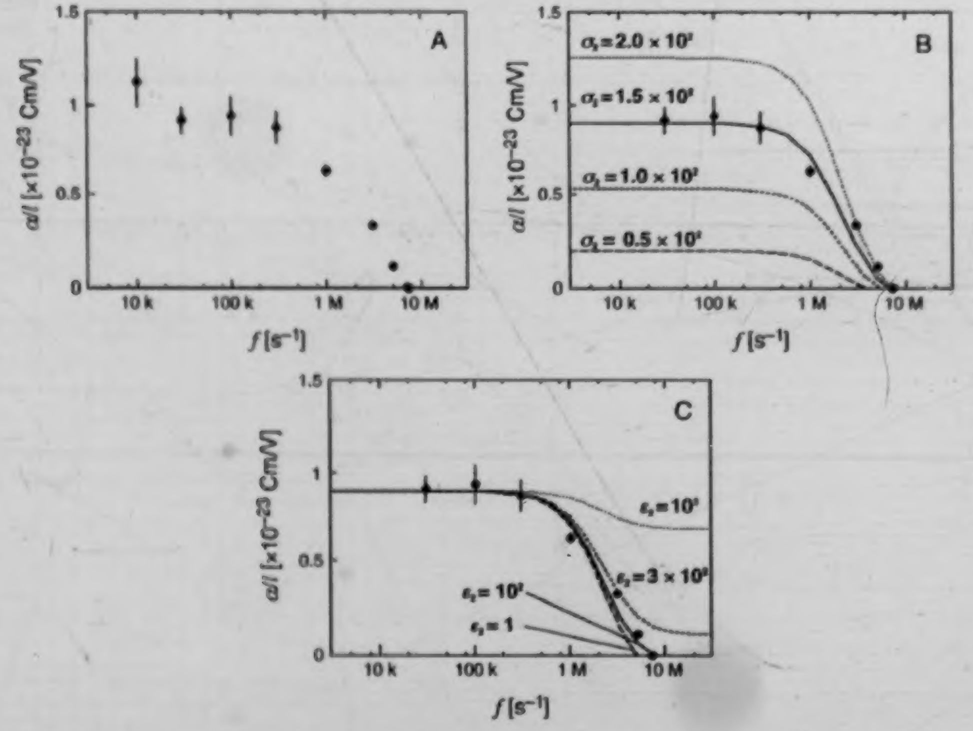

Figure 3.12: Normalized microtubule polarization coefficient versus frequency results for Minoura and Muto microtubule electrorientation experiment. Figure obtained from reference [28] in chapter 3.

The overall picture of an induced dipole moment arising due to the polarizability of the microtubule-counterion system is consistent with another study of ionic conductivity along electrically stimulated microtubules [34]. Isolated taxol-stabilized microtubules were shown to conduct an electric pulse applied through a micropipette. Input signals were of 5–10 ms duration with amplitudes in the range ±200 mV. The current fraction collected with a second micropipette at the other end of the microtubule was 70 % greater than the control current fraction between the same pipettes with no microtubule between them. Hence, the reported data indicates a higher conduction along microtubules than in the buffer.

Finally, Minoura and Muto demonstrate that using the polarization coefficient as a function of the electric field frequency, it is virtually impossible to determine tubulin's dielectric constant as values between 1 and 100 fit the data almost equally well. However, a paper by Sanabria et al. [29] used impedance spectroscopy to measure the dielectric constant of tubulin as $\varepsilon = 8.41$, falling in the Minoura and Muto range. Assuming a microtubule cross-sectional area of 2.5×10^{-16} m^2 the Minoura and Muto conductivity of 150 mS/m corresponds to a resistance of 27 GΩ/µm along the microtubule length. Other measurements of this property for microtubules can be found in the literature. Fritzsche et al. [24] made electrical contacts to single dry microtubules on a substrate containing gold microelectrodes. Their published description suggests the intrinsic resistance of dry microtubules is much greater than the 40 MΩ/µm resistance of their wires. This same group measured microtubules with a 30-nm thick nickel coating [31]. The resistance was found to be orders of magnitude lower and conduction was entirely due to the metallic coating.

Further, Goddard and Whittier [27] reported measurements of samples containing only buffer, tubulin dimers in buffer, microtubules in buffer, and microtubules with MAPs in buffer. Tubulin concentrations were 5 mg/mL with 0.3 mg/mL of MAP2 and tau protein in the last case. The average resistances reported were 999 Ω (buffer), 424 Ω (tubulin), 883 Ω (microtubules) and 836 Ω (microtubules + MAPs). It is not straightforward to translate these results into properties of individual microtubules without assumptions about their geometric arrangements and connectivities. However, by assuming that all tubulin is polymerized in the microtubule cases and that there are uniform microtubule distributions with combinations of parallel and series networks of 10 µm long microtubules, a longitudinal microtubule resistance of 0.8 MΩ/µm was estimated [25]. This compares favorably to an early theoretical estimate, based on a Hubbard model with electrons hopping between tubulin monomers [32, 33]. This model predicts microtubule resistances to be 0.2 MΩ/µm, within the same order of magnitude as the Goddard and Whittier based result, but two orders of magnitude smaller than dry microtubules, which is to be expected. On the other hand, their conductivity value for microtubules is two orders of magnitude smaller than that of the ionic solution surrounding the microtubule as used by Minoura and Muto [28]. Again, this comparison is not unexpected. Recently, Umnov et al. [26] attempted direct measurement of microtubule conductivity. They determined a 90 S/m upper bound on the conductivity of a microtubule, corresponding to a minimum 240 MΩ for a 10 µm MT (24 MΩ/µm), close to the Fritsche et al. result [31]. Minoura and Muto demonstrated that a microtubule's electrical conduction is dependent on its surroundings, providing an experimental conductivity and not just a bound.

These results are seemingly vague leaving direct experimental values of microtubule conductivity in question. While much of this experimental evidence concerning the conductivities of microtubules is still quite scattered and inconclusive, it does provide a broad basis for theoretical models. The conduction properties of microtubules seem to indicate the capability for electrical signal transduction and information processing, but the question remains of how do the delicate, weak, very small scale quantum processes of electron movements within microtubules influence brain cell firing and communication? The following chapter looks at theoretical ideas advanced to explain how microtubules can process information and be implicated in brain functioning.

References

[1] I. B. Levitan, and L. K. Kaczmarek, The Neuron: Cell and Molecular Biology, 3rd Edition, (Oxford University Press, New York, 2002)

[2] W. M. Becker, L. J. Lewis, and J. Hardin, The World of the Cell, 5th Edition, (Pearson Benjamin Cummings, San Fransisco, 2003)

[3] L. A. Amos, and W. B. Amos, Molecules of the Cytoskeleton, (MacMillan Education, Houndmills, Basingstoke, Hampshire, 1991)

[4] Y. Chen, J. Bourne, V. Pieribone, and R. M. Fitzsimonds, *The role of actin in the regulation of dendritic spine morphology and bidirectional synaptic plasticity*, Neuroreport, Vol. 15, No. 5, pp. 829-832, (April 9, 2004)

[5] J. A. Tuszynski, and M. Kurzynski, Introduction to Molecular Biophysics, (CRC Press, Florida, 2003)

[6] P. Dustin, Microtubules, (Springer-Verlag, New York, 1978)

[7] K. Roberts, and J. S. Hyams, Microtubules, (Academic Press, New York, 1979)

[8] R. G. Burns, *Identification of two new members of the tubulin family*, Cell Motility and the Cytoskeleton, Vol. 31, pp. 255-8, (1995)

[9] P. G. McKean, S. Vaughan and K. Gull, *The extended tubulin superfamily*, Journal of Cell Science, Vol. 114, p. 2723, (2001)

[10] J. A. Tuszynski, J. A. Brown, E. Crawford, E. J. Carpenter, M. L. A. Nip, J. M. Dixon, and M. V. Sataric, *Molecular dynamics simulations of tubulin structure and calculations of electrostatic properties of microtubules*, Mathematical and computer modeling, Vol. 41, No. 10, pp. 1055-1070, (May 2005)

[11] A. Mershin, H. Sanabria, J. H. Miller, D. Nawarathna, E. M. C. Skoulakis, N. E. Mavromatos, A. A. Kolomenski, H. A. Schuessler, R. F. Luduena, and D. V. Nanopoulos, *Towards Experimental Tests of Quantum Effects in Cytoskeletal Proteins*, in The Emerging Physics of Consciousness, edited by J. A. Tuszynski, (Springer-Verlag, New York, 2006)

[12] W. D. Howard, and S. N. Timasheff, *GDP state of tubulin: stabilization of double rings*, Biochemistry, Vol. 25, No. 25, pp. 8292-8300, (1986)

[13] R. Melki, M. F. Carlier, D. Pantaloni, and S. N. Timasheff, *Cold depolymerization of microtubules to double rings: Geometric Stabilization of Assemblies*, Biochemistry, Vol. 28, No. 23, pp. 9143-9152, (November 14, 1989)

[14] E. Nogales, M. Whittaker, R. A. Milligan, and K. H. Downing, *High resolution model of the microtubule*, Cell, Vol. 96, pp. 79-88, (1999)

[15] D. Sept, N. A. Baker, and J. A. McCammon, *Physical basis of microtubule structure and stability*, Protein Science, Vol. 12, pp. 2257-2261, (2003)

[16] E. Mandelkow, and E. Mandelkow, *Microtubules and microtubule-associated proteins*, Current Opinion in Cell Biology, Vol. 7, pp. 72-81, (1995)

[17] R. J. Kowalski, *Microtubule -associated protein 2 alters dynamic properties of microtubule assembly and disassembly*, The Journal of Biological Chemistry, Vol. 268, pp. 9847-9855, (May 5 1993)

[18] P. W. Baas, T. P. Pienkowski, and K. S. Kosik, *Processes induced by tau expression in Sf9 cells have an axon-like microtubule organization*, The Journal of Cell Biology, Vol. 115, No. 5, pp. 1333-1344, (December 1991)

[19] D. Panda, H. P. Miller, and L. Wilson, *Rapid treadmilling of brain microtubules free of microtubule associated proteins in vitro and its suppression by tau*, Proceedings of the National Academy of Science USA, Vol. 96, No. 22, pp. 12459-12464, (October 26, 1999)

[20] M. Moritz, M. B. Braunfeld, J. W. Sedat, B. Alberts, and D. A. Agard, *Microtubule nucleation by γ-tubulin-containing rings in the centrosome*, Nature, Vol. 378, pp. 638-640, (December 7, 1995)

[21] Y. Zheng, M. L. Wong, B. Alberts, and T. Mitchison, *Nucleation of microtubule assembly by a γ-tubulin-containing ring complex*, Nature, Vol. 378, pp. 578-583, (December 7, 1995)

[22] C. Papaseit, N. Pochon, and J. Tabony, *Microtuuble self-organization is gravity dependent*, Proceedings of the National Academy of Science USA, Vol. 97, No. 15, pp. 8364-8368, (July 18, 2000)

[23] T. J. Mitchison, and M. W. Kirschner, *Dynamic instability of microtubule growth*, Nature, Vol. 312, pp. 237-242, (1984)

[24] W. Fritsche, K. Bohm, E. Unger, and J. M. Kohlet, *Making electrical contact to single molecules*, Nanotechnology, Vol. 9, No. 3, pp.177-183, (September 1998)

[25] J. A. Tuszynski, A. Priel, J. A. Brown, H. F. Cantiello, and J. M. Dixon, *Electronic and Ionic Conductivities of Microtubules and Actin Filaments Their Consequences for Cell Signaling and Applications to Bioelectronics*, in Nano and Microscience, Engineering, Technology and Medicine, Vol. 9, Nano and Molecular Electronics Handbook, edited by E. Lyshevski, (CRC Press, London, 2007)

[26] M. Umnov, O. A. Palusinski, P. A. Deymier, R. Guzman, J. Hoying, H. Barnaby, Y. Yang, and S. Raghavan, *Experimental evaluation of electrical conductivity of microtubules*, Journal of Material Science, Vol. 42, pp. 373-378, (2007)

[27] G. Goddard, and J. E. Whittier, *Biomolecules as nanomaerials: interface characterization for sensor development*, Proceedings of SPIE, Vol. 6172, Smart Structures and Materials 2006: Smart Electronics, MEMS, BioMEMS, and Nanotechnology, edited by V. K. Varadan, (March 2006)

[28] I. Minoura, and E. Muto, *Dielectric measurement of individual microtubules using the electroorientation method*, Biophyiscal Journal, Vol. 90, pp. 3739-3748, (2006)

[29] H. Sanabria, J. H. Miller Jr., A. Mershin, R. F. Luduena, A. A. Kolomenski, H. A. Schuessler, and D. V. Nanopoulos, *Impedance Spectroscopy of α–β Tubulin Heterodimer Suspensions*, Biophysical Journal, Vol. 90, pp. 4644-4650, (2006)

[30] F. Jülicher, A. Ajdari, and J. Prost, *Modeling molecular motors*, Reviews of Modern Physics, Vol. 69, No. 4, pp. 1269-1282, (October 1997)

[31] W. Fritzsche, J. M. Köhler, K. J. Böhm, E. Unger, T. Wagner, R. Kirsch, M. Mertig, and W. Pompe, *Wiring of metallized microtubules by electron beam-induced structuring*, Nanotechnology Vol. 10, pp. 331–335, (1999)

[32] J. A. Tuszynski, J. A. Brown, and P. Hawrylak, *Dielectric polarization, electrical conduction, information processing and quantum computation in microtubules. Are they plausible?*, Philosophical Transactions of the Royal Society of London A, Vol. 356, pp. 1897–1926, (1998)

[33] J. A. Brown, A study of the interactions between electromagnetic fields and microtubules: ferroelectric effects, signal transduction and electronic conduction, (PhD. Thesis), (University of Alberta, Edmonton, 1999)

[34] A. Priel, A. J. Ramos, J. A. Tuszynski, and H. F. Cantiello. *A biopolymer transistor: electrical amplification by microtubules*, Biophysical Journal Vol. 90, pp. 4639–4643, (2006)

[35] D. Kristofferson, T. Mitchison, and M. Kirschner, *Direct observation of steady-state microtubule dynamics*, Journal of Cell Biology, Vol. 102, pp. 1007-1019, (1986)

[36] P. M. Vassilev, R. T. Dronzine, M. P. Vassileva, and G. A. Georgiev. *Parallel arrays of microtubules in electric and magnetic fields*, Bioscience Reports, Vol. 2, pp. 1025–1029, (1982)

[37] E. D. Kirson, Z. Gurvich, R. Schneiderman, E. Dekel, A. Itzhaki, Y. Wasserman, R. Schatzberger, and Y. Palti, *Disruption of cancer cell replication by alternating electric fields*, Cancer Research, Vol. 64, pp. 3288–3295, (2004)

[38] J. Howard, Mechanics of motor proteins and the cytoskeleton, (Sinauer Associates, Inc., Sunderland, Massachusetts, 2001), Table 6.2

[39] K. Svoboda, and S. M. Block, *Force and velocity measurements for single kinesin molecules*, Cell, Vol. 77, No. 5, pp. 773-784, (1994)

[40] D. Sept, Models of Assembly and Disassembly of Individual Microtubules and their Ensembles, (PhD. Thesis), (University of Alberta, Edmonton, 1997)

[41] I. Segev, *Cable and Compartmental Models of Dendritic Trees*, in The Book of GENESIS: Exploring Realistic Neural Models with the General Neural Simulation System, Second edition, edited by J. Bower, and D. Beeman, (Springer-Verlag, New York, 1998)

[42] S. Hameroff, and R. Penrose, *Conscious Events As Orchestrated Space-Time Selections*, Journal of Consciousness Studies, Vol. 3, No. 1, pp. 36-53, (1996)

[43] L. C. Junqueira, and J. Carneiro, Basic Histology: text and atlas, 11th Edition, (McGraw Hill, New York, 2005), Figure 3.15

[44] N. R. Carlson, Physiology of Behavior, 8th Edition, (Pearson Education, New York, 2004), Figure 2.5

Chapter 4

Information Processing in Microtubules

4.1 An overview of Cellular Automata [1]

4.1.1 History and Background

To understand the natural world, computer simulations have been used to model complex physical phenomena. Realistic detailed models, however, often result in large non-linear systems that are difficult and time consuming to investigate numerically. Complex biological systems commonly follow this trend [2]. One solution to this problem is to model biological systems via cellular automata.

Cellular automata (singular: cellular automaton) are computer models that try to algorithmically simulate natural laws. Specifically, a cellular automaton is a lattice of identically programmed cells that are assigned particular states, which then change stepwise over time according to the states of the surrounding cells and specific rules that determine the system's evolution in time. This updating can occur either synchronously, with all cells updated simultaneously, or asynchronously, with each cell updated individually. The lattice structure of a cellular automaton is commonly referred to as the landscape, and the individual cells are referred to as sites. The surrounding cells make up the neighborhood for a single site, with those neighbors directly adjacent to the site being referred to as nearest neighbors.

It should be noted that the updating method, the method by which the states change over time, has significant impact on the behavior of CAs. It has been shown that the manner of updating can have a profound effect on the overall behavior of a CA system [34]. As such, in order to model a biological system realistically the method of updating should match the real-world system as much as possible. In the case where a "global clock" is present in a system, synchronous updating, in which all cells of the CA are updated simultaneously, is considered the best method of updating. However, when there is no evidence of such a clock an asynchronous method would be better suited to match the system.

In the 1940's Von Neumann and Ulam created the original cellular automaton system to study self-replicating systems. Motivated by the ability of biological organisms to self-replicate the model was based on the simple lattice network model used to study crystal growth and the kinematic model used to describe a physical non-biological self-replicating system. The model mathematically describes a hypothetical machine that could self-replicate using very complicated rules based on a Cartesian lattice where each cell in the lattice could take on 1 of 29 states.

In the 1970's the concept of cellular automata became popularized by Conway's *Game of Life* automaton. In an effort to simplify the original cellular automata model Conway created a cellular automaton using a lattice of cells that could take on 1 of 2 states, dead or alive, which were governed by four simple rules. Even with this simple design the cellular automaton produced diverse behaviour in which the system varied between states of order and randomness, including the frequent occurrence of patterns of cells that moved across the grid known as gliders. These results implied that simple and purely local rules might give rise to complex behaviors that are a result of the phenomena of self-structuring.

In the 1980's Wolfram began a very detailed investigation of cellular automata [3, 4, 5]. Initially basic one-dimensional cellular automata consisting of cells with two possible states interacting with their nearest neighbors were studied. From the 256 possible cellular automata rules (3 cell neighborhood with 2 states each, $2^3 = 8$ patterns; 8 patterns with 2 initial states, $2^8 = 256$) 32 were considered legal based on inessential restrictions. These elementary cellular automata were classified into four broad categories based on the statistical properties and evolving patterns of the automata. Cellular automaton rules were categorized into four classes based on the resulting patterns of an evolving system starting from a "disordered" initial state. The four classes are [4]:

I) Evolution leads to a homogenous state.

II) Evolution leads to a set of separated simple stable or periodic structures.

III) Evolution leads to a chaotic pattern.

IV) Evolution leads to complex localized structures, sometimes long-lived.

Empirical studies of the qualitative properties of the one-dimensional automata were found to be largely independent of properties such as the size of the neighborhood and number of states available to each cell [3]. The investigation was later extended to include two-dimensional automata as well. It was found that two-dimensional automata could be categorized into the same four classes as those used for one-dimensional automata, however there exist a variety of phenomena that depend on the geometry of the two-dimensional lattice [5].

4.1.2 Universal Computation and Cellular Automata

In mathematics, computing science and linguistics the term algorithm is used to denote a systematic procedure representing a finite set of well defined instructions which terminate in a defined end-state after being given initial conditions, or in other words it is a systematic procedure used to accomplish a specific task. At the turn of the twentieth century David Hilbert investigated the considerable importance of algorithms to the nature of mathematics, specifically questioning if any mathematical statements can be proven valid via an algorithm. In his incompleteness theorem Gödel showed that there exist certain statements regarding natural numbers that are primarily true but cannot be solved via mathematical algorithms making the statements inherently non-computable.

To investigate the nature of algorithms Alan Turing, often hailed as the father of modern computer science, proved in the 1930's that formal, simple devices, now called Turing machines (TMs), are capable of performing any conceivable mathematical problem that is represented by an algorithm. A TM capable of simulating any other TM is known as a Universal Turing Machine (UTM). Thus Turing proved that a universal computing machine exists. UTMs are thus capable of universal computation and said to exhibit the property of computational universality.

When Von Neumann showed that his cellular automaton system was capable of constructing a copy of itself, he demonstrated that there exists a universal computing machine which, given a description of an automaton, will construct a copy of it, even if the automaton is another universal computation machine, or a description of itself. Thus, a cellular automaton system is capable of universal computation given the proper automaton description. However, the question remains of which automaton descriptions yield the property of universality.

The Conway's *Game of Life* automaton is known to exhibit the property of computational universality, and according to Wolfram's classification system the *Game of Life* is a class IV automaton. Wolfram hypothesizes that class IV cellular automata may be viewed as computers where data represented by the initial configurations is evolved in time, where computational universality implies that suitable initial configurations can specify arbitrary algorithmic procedures [4], and thus that all class IV automata have the capability of universal computation.

Information in cellular automata is represented by dynamic, self-organizing patterns that are generated through neighboring cell interactions. In order for an automaton to exhibit class IV behaviour the cells of the system must be able to communicate and to transmit information between one another. Class I and II automata, which evolve to homogenous states or static/oscillating patterns, possess cells that are strongly interdependent resulting in little communication between the cells and thus lack the capability to process information usefully. On the other hand, class III automata, which evolve to chaotic patterns, possess cells that are weakly interdependent resulting in over communication between cells and a lack of processing capability. Thus, class IV cellular automata, which exist at the limit between class I and II, and class III, automata are the only ones that possess a moderate interdependence between cells, and are therefore capable of dealing with information in a useful way [6].

4.2 Examples of Cellular Automata

4.2.1 The Ising Spin Model

The Ising spin model was originally defined to describe the behaviour of molecules within lattice structures. This model is a specialized cellular automata model based on the spin states of atoms or molecules, where spin is defined from quantum mechanics as the intrinsic angular momentum of a particle. In the original Ising spin model the landscape consists of a system of nodes, or spins, placed at fixed positions within a lattice. The lattice itself possesses any required dimension to describe the phenomena in question. Spin values for each individual node, analogous to cells in cellular automata, can take one of two values defined according to the specific application (i.e. +1 and -1, up and down, 0 and 1 etc.). The interaction energy between a given node's spin and its nearest neighbors governs the dynamics of the system. At individual time-steps the energy for each node in the lattice is calculated, and then updated in a manner to reduce the systems overall energy. Over time the system will settle down into an energy minimum, with its excess energy being dissipated via several mechanisms depending on the system in question, such as lattice vibrations, bond breaking, radiation in the form of heat, or conformational changes in molecular strucutre.

While the original model focuses on the spin of an individual atom or molecule, any vector value can be used to describe the state of a given node. The nodes themselves can be taken to represent any object located within a lattice structure. Thus the nodes not only represent individual atoms or small molecules, but can represent large macromolecules such as biomolecules, or other similar objects. As such this model has been extended to encompass a wide variety of areas. Phase separation in liquids, gas-liquid critical phenomena, order-disorder transition points in alloys, and magnetic Curie points are a few of the phenomena described using this particular model.

In one dimension the Hamiltonian for the Ising system may be given as,

$$H = -B\sum_{i}\sigma_i - J\sum_{(i,j)}\sigma_i\sigma_j \qquad (4.1)$$

where σ_i and σ_j denotes the z-axis projection of the spin of the i^{th} particle or j^{th} neighbor particle, B is the strength of a magnetic field in the z-direction, and J is the strength of the spin interaction given by half the energy difference between the states. Extensions of the Ising spin model to study the dynamics of microtubules in specific are discussed in section 4.3.2.

4.2.2 Artificial Neural Net/ Hopfield Net Systems

Artificial neural networks are mathematical or computational models of information processing based on the connections of real biological neurons located in the nervous system of higher organisms. The original purpose for this technique was to examine the central nervous system to gain a greater understanding of biological neural networks and their ability to process information. Since then artificial neural networks have advanced to solve intelligence tasks outside the scope of real biological systems.

In its most basic form the cells of an artificial neural network model are a collection of simple nodes, or neurons. However, unlike most cellular automatons the neural network does not base its landscape on a lattice of nearest neighbors. Instead the nodes of a neural network possess a high degree of interconnectedness to represent the large number of connections in biological neural networks. This results in various patterns, sometimes three dimensional, dependent on the type of network being modeled. At no time is a node connected to itself. Individual nodes receive inputs either from other nodes, or from an external source. The inputs received by a given node have an associated weight assigned to them based on the specific model. These inputs are then used to calculate the output of the given node. The outputs can either be discrete or continuous. This output is then passed on as input to other nodes.

During a simulation a single node is selected at random and updated at each timestep in an asynchronous updating manner. When updated the node calculates all its weighted inputs to determine whether it fires or not. Hopfield networks use the specific rule that weights from node 1 to 2 are the same as weights from node 2 to 1. Over time the outputs will produce a specific firing pattern within the net that depends on the information stored in the net weighting.

The similarities between the Hopfield and Ising model can be seen when the energy of the two systems is compared. The energy of a Hopfield net is defined as,

$$H = -\frac{1}{2}\sum_{i<j} w_{ij} s_i s_j + \sum_i \theta_i s_i \tag{4.2}$$

where w_{ij} is the connection strength between units i and j, s_i is the state of unit i, and θ_i is the threshold of unit i.

4.3 Previous Computer Models of Microtubules

Much of the investigation into the capability of microtubules to process information has been conducted via computer simulation. A fair number of groups have published models of cytoskeletal information processing, including information processing in microtubules, which relate cytoskeletal function to computer related technologies [7]. The method of cellular automata has been used to a great extent to show the potential for information processing in microtubules. Cellular automata with rules based on various biological interactions are good models of biological pattern formation offering examples of universal computation and self-organization in self-organizing systems. The interactions of the individual unit cells with one another can lead to complex behaviour capable of computation. Cellular automata models of microtubules based on tubulin dipole oscillations represented as a discrete charge within the tubulin dimer have demonstrated self-organizing patterns suggesting the potential for microtubules to process information [8, 9, 10]. It has been shown that microtubule cellular automata networks may signal, adapt, recognize, and subserve neural-level learning [11]. Such models have also been used to simulate associative learning in microtubule networks as well as the dynamics of microtubule assembly and disassembly [9]. These results suggest that such activities in microtubules may have importance in biological regulatory functions as well as cognition. The next sections describe previous cellular automata models of microtubules in detail.

4.3.1 Original Cellular Automata Models of Microtubules

In 1984 Smith, Watt and Hameroff investigated biological regulation and information processing in microtubule lattices via cellular automata based on the electrostatic forces between tubulin subunits in a hexagonal A6-type lattice geometric arrangement [8, 12] with reflections at the microtubule ends. Tubulin subunits were allowed to exist in one of two states determined by the position of a discrete mobile electron. The location of this discrete charge was taken to represent the overall protein dipole orientation. The states, labeled as α, and β states, corresponded to the tubulin monomer that held the electron thus determining which monomer the overall dipole was oriented towards. The state of each dimer was determined via the components of the electrostatic force along the protofilament length y from each of six surrounding neighbor dimers. When the forces from the neighboring dipoles were predominately oriented towards the α-monomer the dimer was assigned an α-state and vice versa for the β-state. That is,

$$\begin{aligned} state = \alpha \quad if \quad \sum_{i=1}^{N} f_i(y) > 0 \\ state = \beta \quad if \quad \sum_{i=1}^{N} f_i(y) < 0 \end{aligned} \tag{4.3}$$

where the force is given by,

$$f_i(y) = K\frac{y_i}{r_i^3} \tag{4.4}$$

with K a constant determining the strength of the force, r_i is the distance between the central dimer and neighbor i, and y_i is the component of the distance r_i along the protofilament length.

Computer simulations of the cellular automata were run with the initial condition that all dimers were set to the β state except for a few that were in an arbitrary pattern of α states. The states of the dimers were updated stepwise with all electrostatic forces on each dimer being calculated first, then changing the dipole orientations to their new configuration. The resulting dipole configurations that formed on the microtubule lattice over time showed stable patterns, oscillating patterns and traveling patterns termed as gliders.

From these results it was concluded that stable and oscillating dipole patterns within microtubules could play a role in the orchestration of biomolecular activities, protein binding and transport, as well as potentially serving as information storage and memory. The interaction and interference of gliders within the microtubule was deemed as an indication that microtubules could potentially process information. While the cellular automata rules and patterns discovered by this investigation were somewhat arbitrary, they demonstrated that cellular automata-like information processing within microtubule lattices is feasible.

In 1989 Hameroff, Rasmussen and Mansson [13] expanded on the cellular automata microtubule model of Smith et. al. A threshold parameter was added to the cellular automata rules to take into account biological factors affecting the tubulin dipole such as temperature, pH, voltage gradients, ionic concentration, genetically determined variables in individual dimers, and binding of molecules. Electrostatic forces from neighboring dimers had to exceed this threshold value before the dipole of a dimer could switch states. Situations in which the switching thresholds between the two states were taken as symmetric and antisymmetric were both considered. In addition to this modification the boundary conditions were varied from the original reflective ends. In one case the conditions were chosen such that the ends of the microtubule were considered joined thus forming a torus and providing continuous toroidal boundary conditions. The second type of boundary condition selected allowed both microtubule ends to be open and independent from one another. In this second type the dimers at the plus end of the microtubule were given random states at each time step, while the minus end dimers were set to be in a constant β-state.

The results from simulations run under toroidal boundary conditions demonstrated general cellular automata behaviour such as virtual automata, gliders and blinkers as well as microtubule specific behaviour such as perturbation stable gliders, wedge patterns and unique orientation patterns. A number of these resulting patterns including single and bidirectional gliders, traveling and standing wave patterns, oscillating patterns, linearly growing patterns, and stable frozen patterns were attributed to be threshold dependent.

The results from these simulations indicated a potential capacity for microtubule automata to process information in a single microtubule. As well, individual microtubule specific automata behaviour was concluded to be indicative of certain activities in the brain such as back-propagating information transport (bi-directional automata), imprinting, pattern recognition and memory (static patters or oscillators), and traveling waves coupled to nerve membrane depolarizations (gliders). The self-organizing patterns, traveling waves, gliders and blinkers that were observed to form from random input at the plus end of the microtubule in the open-ended microtubule case was suggested to be a form of signal processing that may occur in real microtubules.

In 1990 Rasmussen, Karampurwala, Vaidyanath, Jensen and Hameroff extended the model of Hameroff, Rasmussen and Mansson to study and investigate simple adaptive microtubule networks as well as microtubule assembly/disassembly. In the case of microtubule networks two parallel microtubules were considered. The microtubule automata were connected via MAP-like connections to allow the two automata to communicate. The connections were considered unidirectional transferring a signal from one microtubule to the other. The state of the tubulin dimer on the input microtubule was used to determine the state of the dimer on the output microtubule. The resulting dynamics of the network thus depended not only on the threshold parameters, but also on the number, location and direction of the MAP-like attachments.

Each microtubule automata was assigned an input area at the right end of the microtubule and an output at the left end. The threshold values were chosen based on the dynamics of the system. A single connection between the two microtubules was placed at random locations. Input patterns were then entered into both microtubule automata and the resulting output pattern was compared against a desired output by measuring the Hamming distance, which is the number of substitutions required to make the two patterns match. The connection location with the lowest Hamming distance was then kept and a second MAP-like attachment was added at random. The second connection with the lowest Hamming distance was then kept and a third connection was chosen at random. This process was repeated until an acceptable Hamming distance was reached. At this point new input patterns were entered into the automata and new connections added in the same random manner until the Hamming distance for the new output patterns was deemed acceptable. The original input pattern was then reentered. If the output was still acceptable the adaptive sequence was considered to have finished satisfactorily.

The results of the simulation run on microtubule networks indicated that simple networks of paired microtubules were capable of learning two different patterns via the use of an evolutionary-like selection mechanism and associate nearby patterns. Nevertheless, it was noted that many improvements could be made to allow the system to more closely resemble biological activities, as well as improve the overall network performance. Despite these concerns however, the results indicated the possibility of associative learning in microtubule networks.

In the case of microtubule assembly/disassembly the microtubule was modeled as a lattice with each site existing in one of five states: GTP-bound polymerized tubulin, GDP-bound polymerized tubulin, GTP-bound free tubulin, GDP-bound free tubulin, and water. Hydrolysis of tubulin bound GTP to GDP was represented as lattice sites in a GTP-bound polymerized tubulin state switching to a GDP-bound polymerized state with a predetermined probability. Disassembly of GDP-tubulin was based on the concentration of GTP-bound free tubulin, so that lower concentrations of GTP-bound free tubulin increased the rate of disassembly. This was represented by GDP-bound polymerized tubulin located at the edges of the polymerized microtubule switching to states of GDP-bound free tubulin if three of more of its neighbors were in a state of either GDP-bound free tubulin, GTP-bound polymerized tubulin or water. To model the movement and changes in concentration of free tubulin and water transitions between GTP-bound free tubulin, GDP-bound free tubulin and water states were allowed based on stochastic processes. Polymerization of GTP-bound free tubulin to GTP-bound polymerized tubulin was allowed if any GTP-bound free tubulin sites were aligned with at least two GTP-bound polymerized tubulin states.

Simulations of microtubule assembly and disassembly displayed the behaviour of dynamic instability such as microtubule catastrophe and rescue. However, when compared with the elongation rate of dendrite microtubules in vivo (1 mm/day) it was found that the simulation elongation rate was much faster (1 nm/s). This suggests that the time scale for updating in the assembly/ disassembly model is not the same as in the signal propagation model.

The model of Hameroff, Rasmussen and Mansson was further extended in 2000 by Campbell to take into account the B8-Lattice configuration of the microtubule [10]. It was assumed that in vivo microtubules possessed tubulin monomers arranged in the A6-Lattice structure. However, in the 1990's evidence suggesting that microtubules in living cells are rather constructed with the B8-Lattice arrangement of tubulin [14, 15]. The model used the same electrostatic governing rules and threshold parameters as the Hameroff, Rasmussen, and Mansson model but was based on a neighborhood of eight surrounding tubulin dimers according to the B8-Lattice structure. Also, since the B8-Lattice structure exhibits the physical discontinuity of a seam between the 1st and 13th protofilaments the neighbor rules along the seam were modified. The dimers of the 1st and 13th protofilaments along the seam were modeled as having only seven neighboring dimers.

Simulations were run with both toroidal and open-ended boundary conditions as described by the Hameroff, Rasmussen, Mansson A6-Lattice model. While the actual shapes of the patterns formed on the B8-Lattice were generally different from those generated by the A6-Lattice model, the same types of behaviour were observed. Despite the overall difference in the lattice structures the simulations did not show any significant behavioral differences between the two lattices. These results lead to the conclusion that the type of lattice structure employed by a microtubule does not affect its ability to process information or fulfill its role in the cell.

4.3.2 Ising Spin Based Ferroelectric Models

Due to the dipolar nature of the microtubule subunit tubulin and the regular arrangement of tubulin molecules within the microtubule structure, microtubules may be viewed as an electret, which is an assembly of ordered dipoles, indicating that they may possess dielectric properties. Based on this indication it has been predicted that microtubules are ferroelectric in nature.

In 1993 Sataric et. al. investigated a ferroelectric model of microtubules [16]. The model attempted to give a physical description of energy transfer mechanisms in cell microtubules. The model was based on the creation of kink-like excitations in microtubules linked to the energy release associated with GTP hydrolysis, and their propagation due to an intrinsic electric force generated by the microtubule. Due to the structural symmetry of microtubules the dynamics of the system were described in terms of the non-linear dynamics of dimer dipoles in one protofilament in terms of a double-well potential model based on tubulin conformational changes due to GTP hydrolysis. The one dimensional Hamiltonian for the microtubule system is given as,

$$H = \sum_{i=1}^{N}\left(\frac{M}{2}\left(\frac{du_i}{dt}\right)^2 + \frac{K}{4}(u_{i+1} - u_i)^2 - \frac{A}{2}u_i^{\,2} + \frac{B}{4}u_i^{\,4} - Cu_n\right) \tag{4.6}$$

where u_i is the longitudinal displacement of the i^{th} dimer, M is the tubulin dimer mass, K is the spring constant determining the stiffness between dimers, A and B are parameters describing the shape of the quartic double well potential, and C is the additional potential energy due to each dipole interacting with the intrinsic electric field of the microtubule.

It was found that kink-like excitations could propagate along the microtubule length with a velocity proportional to the intrinsic electric field. This result is consistent with the observed growth rates of microtubules including dynamic instability and treadmilling, as well as the stability of microtubules induced by the presence of microtubule-associated-proteins. Suggestions were also proposed that the kink-like excitations could be observed experimentally via neutron scattering and polarization experiments.

Theoretical ferroelectric behaviour was further examined by Tuszynski et. al. a few years later [17]. In this case the microtubule was modeled as a lattice array of coupled local dipole states interacting with their immediate neighbors. The situation was represented as an anisotropic two-dimensional Ising model on a triangular lattice. It was shown that the dipoles of the microtubule were likely to exist in two ordered phases, a ferroelectric phase and a length dependent intermediate weakly ferroelectric phase, which varied between one another through variation of temperature and an external electric field. The ferroelectric phase, in which the dipoles were aligned parallel, showed long-range order and alignment among the dipoles with the capability to transmit kink-like excitations, akin to the findings of Sataric et. al., as well as optimal conditions for microtubule signaling and assembly/disassembly. The intermediate phase, in which the dipoles exhibited a conflict in resolving the dipole couplings, showed properties suitable for information processing and computation.

Extensions of the dipole lattice model revealed several interesting results concerning the ability of the dielectric microtubule to signal and process information. Investigations into the information storage capacity of microtubules indicated that in the ferroelectric phase there is no capacity for storage, but the capacity begins to increase as the phase makes a transition into the paraelectric phase, and that the capacity not only depends on the dipole configuration but on their orientation to the microtubule as well [18]. The same investigation indicated that microtubules possess a capacity to store information at temperatures above 0 K. It has been shown that in the presence of large transient electric fields, such as a propagating nerve impulse, microtubules are more likely to be in a ferroelectric phase due to the alignment of the lattice dipoles with the field [19, 20] thus indicating conditions for signaling rather than information processing. It has also been shown that microtubule-associated-proteins bound to a microtubule affect the overall configuration of the dipole lattice [20]. Associated-proteins that fix dimer dipoles into a single state were observed to enhance the number of dipoles in the lattice pointing in the same direction moving the microtubule towards a signaling phase, while associated-proteins that neutralized the dipole lower the transitions temperature between the ordered signaling phase and disordered information processing phase. Overall microtubules with microtubule-associated-proteins possessed configurations with higher complexity than microtubules without.

4.3.3 Hopfield Network Microtubule Model

Microtubules have also been modeled as quantum Hopfield networks [21]. A Hopfield network consists of individual processing units, usually neurons, existing in one of two states. The units of this Hopfield system are fully connected to all other units in the system via multiplicative weights that add up to determine whether the individual unit changes state or not. The quantum Hopfield network model of a microtubule investigates the suggestion of quantum computation in microtubule protein assemblies numerically with qubits representing tubulin molecules interacting via Coulomb forces at finite temperature. The Hamiltonian for a microtubule as a quantum Hopfield network is given as,

$$H = \sum_j \left(K\sigma_{xj} + A\sigma_{zj} \right) \tag{4.7}$$

where σ_x and σ_j are the Pauli matrices, K is the flipping amplitude for a given qubit, and A is half the energy difference between two states.

It was found that quantum information processing in microtubules is feasible although at temperatures of approximately 6 K. However in this model environmental factors such as energy losses and dissipation are neglected, and several of the parameters used in simulation are not based on experiment suggesting that modifications of the model could affect the scale at which the phenomena occur.

4.4 Current Ideas on Dendritic Cytoskeletal Computation

4.4.1 C-termini based Signaling and Information Processing

Alterations of the structural microtubule associated protein MAP2 have been shown to alter contextual memory [22] and the expression of the motor MAP kinesin has been shown to affect learning [23]. As well, the transport of mRNA's along dendritic microtubules to the specialized cytoskeleton located at neuronal synapses, known as the postsynaptic density, has been suggested to play a role in learning and long-term potentiation [24]. Priel et. al. examined the role of the tubulin C-termini tails in the microtubule's ability to transduce and process signals [25]. The biophysical properties of the C-termini have been shown to affect the attachment of MAPs including kinesin and MAP2 [26].

To investigate the role of C-termini in the functioning of dendrites, Priel et. al. developed a computational model based on the biochemical data of tubulin, their C-termini tails, and MAP2. Using molecular dynamics simulations the conformational states of the C-termini protruding from the microtubules outer surface were calculated. The 3D structure of the tubulin dimer was determined by Nogales et. al. [27] but several amino acids including some at the C-terminus of the protein were unresolved resulting in their omission from the Protein Data Bank. Structure files were created that include the C-termini of tubulin. Each tubulin dimer possesses two C-termini tails that can exist in several conformational states. According to the model the negatively charged C-termini interact electrostatically with the dimer surface, neighboring C-termini, and adjacent MAPs. The minimization of the overall interaction energy of the C-termini is believed to govern the system as it evolves in time. The surface of the tubulin dimer is highly negatively charged, with regions of positive charge attracting the C-termini tails causing them to bend into a "downward" state. The "up" state, in which the C-terminus extends perpendicularly out from the dimer, was found to have the lowest energy. For situations in which the energy of the C-termini was less than 50 meV plus the lowest energy state, the C-termini tail was allowed to move freely due to thermal fluctuations. This corresponds to a cone with an angle of 40° from the dimer surface. A local minimum corresponding to the "downward" state was found at 100 meV above the lowest energy state, and a saddle-point was found 160 meV above the lowest energy. It was deduced from these findings that two major metastable states exist with an energy difference between the two on the order of a few k_bT [25].

To facilitate the calculation a bead-spring model was developed in which the C-termini tails are taken as strings of beads with flexible connections. The electric field exerted by the dimer, the external field from the environment and interactions within individual C-termini were taken into account. Simulations of the bead-spring model indicated the ability of ionic waves to create waves of C-termini state changes from upright to downward orientations. Calculations performed on the model to find the minimum energy positions of the individual beads, corresponding to the C-termini amino acids, in two equal forms revealed a 15% probability for the tail to exist in a full or partial "downward" position. This indicates that the system favors the "up" state unless driven towards the "downward" state by outside influences.

The interaction between MAP2 and its ionic environment was modeled using counter-ions in order to investigate the ability of MAP2 to function as a wave-guide. The binding region is located at the C-terminus and the bond between MAP2 and a microtubule appears to be electrostatic in nature. It has been shown that MAP2 binds to microtubules in a concentration-dependent manner [28]. However since the 3D structure of MAP2 is unknown at this point in time, as it has not been crystallized, it is not known whether or not MAP2 actually makes physical contact with microtubules, but at the very least MAP2 enters into the immediate vicinity of the microtubule. As a simplification of the model Priel et. al. assumed MAP2 to be a straight chain along which the attraction sites for the counterions were equally spaced and arranged, and that the counterions move only in a plane perpendicular to the MAP2 cylinder. It was found that perturbations applied to the counterions at one end of the MAP2 chain initiated a wave traveling along the MAP2 moving the counterions out of equilibrium. The profile of the ion displacements revealed a "kink"-like perturbation along the MAP2 chain with a phase velocity on the order of 2 nm/ps.

The results of molecular dynamic modeling of microtubules raise the possibility that microtubules are capable of transmitting electrostatic disturbances. The propagation of ionic waves along MAP2 can be seen to influence the conformational states of surrounding C-termini that in turn affect other C-termini along the microtubule. Thus electrostatic disturbances can be understood to propagate along microtubules in the form of collective disturbances among neighboring C-termini, or between neighboring microtubules via MAP2 connections. The relation of these ideas to the cognitive functions of the brain is discussed in the next section.

4.4.2 Computation within the Dendritic Cytoskeleton

The transport of proteins and receptors along neuronal microtubules is likely to have an electromagnetic basis indicating that this function is possibly dependent on microtubule information processing. As discussed above kinesin mediated transport of mRNA has been implicated in memory and learning. Kinesin mediated transport along microtubules is affected by both the protein conformation of tubulin and the nature of the C-termini [25, 26]. The conformational state of tubulin, which is key to the notion of information processing within microtubules and therefore the notion of quantum brain function, is not only critical to effective transport, but appears to be altered in turn by motor proteins and MAPs. The binding of kinesin and the MAP tau have been observed to significantly alter the direction of the protruding protofilament ridges along microtubules, which in turn influences their further binding abilities [29]. In fact it has been suggested that tubulin dimers along microtubules alter their conformational state ahead of kinesin motor movement [30]. The conformational state of tubulin within a microtubule determines the dipole moment of the dimer and thus the electromagnetic field of the microtubule [31].

Priel et. al. building on the ideas discussed in the previous section suggested a direct regulation of ion channels, and thus the electrical response of neurons, by cytoskeletal structures [25]. It is envisioned that arrays of dendritic microtubules, equally arranged in parallel and anti-parallel fashion, receive signals from neuronal synapses either via actin filaments connected to the array via MAP2, or via direct connection of the array to the post synaptic density located at the synapse. Once the input signal is received the microtubule network evolves the signal by dynamically altering its C-termini conformations. The output of the signal moving through the microtubule network may then propagate along via actin filaments to distant ion channels eliciting the channel to open or close. This process thus affects the electrical response of the neuron by regulating the temporal gating state of the voltage-sensitive channels. For this reason the process controls the membrane conductive properties as well as the axon hillock behavior by changing the rate, distribution and topology of open/closed channels. The overall functions of the dendrite and neuron can thus be directed in this manner.

Recall that the binding of kinesin and MAP2 are affected by the conformational state of tubulin's C-termini as discussed in the previous section. Thus, the incoming signal from a neuronal synapse not only alters the C-termini conformational states along the microtubule, but also alters the binding of kinesin and MAP2. Through alterations of kinesin and MAP2 binding the tubulin conformational state is affected, thus the electromagnetic fields created by microtubules could be altered by synaptic inputs.

MAP2 bridges keep the microtubule networks within the dendritic core aligned in parallel and antiparallel arrangement by aligning portions of polarized microtubules. The antiparallel alignment of microtubules, which specifically occurs in dendrites, can be understood to severely attenuate any electromagnetic field generated by microtubules. It is expected that kinesin mediated transport is enhanced during heightened synaptic activity. Due to kinesin's effect on tubulin's conformational state it is expected that during this period microtubule bound MAP2 would be perturbed and may even detach from the microtubule temporarily. If it is assumed that some MAP2 remain connected to the microtubule, thus keeping the microtubule network intact, any net unidirectional transport along the array should enhance the strength of its associated electromagnetic field resulting in the spread of that field to adjacent microtubules. If a sufficient number of microtubules engage in this activity it can be imagined that entire dendrites might be expected to interact. Due to lengthwise electric dipoles of tubulin dimers, information in the form of traveling waves propagated along microtubules can, in principle, be transmitted between synapses with high fidelity [32]. Due to the parallel/antiparallel arrangement of microtubules in cortical dendrites and the ability of electromagnetic fields to pass from one dendrite to adjacent dendrites, information could, in principle, pass between neurons when such electromagnetic fields were sufficiently amplified as a result of changes in the binding of MAPs or kinesin.

The idea that there is one common type of energy responsible for perceptual and cognitive processes appears likely [33]. This may be a particular electromagnetic state of a network of microtubules that corresponds to a unique cognitive event. This has been referred to as an electromagnetic fingerprint [25]. Due to the high degree of interaction described above, activation of one electromagnetic fingerprint could, in turn, activate another electromagnetic fingerprint, independent of sensory input giving rise to the so-called stream of consciousness. Moreover, the subjective feels of this widespread pattern of electromagnetic energy can be specified according to those key physical properties of microtubules that influence the transport of proteins to synapses.

References

[1] A. Deutsch, and S. Dormann, Cellular automaton modeling of biological pattern formation: characterization, applications, and analysis, (Birkhauser, Boston, 2005)

[2] G. B. Ermentrout and L. Edelstein-Keshet, *Cellular Automata Approaches to Biological Modeling*, Journal of Theoretical Biology, Vol. 160, No. 1, pp. 97-133, (January 7, 1993)

[3] S. Wolfram, *Statistical Mechanics of Cellular Automata*, Review of Modern Physics, Vol. 55, pp. 601-644, (July 1983)

[4] S. Wolfram, *Universality and Complexity in Cellular Automata*, Physica D, Vol. 10, pp. 1-35, (1984)

[5] N. H. Packard, and S. Wolfram, *Two-Dimensional Cellular Automata*, Journal of Statistical Physics, Vol. 38, pp. 901-946, (1985)

[6] H. A. Gutowitz, and C. Langton. *Methods for designing Cellular Automata with "Interesting Behaviour"*, in Center for Nonlinear Studies (CNLS) News Letter, (University of Santa Fe Press, Santa Fe, 1988)

[7] S. Hameroff, Ultimate Computing, (North Holland, Amsterdam, 1987)

[8] S. A. Smith, R. C. Watt, and S. R. Hameroff, *Cellular automata in cytoskeletal lattices*, Physica D, Vol. 10, p. 168-174, (January 1984)

[9] S. Rasmussen, H. Karampurwala, R. Vaidyanath, K. S. Jensen, and S. Hameroff, *Computational connectionism within neurons: a model of cytoskeletal automata subserving neural networks*, Physica D, Vol. 42, No. 1-3, pp. 428-449, (June 1990)

[10] R. D. J. Campbell, Information processing in microtubules (PhD. Thesis), (Queensland University of Technology, Australia, 2002)

[11] S. R. Hameroff, J. E. Dayhoff, R. Lahoz-Beltra, A. V. Samsonovich, and S. Rasmussen, *Models for molecular computation: Conformational automata in the cytoskeleton*, Computer, Vol. 25, No. 11, pp. 30-39, (November 1992)

[12] S. R. Hameroff, S. A. Smith, and R. C. Watt, *Automaton model of dynamic organization in microtubules*, Annals of the New York Academy of Sciences, Vol. 466, pp. 949-952, (June 1, 1986)

[13] S. Hameroff, S. Rasmussen, and B. Mansson, *Molecular automata in microtubules: basic computational logic of the living state*, in Artificial Life: Santa Fe Institute Studies in the Science of Complexity, Vol. 6, pp. 521-553, edited by C. Langton, (Addison-Wesley, Boston, 1988)

[14] Y. Song, and E. Mandelkow, *Recombinant kinesin motor domain binds to β-tubulin and decorates microtubules with a B surface lattice*, Proceedings of the National Academy of Sciences, Vol. 90, pp. 1671-1675, (1993)

[15] E. Nogales, M. Whittaker, R.A. Milligan, K.H. Downing, *High Resolution model of the microtubule*, Cell, Vol. 96, pp. 79-88, (1999)

[16] M. V. Sataric, J. A. Tuszynski, and R. B. Zakula, *Kinklike excitations as an energy transfer mechanism in microtubules*, Physical Review E, Vol. 48, pp. 589-597, (1993)

[17] J. A. Tuszynski, S. Hameroff, M. V. Sataric, B. Trpisová, and M. L. A. Nip, *Ferroelectric behaviour in microtubule dipole lattices: implications for information processing, signaling and assembly/ disassembly*, Journal of Theoretical Biology, Vol. 174, pp. 371-380, (1995)

[18] B. Trpisová, Dielectric phases, solitary waves, and information capacity in microtubules (PhD. Thesis), (University of Alberta, Edmonton, 1996)

[19] J. A. Brown, and J. A. Tuszynski, *Dipole interactions in axonal microtubules as a mechanism of signal propagation*, Physical Review E, Vol. 56, No. 5, pp. 5834-5840, (November 1997)

[20] B. Trpisová, and J. A. Brown, *Ordering of dipoles in different types of microtubule lattice*, International Journal of Modern Physics B, Vol. 12, No. 5, pp. 543-578, (1998)

[21] E. C. Behrman, K. Gaddam, J. E. Steck, and S. R. Skinner, *Microtubules as a quantum Hopfield network*, in The Emerging Physics of Consciousness, edited by J. A. Tuszynski, (Springer-Verlag, New York, 2006)

[22] Z. Khuchua, D. F. Wozniak, M. E. Bardgett, Z. Yue, M. McDonald, J. Boero, R. E. Hartman, H. Sims, and A. W. Strauss, *Deletion of the N-terminus of murine MAP2 by gene targeting disrupts hippocampal CA1 neuron architecture and alters contextual memory*, Neuroscience, Vol. 119, pp. 101-111, (2003)

[23] R. W. Wong, M. Setou, J. Teng, Y. Takei, and N. Hirokawa, *Overexpression of motor protein KIF17 enhances spatial and working memory in transgenic mice*, Proceedings of the National Academy of Sciences of the United States of America, Vol. 99, pp. 14500-14505, (2002)

[24] M. A. Kiebler, and L. DesGroseillers, *Molecular insights into mRNA transport and local translation in the mammalian nervous system*, Neuron, Vol. 25, pp. 19-28, (2000)

[25] A. Priel, J. A. Tuszynski, and H. F. Cantiello, *The dendritic cytoskeleton as a computational device: An hypothesis*, in The Emerging Physics of Consciousness, edited by J. A. Tuszynski, (Springer-Verlag, New York, 2006)

[26] D. L. Sackett, *Structure and function in the tubulin dimer and the role of the acid carboxyl terminus*, in Subcellular Biochemistry – Proteins: Structure, Function and Engineering, Vol. 24, pp. 255-302, edited by B.B. Biswas and S. Roy, (Kluwer Academic Publishers, Dordrecht, 1995)

[27] E. Nogales, S. G. Wolf, and K. H. Downing, *Structure of the alpha beta tubulin dimer by electron crystallography*, Nature, Vol. 291, pp. 199-203, (1998)

[28] B. Pedrotti, R. Colombo, and K. Islam, *Interactions of microtubule associated protein MAP2 with unpolyermized and polymerized tubulin and actin using a 96-Well microtier plate solid-phase immunoassay*, Biochemistry, Vol. 33, pp. 8798-8806, (1994)

[29] R. A. Santarella, G. Skiniotis, K. N. Goldie, P. Tittmann, H. Gross, E. M. Mandelkow, E. Mandelkow, and A. Hoenger, *Surface deterioration of microtubules by human tau*, Journal of Molecular Biology, Vol. 339, pp. 539-553, (2004)

[30] A. Krebs, K. N. Goldie, and A. Hoenger, *Complex formation with kinesin motor domains affects the structure of microtubules*, Journal of Molecular Biology, Vol. 335, pp. 139-153, (2003)

[31] S. Hagan, S. R. Hameroff, and J. A. Tuszynski, *Quantum computation in brain microtubules: Decoherence and biological feasibility*, Physical Review E, Vol. 65, pp. 061901 1-11, (2002)

[32] J. A. Tuszynski, J. A. Brown, and P. Hawrylak, *Dielectric polarization, electrical conduction, information processing and quantum computation in microtubules. Are they plausible?*, Philosophical Transactions of the Royal Society of London A, Vol. 356, pp. 1897-1926, (1998)

[33] J. Cronly-Dillon, and G. W. Perry, *Effect of visual experience on tubulin during a critical period of visual cortex development in the hooded rat*, The Journal of Physiology, Vol. 293, pp. 469-484, (1979)

[34] D. Conforth, D. G. Green, and D. Newth, *Ordered asynchronous processes in multi-agent systems*, Physica D, Vol. **204**, p. 70-82, (2005)

Chapter 5

A Cellular Automata Model of a Microtubule at Physiological Temperature

5.1 Quantum Cellular Automata

As stated in section 4.1.1, a cellular automata model is composed of a lattice of identically programmed cells that are assigned particular states, which then change stepwise over time according to the states of the surrounding cells and specific rules that determine the system's evolution in time. Quantum cellular automata (QCA) use geometrically arranged lattices of quantum wells, with the configuration of electron within the wells encoding and processing information [24]. Cellular automata cells may consist of one or more quantum wells coupled togther, such that electrons in the well confining potentials can tunnel between wells in the same cell, but not between different cells. Quantum mechanics and the Coulomb interaction in each cell can determine the possible cell states, and the Coulomb interaction between electrons in different cells can provide a local intercellular coupling mechanism [25]. Typical QCA cells consist of four or five coupled quantum wells containing two electrons [24-27], however single electron devices have been conceived [24, 28, 29]. In the following sections a possible double well potential site in tubulin is discussed as a cell for a quantum cellular automata in a microtubule. The computer code used to simulate the microtubule cellular automata may be found in the Appendix.

5.2 The Cellular Automata Lattice Structure

5.2.1 The Microtubule Lattice

To simulate microtubule automata the standard 13-protofilament microtubule structure is represented as a two-dimensional lattice in which the cylindrical microtubule has been split open between the 1st and 13th protofilaments, and flattened. The lattice, composed of microtubule subunit tubulin dimers, is positioned such that the minus end of the microtubule is to the left, and the first protofilament is at the top of the array. Thus, the lattice is taken to have 13 rows, corresponding to individual protofilaments. The lattice is chosen to have 100 columns, denoting individual dimers along the length of the microtubule, thus representing a microtubule of approximately 0.8 μm in length. To be consistent with the MT-13A-6 structure the top and bottom rows of the array were considered joined as in Figure 5.1.

5.2.2 The Seven Dimer Hexagonal Neighborhood

Dimer neighborhoods were constructed according to the tilted hexagonal shape of the MT-13A-6 structure (see Figure 5.4). The neighbors of a single dimer (i, j) were defined as follows: N_0 (i-1, j-1), N_1 (i-1, j), N_2 (i, j+1), N_3 (i+1, j+1), N_4 (i+1, j), N_5 (i, j-1). Neighbors N_0 and N_1 of dimers in the first row were located in the thirteenth row in accord with the three-start helical winding pattern. Neighbors N_3 and N_4 of dimers in the bottom row were located in the first row and likewise shifted down according to the wrapping scheme described in Figure 5.2 so that the joining dimers between the top and bottom row are separated by eight columns. The microtubule ends were considered joined creating continuous toroidal boundary conditions.

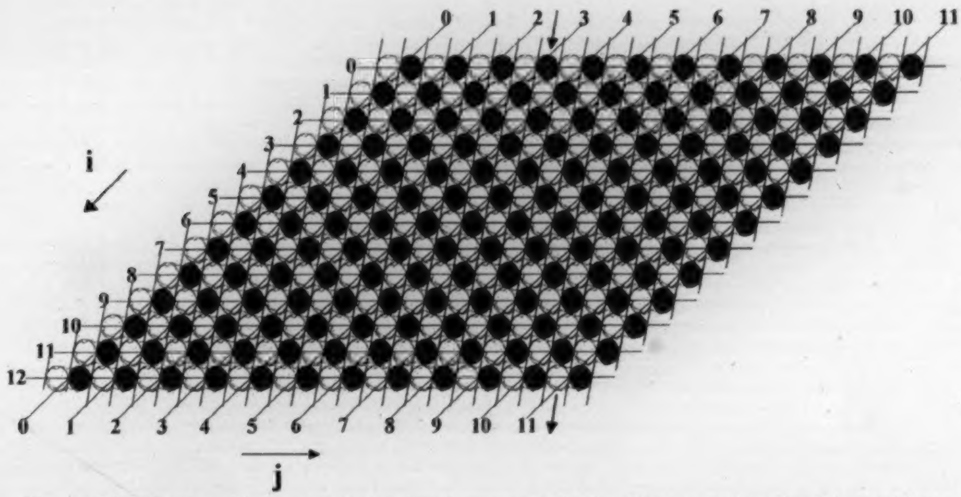

Figure 5.1: Section of the two dimensional array of tubulin dimers used in the CA model to represent a Type A lattice microtubule. Label i denotes individual protofilaments while label j denotes dimers along each protofilament. Also shown are the helices of monomers. Black arrows pointing along monomer helices indicate where monomer helices join between 0th and 12th protofilaments.

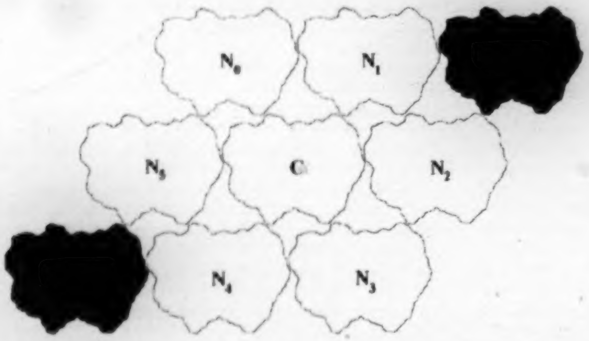

Figure 5.2: Seven dimer tilted hexagonal neighborhood of an individual tubulin dimer in a MT-13A-6 lattice structure.

5.3 The Cellular Automata Cell

5.3.1 The Electrostatic Properties of the Tubulin Dimer

Individual cells of the cellular automata microtubule model were taken to represent tubulin dimers, and in order for comparison to previous models the cells were allowed to exist in one of two possible. The work of Fröhlich discussed previously in section 2.3.3 suggests that quantum oscillations within hydrophobic pockets located within a protein's interior engage in macroscopic quantum coherence [1]. Thus, the cells were taken to exist in two possible states corresponding to the position of a mobile electron within the tubulin dimer.

To investigate the electrostatic properties of tubulin the Poisson-Boltzmann Equation (PBE), which describes electrostatic interactions between molecular solutes and aqueous media, was solved with the solute molecule tubulin in a solvent composed of an ionic aqueous solution with a dielectric constant of 78.54 and 0.1 M of both +*e* and –*e* ionic species, where *e* is the charge of the electron. The PBE is given by,

$$\vec{\nabla}[\varepsilon(\vec{r})\vec{\nabla}\Psi(\vec{r})] = -4\pi\rho^{f}(\vec{r}) - 4\pi\sum_{i} c_i^{\infty} z_i \lambda(\vec{r}) q e^{\frac{-z_i q \Psi(\vec{r})}{kT}} \tag{5.1}$$

where $\varepsilon(\vec{r})$ represents the position-dependent dielectric constant describing the dielectric properties of the solute and solvent, $\Psi(\vec{r})$ represents the electrostatic potential, $\rho^{f}(\vec{r})$ represents the charge density of the solute, c_i^{∞} represents the concentration of the ion *i* at a distance of infinity from the solute, z_i is the charge of the ion, *q* is the charge of a proton, k is the Boltzmann constant, *T* is the temperature, and $\lambda(\vec{r})$ is a factor describing the position-dependent ionic strength of the solution and accessibility of ions to the solute interior.

Since, the PBE describes electrostatic interactions between molecular solutes and aqueous media, and thus can be used to the find the electrostatic potential of macromolecules. Recent studies using electron crystallography on zinc-induced tubulin sheets have yielded a refined high-resolution structure of the tubulin molecule with a 3.5 Å resolution [3]. Solving the Poisson-Boltzmann equation for this structure via the Adaptive Poisson-Boltzmann Solver (APBS) software [4] produced an electrostatic potential map of the protein.

Two regions of positive potential surrounded by negative potential were observed by taking cross sections of the resulting electrostatic map along the x, y and z coordinates (see Figure 5.3). This region is located near the separation between α-tubulin and β-tubulin, approximately 4.5 nm from the tip of the α-monomer, with the positive potential regions separated by 2 nm. This structure may provide a local double well potential for a mobile electron that may undergo an electron transfer process within the protein.

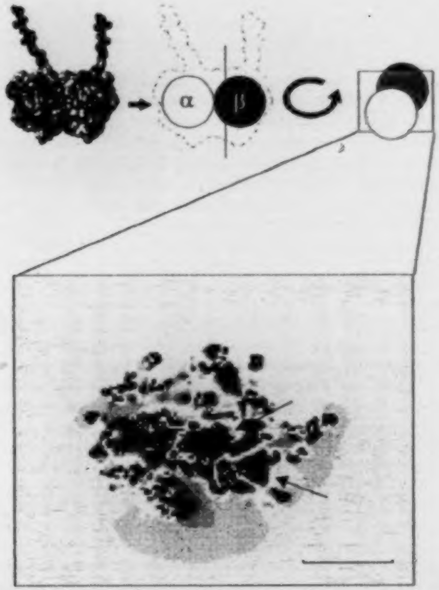

Figure 5.3: Cross section of an electrostatic map of the tubulin dimer showing the proteins interior. Black arrows indicate the regions of positive potential taken to constitute the double well structure. Scale bar = 2 nm.

The electron donor and acceptor properties of biologically important molecules have been evaluated by quantum-mechanical calculations based on the molecular-orbital method by Pullman and Pullman [12]. From their evaluations it was determined that histidine, an aromatic amino acid present in the tubulin protein, is a moderate electron donor. The imidazole side chain in the histidine structure is a heterocyclic aromatic organic compound that contains nitrogen capable of donating electrons [13]. The isoelectric point of histidine is 7.47, which is above the 6.8-7.3 pH of the intracellular environment, indicating a potential for electron donation. Overlays of the histidine locations on the electrostatic map revealed that Histidine (β-28) given by [3] is the closest to the right well of the double-well structure being approximately 11 Å away.

The typical distance between electron donors and acceptors has been given around 10-15 Å [14, 15], indicating that Histidine (β-28) would be capable of supplying a mobile electron to the double-well structure for use in ET processes. This is consistent with the findings of Tuszynski et. al. [2] who found that the hydrophobic interior of the tubulin protein gives rise to a symmetric electrostatic potential, characteristic of a double-well structure, where the structure was taken to indicate that charged groups present in the region of the potential could execute tunneling motion between its two equivalent energy minima. Nonetheless, ultimately experimental confirmation is needed to establish the origin and properties of electron transfer processes in tubulin. Recently, several studies have initiated investigation of conduction properties of microtubules, which is an important first step in this direction [9, 10, 16-19].

5.3.2 Tubulin Dimer as a Double Potential Well

From the electrostatic potential of tubulin, as discussed in the previous section, it was seen that the interior of the tubulin dimer possesses a region that is representative of a double well structure for an electron. As stated previously the crystallographic structure of tubulin that provided the electrostatic map was determined to a resolution of 3.5 Å [3]. To noticeably alter the electrostatic map the movement of an electron in the double well structure would need to distort the map by more than 3.5 Å. Since the majority of the charges defining the electrostatic map are bound charges, the minimum work *W* required to noticeably distort the structure of the tubulin dimer is given as,

$$\begin{aligned} W &= F\Delta x \\ &= \frac{1}{2}k\Delta x^2 \end{aligned} \tag{5.2}$$

where k is the spring constant for a single tubulin dimer which has been estimated as approximately 4 N/m [20], and Δx is the distance by which the structure is distorted which is taken as 3.5 Å. Thus, the minimum work required to distort the map is approximately 1.53 eV. As seen below in Table 5.1 the energies of a single electron to move from one side of the well to the other is well below the energy required to appreciably distort the electrostatic map. With the addition of surrounding dimers containing electrons, the interaction of electrons would raise an individual electron's energy. However, the interaction between dimers would also be expected to increase the spring constant due to the binding of the proteins and therefore is not expected to affect this result. As well, as shall be shown in Section 5.5.2 the timescale of transitions for an electron to switch between wells is on the order of 100 fs, where fs is femtoseconds (1 fs = 10^{-15} s). The average time for protein structural conformation changes, based on protein hinge motion, is approximately 10^{-9}-10^{-8} s, a value several orders of magnitude larger [31]. Thus, the map shown above may be considered static for our purposes.

From the information in the following sections describing the model it can be found that the maximum energy of an individual electron when interacting with surrounding electrons is approximately 0.6 eV, as given in Table 5.1. While the energy gap to the conduction band in tubulin is unknown, a typical gap value between 2.57 – 3.12 eV has been reported for a number of proteins with 1.2 eV being the lowest value recorded for cytochrome C [21]. As such it is reasonable to assume that the energies of the mobile valence electrons in the double well structures are insufficient to move the electrons to the conduction band in tubulin. Thus, for the purpose of the model investigated here, the double-well structure of tubulin was approximated by an infinite square double- well potential. The potential is described as,

$$\begin{aligned} V(x) &= +\infty && x \le -L/2 \\ &= 0 && -L/2 < x < -a \\ &= V_0 && -a \le x \le a \\ &= 0 && a < x < L/2 \\ &= +\infty && x \ge L/2 \end{aligned} \tag{5.3}$$

where x is the position about an axis centered between the two wells within tubulin, L is the width of the double well structure, $2a$ is the width of the potential barrier and V_0 is the height of the potential barrier. A schematic diagram of the potential is given in Figure 5.4.

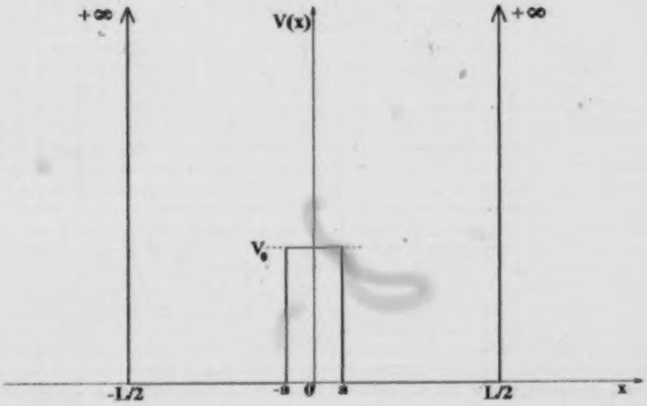

Figure 5.4: A typical infinite square double well potential, with total length of L, barrier width of 2a, and finite barrier height V_0.

The Schrödinger equation describes the quantum mechanical behaviour of an electron in a potential, such as the one described above. The time-dependent Schrödinger equation is given as,

$$-\frac{\hbar^2}{2m_e}\frac{d^2\Psi(x,t)}{dx^2}+V(x)\Psi(x,t)=E\Psi(x,t) \tag{5.4}$$

where $\hbar$ is Planck's constant divided by 2π, m_e is the mass of the electron, E is the energy of the electron, and $\Psi(x,t)$ is the solution to the equation otherwise known as the energy eigenfunction or wavefunction. The square modulus of the wavefunction provides the probability of finding the particle at a given position, at a given time. However, it is only the probability of a particle to tunnel through the potential barrier that is of consequence to the dynamics of the microtubule system.

The quantum solutions for the behaviour of a wave packet in a one-dimensional infinite double square well potential separated by a finite barrier have been evaluated to find the eigenvalues of the Schrödinger equation and the energy level splitting [5, 6], as well as the motion of a wave packet inside such a potential as time progresses [5]. Thus, the probability of finding a particle in one well or the other can be determined and used to evaluate the tunneling probability, however these solutions to the time-dependent equations for a particle in a double well are solved for particles of constant energy. In the microtubule model the energy of an electron in a given dimer is determined by the relative positions of the electrons in the surrounding dimers. The positions of these electrons are updated at discrete timesteps, and thus the energy of a given electron varies discretely with time. Thus, the difficulty in finding the tunneling probability lies in the constant updating of the electron energy at each timestep.

The most widely used approximation for solving tunneling problems is the semi-classical Wentzel, Kramers, Brillouin (WKB) method. The WKB method yields a tunneling probability P, dependent on the energy E of a particle, of,

$$P(E)=\frac{e^{-2\sigma}}{(1+\frac{1}{4}e^{-2\sigma})^2} \tag{5.5}$$

with,

$$\sigma=\int_p^q\sqrt{\frac{2m_e}{\hbar^2}(V(x)-E)}dx \tag{5.6}$$

where p and q denote the points where a classical particle would be reflected by the potential, also known as the classical turning points, and $V(x)$ is a potential that is a slowly varying function of x. When the condition is met that $\sigma > 1$ the tunneling probability is given by,

$$P(E) = e^{-2\int_{p}^{q}\sqrt{\frac{2m_e}{\hbar^2}(V(x)-E)}dx} \tag{5.7}$$

which agrees with the semi-classical approximation of Miller and Good [7]. Using the values defined in Section 5.5.1 it can be found that the condition of $\sigma > 1$ is met thus allowing the use of Equation 5.7 for the tunneling probability.

5.4 The Cellular Automata Dynamic Governing Rules

5.4.1 The Energy Dynamics of the System

The dynamics of the system are based on the organization in time of mobile electrons located in the double well potential structure in each of the tubulin dimers. Electrons were considered confined to individual tubulin dimers, but were allowed to move between the two potential wells localized within each dimer. The position of this mobile electron in the double well was used to designate the state of the tubulin cell. An electron in the left well designates the tubulin as being in an α-state since the left well is positioned closer to the α–tubulin monomer. An electron in the right well designates a β-state.

The energy, E, of a single electron in a central dimer C was determined by its Coulomb interaction with its neighbors:

$$E(C) = \sum_{m=0}^{5} \frac{e^2}{4\pi\varepsilon\varepsilon_0 r(C,N_m)} \tag{5.8}$$

where e is the charge of the electron, ε is the dielectric constant of tubulin, ε_0 is the permittivity of free space, $r(C,N_m)$ is the separation between the central dimer electron and its m^{th} neighbor electron, and m is the index labeling the neighbors from 0-5. The distance values, r_i, between the central dimer electron and its neighbor electrons are given in Figure 5.5.

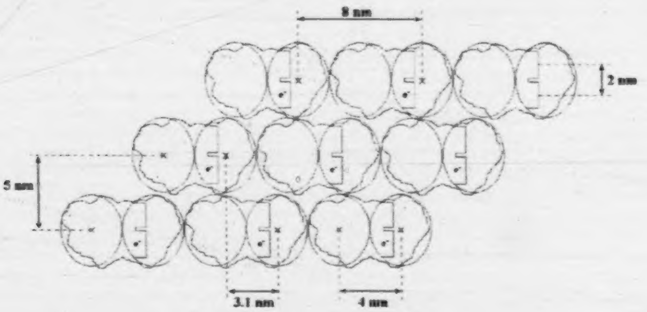

Figure 5.5: Dimensions of a MT-13A Lattice with a double well structure located in tubulin.

Since the dynamics of the system aim to minimize the system's total energy, the energy difference between a central dimer electron in an α-state and a β-state with the same configuration of neighbor dimer electrons determines whether or not an electron will switch from one well to the other. The energy difference, *ΔE*, is determined by the energy of the original state minus the energy of the new state as given by:

$$\Delta E(C) = A\sum_{m=0}^{5}\left(\frac{1}{r(C_f,N_m)} - \frac{1}{r(C_i,N_m)}\right) \quad (5.9)$$

where,

$$A = \frac{e^2}{4\pi\varepsilon\varepsilon_0} \quad (5.10)$$

The values for *E(C)* and *ΔE(C)*, given by Equations (5.8) and (5.9) respectively, are the two main parameters used to define the transition rules that govern the dynamics of the electrons in the microtubule system. The transition rules for both classical and quantum based scenarios are discussed in the following sections.

While it is commonly accepted that most proteins possess a dielectric constant in the range of 2-4, the dielectric constant of tubulin has yet to be precisely determined by experiment. There have recently been experimental tests performed that point to a value that differs from expectations. Surface plasmon resonance and refractometry measurements of the high-frequency dielectric constant have yielded a value of ~8.41 [9]. Other measurements of the dielectric constant of individual microtubules via a method of electroorientation give a very broad range of values between 0 and 100 [10], consequently offering no useful information. While this is not a precise measurement by any means, and it is doubtful that tubulin would have a dielectric constant greater than that of water, it does indicate the difficulty in obtaining a precise value for tubulin's dielectric constant. As such, the tubulin dielectric constant was allowed to range between 2 and 10. Table 5.1 give energy scales for varying tubulin dielectric constants.

Table 5.1 : Electron's total energy range, and the maximum energy difference between wells for tubulin dielectric constant values between 2 and 10.

[illegible]	[illegible]	[illegible]
2	578.17 – 697.45 meV	25.44 meV
4	289.07 – 348.71 meV	12.72 meV
6	192.72 – 232.48 meV	8.48 meV
8	144.54 – 174.36 meV	6.36 meV
10	115.63 – 139.49 meV	5.09 meV

5.4.2 The Transition Rules

The system is in contact with the environment, a temperature heat bath, it is necessary to include local rules that incorporate thermal noise. As stated by Wolfram [8] the simplest procedure is to impose that at each timestep the position of the electron be switched with a probability *P*, where *P* is given by the Boltzmann factor corresponding to a finite temperature heat bath. The probability of the thermal energy to cause an unfavorable transition is determined by the Boltzmann factor, which gives the probability for an electron to be in the new state, as $e^{-\Delta E/kT}$, where *k* is Boltzmann's constant and *T* is the temperature of the system. Thus,

Rule (i) if $E > V_0$ and $\Delta E > 0$ then a transition occurs with probability

$$P(E) = e^{\frac{-\Delta E}{kT}}.$$

This yields a probability between 0 and 1 for positive differences in energy, however, it yields a value greater than 1 for negative differences. Thus, if the electron possesses enough energy to cross the potential barrier, and the transition between states lowers its energy, then it will switch states automatically. That is,

Rule (ii) if $E > V_0$ and $\Delta E \le 0$ then a transition automatically occurs.

The electron is allowed to pass through the potential barrier via quantum tunneling with a finite probability. If the electron does not have enough energy to overcome the potential barrier, of height V_0, then it can still make the transition with a tunneling probability defined by the parameters of the potential barrier between the two wells. This transition still depends on whether or not the energy of the electron will be minimized. Thus according to Equation 5.7,

Rule (iii) if $E \le V_0$ and $\Delta E \le 0$ then a transition occurs with probability

$$P(E) = e^{-2\int_{-a}^{a}\sqrt{\frac{2m}{\hbar^2}(V(x)-E)}dx}.$$

where *2a* is the width of the potential barrier, and $\hbar$ is Planck's constant divided by 2π. However, if the transition requires an increase in energy,

Rule (iv) if $E \le V_0$ and $\Delta E > 0$ then a transition occurs with probability

$$P(E) = e^{\frac{-\Delta E}{kT}} e^{-2\int_{-a}^{a}\sqrt{\frac{2m}{\hbar^2}(V(x)-E)}dx}.$$

At each lattice site for a given timestep the electron has two choices: stay in the current position, or make a transition to a new position. The probability of making a transition $P_1(E)$ is given by the transition rules expressed above. Probability $P_1(E)$ ranges between 0 and 1 depending on the choices of parameters (i.e. DE and T for Rule (i), E and V(x) for Rule (ii) and all the previous parameters for Rule (iv)). The probability of staying in the same position $P_2(E)$ is then taken as $P_2(E) = 1 - P_1(E)$, ensuring that all probabilities add up to 1.

Bolteraruer, Limbach and Tuszynski discuss the equivalence between transition probabilities and kinetic rates in differential equations in [33]. They find a simple proportionality between probabilities P and the reaction rates k, given as,

$$P = k\Delta t \tag{5.11}$$

where Δt is the time step of the simulation. As the cellular automata uses discrete timesteps it is possible to use either probabilities or rates to describe the evolution of the system. By choosing the timestep of the simulation to coincide with the occurrence of a single transition, as discussed in section 5.5.2, the four transition rules, (i) – (iv), based on probabilities, can be taken to govern the dynamics of the electrons in the microtubule system.

5.5 The Cellular Automata Simulation

5.5.1 Simulation Conditions

The model described above aims to describe realistically a microtubule in an environment at physiological temperature. However, there are several factors about the microtubule and its environment that are currently unknown. As such, simulations were run over various conditions in an effort to account for these factors that are unknown through experiment. The two main parameters varied during simulations were the tubulin's potential well depth V_0 described above, and tubulin's dielectric constant ε defining the permittivity of the microtubule environment. The ranges of these parameters are discussed in the following paragraphs. The normal temperature of the microtubule environment is taken as 310 K, but to account for variations in the environmental temperature, such as in the case of fever or hypothermia, T was varied between 290 K and 330 K in increments of 10 K.

While it is commonly accepted that most proteins possess a dielectric constant in the range of 2-4, the dielectric constant of tubulin has yet to be precisely determined by experiment. There have recently been experimental tests performed that point to a value that differs from expectations. Surface plasmon resonance and refractometry measurements of the high-frequency dielectric constant have yielded a value of ~8.41 [9]. Other measurements of the dielectric constant of individual microtubules via a method of electroorientation give a very broad range of values between 0 and 100 [10], consequently offering no useful information. While this is not a precise measurement by any means, and it is doubtful that tubulin would have a dielectric constant greater than that of water, it does indicate the difficulty in obtaining a precise value for tubulin's dielectric constant. As discussed in Section 5.4.1 the tubulin dielectric constant was allowed to range between 2 and 10. This range was covered in increments of 0.1 in order to cover a plausible range of dielectric constant values. From the electrostatic map of the tubulin interior seen in Figure 5.3, the width of the potential barrier between the two positive potential regions was determined to be 2 Å, thus the value a from Equation 5.3 was taken as 1 Å. As the separation of the two positive wells was determined to be 2 nm, the overall length of the double-well system L, as defined in Equation 5.3, was taken to be 3.6 nm. The potential well depth V_0 in the tubulin dimer was taken to range between 100-150 meV, a value indicated previously by Hameroff and Tuszynski [11], and simulations were performed at 1 meV intervals. With the values defined above it can be found from Equation 5.5 that $\sigma > 1$ thus allowing the semi-classical approximation for the tunneling probability given in Equation 5.6 to be used.

The final factor that needs to be addressed is the method of updating. Currently there is no known experimental evidence suggesting the presence of a "global clock" to affect the microtubule system. As such, it is appropriate that an asynchronous method of updating be used during CA simulations to realistically model the system. However, it has been proposed that dendrite and neuron function are regulated by the propagation of ionic waves along the cytoskeleton [22, 23]. The propagation of signals via ionic waves as they pass along microtubules in the cytoskeletal network may serve as a mechanism to synchronize electron behavior. In this case it would be appropriate to use a synchronous, or sequential method of updating. Since these issues are not conclusively resolved it was deemed appropriate to investigate both synchronous and asynchronous methods of updating in the model described above.

In all simulations the lattice of dimers was set to an initial configuration of α-states randomly seeded with β-state dimers with a probability of 1% for a given dimer to exist in a β-state. In the case of synchronous updating a timestep consisted of systematically evaluating the preferred position of all the electrons in the lattice according to (i)-(iv) while holding all electrons in their original position, and then moving all the electrons simultaneously to their new positions. Thus, all dimers are updated in parallel at each timestep. These simulations were run for 300 time steps to allow adequate time for patterns to develop. In the case of asynchronous updating, a random order asynchronous method was used, as defined by Conforth et. al. [30]. A random order asynchronous timestep consisted of continually choosing individual tubulin dimers on the microtubule lattice at random, without replacement, and changing the position of the electron according to the rules (i)-(iv) described above until all dimers had been updated completing a single timestep. Thus, at each time step, all dimers are updated, but in random order, with each dimer being updated exactly once. Random order asynchronous simulations were run for 300 timesteps to allow adequate time for patterns to develop. Simulations were run under these conditions for lattices considered joined in the manner shown in Figure 5.1 with the ends of the microtubule joined to form continuous toroidal boundary conditions.

5.5.2 Simulation Procedure and Timing

Simulations of cellular automata follow a set of steps based on the transition rules defined in section 5.4.2, and the method of updating. These steps constitute a single timestep in the evolution of the system. For synchronous updating the procedure for one timestep is as follows:

1. A single tubulin cell in the microtubule lattice is chosen.
2. The energy for the electron in its current state is calculated according to Equation 5.8.
3. The energy for the electron in its alternate state is calculated according to Equation 5.8.
4. The energy difference between these energies is calculated according to Equation 5.9.
5. Using the transition rules in section 5.4.2, and random number generation to determine probability, the preferred state of the electron is determined.
6. The preferred state is held in memory, and the electron is allowed to remain in its current state.
7. Steps 2-7 are repeated until all cells in the lattice have been selected.
8. The electrons in all tubulin cells are placed in their preferred states.
9. The lattice is updated and the procedure begins again at step 1 for the next timestep.

For asynchronous updating the procedure for one timestep is as follows:

1. A single tubulin cell in the microtubule lattice is chosen, at random via random number generation, without replacement.
2. The energy for the electron in its current state is calculated according to Equation 5.8.
3. The energy for the electron in its alternate state is calculated according to Equation 5.8.
4. The energy difference between these energies is calculated according to Equation 5.9.
5. Using the transition rules in section 5.4.2, and random number generation to determine probability, the preferred state of the electron is determined.
6. The electron is placed in its preferred state.
7. The next cell in the lattice is chosen and steps 2-7 are repeated until all cells in the lattice have been selected.
8. The lattice is updated and the procedure begins again at step 1 for the next timestep

The rules described in section 5.4.2 are based on probabilities for a single transition. The length of time for a single transition therefore defines the time in a single timestep. When energy is below the barrier, the time for transition is defined by electron tunneling. As physicist Paul Davies points out, the definition of tunneling time is still under debate and the attempts to define it are extensive [32]. As a naïve approach he suggest the use of the energy time uncertainty pricinple, which yields $\Delta t = \hbar/\Delta E$. Thus, for the energy differences give in Table 5.1, in which the electron energy is less than the barrier height,

$$100fs \leq \Delta t \leq 130fs \tag{5.12}$$

where *fs* is femtoseconds (1 fs = 10^{-15} s). This, however, gives the transition time at 0 K temperature. The Arrhenius equation is a formula from transition state theory that describes the temperature dependence *T* of the escape rate *k* for a particle making a transiton between states, and is given as,

$$k = \frac{E}{2\pi\hbar} e^{-\frac{V_0}{k_B T}} \tag{5.15}$$

where *E* is the energy of the particle, V_0 is a potential barrier binding the particle, k_B is Boltzmann's constant and $\hbar$ is Planck's constant [34]. The transition time *t*, can be found as $t = 1/k$. Thus, for the ranges of *E* given in Table 5.1, and the range of V_0 discussed in section 5.5.1

$$308fs \leq t \leq 13.5ps \tag{5.14}$$

where *ps* is picoseconds (1 ps = 10^{-12} s). This, however, is a strictly classical description. As discussed in [35], the incorporation of quantum effects into a description of transition rates via transition state theory has been problematic, and therefore a detailed discussion of this topic is not included. The ranges given in Equation 5.12 and 5.14 provide an order of magnitude estimate of the timestep. Therefore, a single timestep, in the cellular automata simulations, is taken on the order of 100 fs.

5.6 Results of Simulations

5.6.1 Typical automata pattern evolution for synchronous updating

Evolution of the system from the initial random configuration was visually observed for 300 timesteps to determine the type of pattern developed. The patterns observed were classified according to the classification scheme of Wolfram given above. For synchronous updating type II, III, and IV behaviors were observed over the range of parameters described above. The patterns of evolution are shown in Figures 5.6-5.8 and are described in the following sections to give clarity to the discussion that follows.

Evolution of the microtubule system to Type II behavior is the most common form of evolution observed. Type II behavior, as shown in Figure 5.6, is characterized by the dimers forming alternating bands of α and β states stretching in the horizontal protofilament N_2-C-N_5 direction. These horizontal bands alternate from one protofilament to the next and are broken along the protofilament length by patterns of α and β states determined by the initial random seeding of β-states, as well as the randomness of thermal effects during the evolution to the pattern described. As time progresses the pattern of bands oscillates such that α-state dimers make a transition to the β-state, and β-state dimers change to α-states. Thus, Type II behavior is defined by the entire system of dimers oscillating in unison between two opposite patterns.

Type III behavior, as pictured in Figure 5.7, displays constant change and no pattern formation. The initial pattern of β-seeds on an α-background evolves into a constant switching of dimers between α-states and β-states. The duration for a single dimer to remain in one state, or the other, was unable to be determined and thus no visible patterns were discerned.

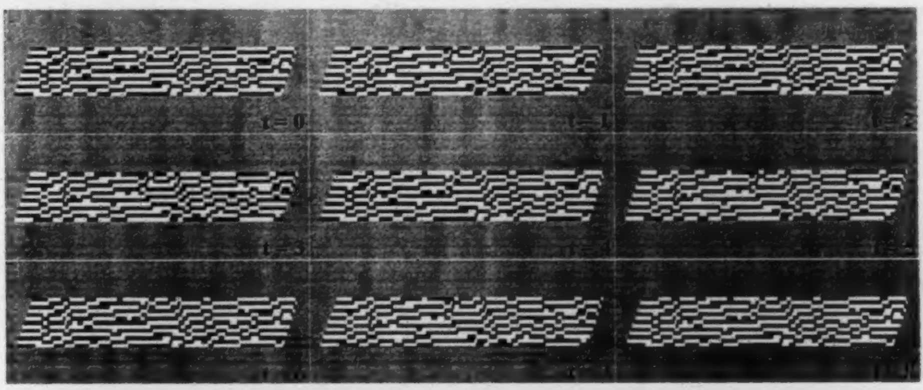

Figure 5.6: Type II evolution for synchronous updating.

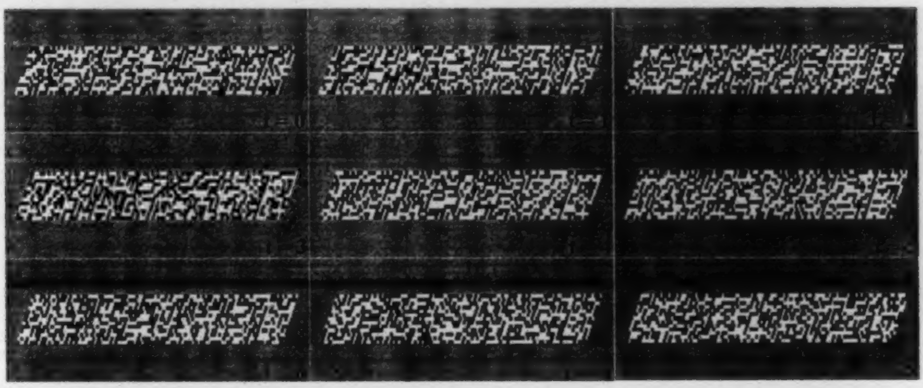

Figure 5.7: Type III evolution for synchronous updating.

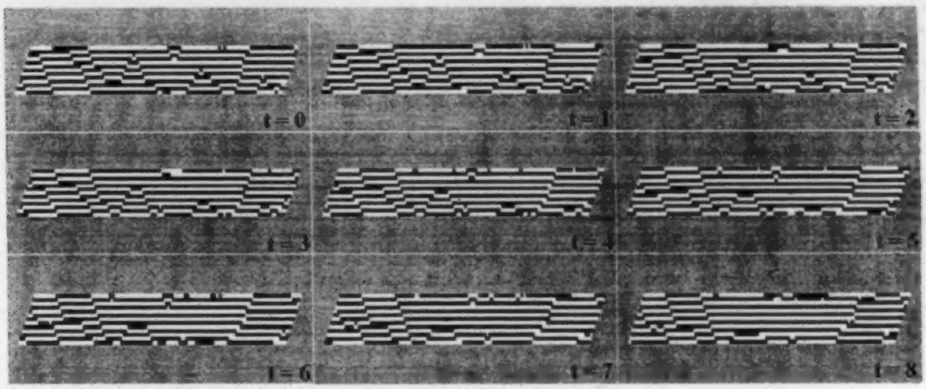

Figure 5.8: Type IV evolution for synchronous updating.

Type IV evolution is marked by the presence of rippling patterns moving around the microtubule (see Figure 5.8). Type IV, like Type II, behavior is characterized by dimers forming alternating bands of α and β states stretching in the N_2–C-N_5 direction. These horizontal bands alternate from one protofilament to the next and are broken along the protofilament length by patterns of α and β states determined by the initial random seeding of β-states as well as the randomness of thermal effects during the evolution to the pattern described.

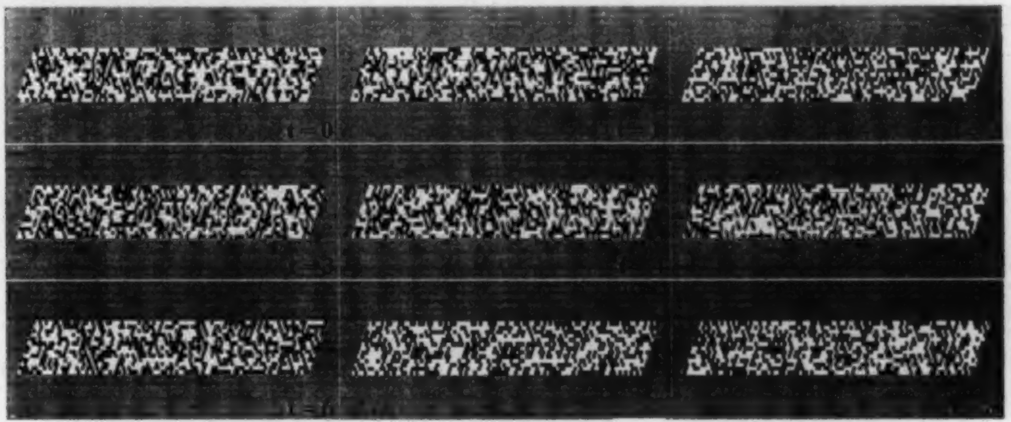

Figure 5.9: Type III evolution for asynchronous updating.

5.6.2 Typical pattern evolution for asynchronous updates

Evolution of the system from the initial random configuration was visually observed for 10^4 timesteps to determine the type of pattern developed. For asynchronous updating only Type III behavior was observed over the range of parameters described above. Type III behavior, as shown in Figure 5.9, displays constant change and no pattern formation.

The initial pattern of β-seeds on an α-background slowly evolves as dimers are selected randomly for update. The duration for a single dimer to remain in one state, or the other, was unable to be determined and no visible patterns were discerned.

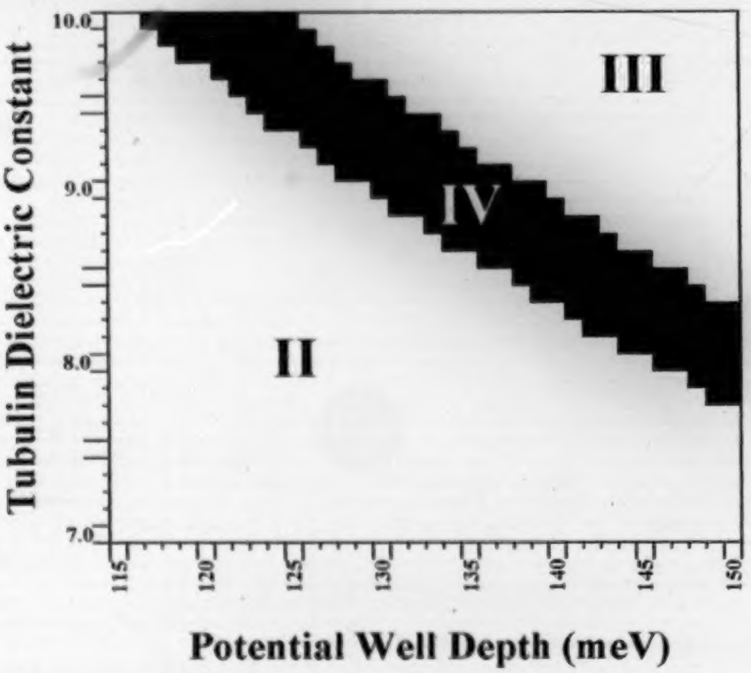

Figure 5.10: Tubulin dielectric constant versus tubulin potential well depth showing CA evolution for synchronous updating based on a system temperature of 310 K.

5.6.3 Discussion of results

In this section it was shown that even with a simplifying assumption about the double well potential within each dimer, the resultant dynamical behavior of the electronic states can depend heavily on the type of updating used. In both the synchronous and asynchronous simulations the overall behavior of the system did not vary greatly as temperature was varied between 290 K and 330 K. Although overall behavior did not depend on temperature, as the temperature was increased, the time taken to reach the corresponding asymptotic behavior did vary. For behaviors of Type II and IV the increasing temperature delayed the onset of the patterns observed, whereas the onset of behavior of Type III evolutions was accelerated with increasing temperature. In all cases the typical behavior patterns were reached within the 300-time step period. Taking the energy of the electrons on the order of ~100 meV, and the distance between wells as 2 nm, the time interval for a single transition would be on the order of femtoseconds, as shown above. Thus, all behaviors are reached on the timescale of picoseconds.

However, this is assuming the movement of the electron is through a vacuum. Taking into account the medium may increase this timescale by several factors. Assuming transitions on the order of 100 femtoseconds indicates that the movement of such objects or patterns around the microtubule occurs at speeds of $\sim 10^4$-10^5 m/s.

Figure 5.10 gives the behavior of the synchronous system in terms of the tubulin parameters at a temperature of 310 K, which is relevant to the temperature of the typical microtubule environment. It should be noted that the regions marked in Fig. 6 should not be taken as firm boundaries but rather as transition regions between the three types of behavior. The behavior observed in type II evolution is characteristic of automata cells that are too strongly interdependent, while the type III behavior is characteristic of cells with too weak interdependence. The onset of type IV behavior approaching from the type II region is marked by the oscillating bands of type II slowly varying to give rise to the discontinuities described for type IV evolution. These discontinuities allow the formation of moving objects and increase in size and movement in the further regions of type IV behavior. As the region of type III behavior is neared the moving objects become larger and interact giving rise to more complex behavior. Eventually this results in the loss of observable patterns and properties giving rise to type III behavior. Interestingly, below a tubulin dielectric constant of 7.8 only type II behavior is observed independent of the potential well depth which gives an empirically testable hypothesis. This was also observed for barrier heights below 116 meV with no dependence on the dielectric constant. The behavior of the system with a tubulin dielectric constant of 7.8 or higher and barrier height above 116 meV can be seen to depend on both the dielectric constant and the potential well depth. However, there are no concrete experimental findings to indicate either of these values leaving this problem open to future experimental investigation.

The results of these simulations depend heavily on the electrostatic properties of the tubulin dimer and on the nature of the microtubule with its environment. The stable and oscillating patterns of microtubule automata observed via the synchronous simulations could possibly function as specific sites of ion or protein binding and transport thus performing some role in the orchestration of biomolecular activities. It is expected that the addition of microtubule associated proteins (MAPs) and other proteins known to normally interact with microtubules will affect the overall patterns of behavior by altering the dynamics of electrons at specific MAP attachment sites and other locations. As well, these simulations have shown that information processing at temperatures relevant to the microtubule environment is feasible so long as a global clocking mechanism is present. The notion of sub-neuronal information processing and signaling suggested to occur in microtubules, at relevant temperatures, thus remains a possibility and is open to further investigation. Again it is stated that many of the simulation parameters are not known through experiment, thus the importance of the electrical properties of microtubules and tubulin to the functioning of information processing and signaling mechanisms, as well as other biological activities is stressed.

References

[1] H. Fröhlich, *Long-Range Coherence and Energy Storage in Biological Systems*, International Journal of Quantum Chemistry, Vol. 2, pp. 641-649, (1968)

[2] J. A. Tuszynski, J. A. Brown, E. Crawford, E. J. Carpenter, M. L. A. Nip, J. M. Dixon, and M. V. Sataric, *Molecular dynamics simulations of tubulin structure and calculations of electrostatic properties of microtubules*, Mathematical and computer modeling, Vol. 41, No. 10, pp. 1055-1070, (May 2005)

[3] J. Lowe, H. Li, K. H. Downing, and E. Nogales, *Refined structure of αβ-tubulin at 3.5 Å resolution*, Journal of Molecular Biology, Vol. 313, No. 5, pp. 1045-1057, (November 2001)

[4] N. A. Baker, D. Sept, S. Joseph, M. J. Holst, J. A. McCammon. *Electrostatics of nanosystems: application to microtubules and the ribosome*, Proceedings of the National Academy of Sciences of the United States of America, Vol. 98, No. 18, pp. 10037-10041, (August 21, 2001)

[5] E. A. Johnson, and H. T. Williams, *Quantum solutions for a symmetric double square well*, American Journal of Physics, Vol. 50, pp.239-243, (March 1982)

[6] M. Razavy, Quantum theory of tunneling, (World Scientific, River Edge, NJ, 2003)

[7] S.C. Miller Jr., and R. H. Good Jr., *A WKB-type approximation to the Schrödinger equation*, Physical Review, Vol. 91, No. 1, pp. 174-179, (July 1953)

[8] S. Wolfram, *Statistical Mechanics of Cellular Automata*, Review of Modern Physics, Vol. 55, pp. 601-644, (July 1983)

[9] A. Mershin, A. A. Kolomenski, H. A. Schuessler, and D. V. Nanopoulos, *Tubulin dipole moment, dielectric constant and quantum behavior: computer simulations, experimental results and suggestions*, Biosystems, Vol. 77, pp. 73-85, (2004)

[10] I. Minoura, and E. Muto, *Dielectric measurement of individual microtubules using the electroorientation method*, Biophysical Journal, Vol. 90, pp. 3739-3748, (May 2006)

[11] S. R. Hameroff, and J. A. Tuszynski, *Search for quantum and classical modes of information processing in microtubules: implications for "the living state"*,

Bioenergetic Organization in Living Systems, Eds. Franco Musmeci and Mae-Wan Ho, (World Scientific, Singapore 2003)

[12] B. Pullman, and A. Pullman, *Electron-Donor and –Acceptor Properties of Biologically Important Purines, Pyrimidines, Pteridines, Flavins, and Aromatic Amino Acids*, Proceedings of the National Academy of Sciences of the United States of America, Vol. 44, No. 12, pp. 1197-1202, (1958)

[13] E. Kimura, and A. Szent-Györgyi, *Donor-Acceptor Interactions of Nitrogen*, Proceedings of the National Academy of Sciences of the United States of America, Vol. 62, No. 1, pp. 286-288, (1969)

[14] G. W. Canters, and C. Dennison, *Biological electron transfer: Structural and mechanistic studies*, Biochimie, Vol. 77, pp. 506-515, (1995)

[15] R. M. Baum, *Views on biological, long-range electron transfer stir debate*, Chemical and Engineering News, Vol. 22, pp. 20-23, (1993)

[16] W. Fritzsche, K. Boehm, E. Unger and J. M. Koehler, *Making electrical contact to single molecules*, Nanotechnology, Vol. 9, pp. 177-183, (1998)

[17] W. Fritzsche, J.M. Koehler, K. Boehm, E. Unger, T. Wagner, R. Kirsch, M. Mertig and W. Pompe, *Wiring of metallized microtubules by electron beam-induced structuring*, Nanotechnology, Vol. 10, pp. 331-335, (1999)

[18] G. Goddard, and J. E. Whittier, *Biomolecules as nanomaterials: interface characterization for sensor development*, Proceedings of SPIE, Vol. 6172, Smart Structures and Materials 2006: Smart Electronics, MEMS, BioMEMS, and Nanotechnology, edited by V. K. Varadan, (March 2006)

[19] M. Umnov, O. A. Palusinski, P. A. Deymier, R. Guzman, J. Hoying, H. Barnaby, Y. Yang, S. Raghavan, *Experimental evaluation of electrical conductivity of microtubules*, Journal of Materials Science, Vol. 42, pp. 373-378, (2007)

[20] S. Portet, J. A. Tuszynski, C. W. V. Hogue, and J. M. Dixon, *Elastic vibrations in seamless microtubules*, European Biophysics Journal, Vol. 34, pp. 912-920, (2005)

[21] D. D. Eley, *Studies of Organic Semiconductors for 40 Years – I The Mobile π-Electron – 40 Years on*, Molecular Crystals and Liquid Crystals, Vol. 171, pp. 1-21, (1989)

[22] A. Priel, J. A. Tuszynski, and N. J. Woolf, *Transitions in microtubule C-termini conformations as possible dendritic signaling phenomenon*, European Biophysics Journal, Vol. 35, pp. 40-52, (2005)

[23] A. Priel, J. A. Tuszynski, and H. F. Cantiello, *The dendritic cytoskeleton as a computational device: An hypothesis*, in The Emerging Physics of Consciousness, edited by J. A. Tuszynski, (Springer-Verlag, New York, 2006)

[24] A. O. Orlov, R. Kummamuru, J. Timler, C. S. Lent, G. L. Snider and G. H. Bernstein, *Experimental studies of quantum-dot cellular automata devices*, Mesoscopic Tunneling Devices, 2004, edited by H. Nakashima, (Research Signpost, India, 2004) pp. 125-160

[25] C. S. Lent, P. D. Tougaw, and W. Porod, *Bistable saturation in coupled quantum dots for quantum cellular automata*, Applied Physics Letters, Vol. 62, No. 7, pp. 714-716, (February 15, 1993)

[26] C. S. Lent, B. Isaksen, and M. Lieberman, *Molecular Quantum-Dot Cellular Automata*, Journal of the American Chemical Society, Vol. 125, No. 4, pp. 1056-1063, (2003)

[27] C. S. Lent, P. D. Tougaw, W. Porod, and G. H. Bernstein, *Quantum cellular automata*, Nanotechnology, Vol. 4, pp. 49-57, (1993)

[28] Y. A. Pashkin, Y. Nakamura, and J. S. Tsai, *Room-temperature Al single-electron transistor made by electron-beam lithography*, Applied Physics Letters, Vol. 76, No. 16, pp. 2256-2258, (April 17, 2000)

[29] P. Bakshi, D. A. Broido, and K. Kempa, *Spontaneous polarization of electrons in quantum dashes*, Journal of Applied Physics, Vol. 70, No. 9, pp. 5150-5152, (November 1, 1991)

[30] D. Conforth, D. G. Green, and D. Newth, *Ordered asynchronous processes in multi-agent systems*, Physica D, Vol. **204**, p. 70-82, (2005)

[31] L. Stryer, Biochemistry, Third Edition, (W.H. Freeman and Co., New York, 1988)

[32] P. C. W. Davies, *Quantum Tunneling Time*, American Journal of Physics, Vol. 73, No. 1, pp. 23-27, (January 2005)

[33] H. Bolterauer, H. J. Limbach, and J. A. Tuszynski, *Models of Assembly and Disassembly of Individual Microtubules: Stochastic and Averaged Equations*, Journal of Biological Physics, Vol. 25, pp. 1-22, (1999)

[34] U. Weiss, Quantum Dissipative Systems, 2nd Edition, (World Scientific, Singapore, 1999)

[35] D. G. Truhlar, A. D. Iasaacson, R. T. Skodje, and B. C. Garrett, *Incorporation of Quantum Effects in Generalized-Transition-State Theory*, Journal of Physical Chemistry, Vol. 86, pp. 2252-2261, (1982)

Chapter 6

An Examination of Possible Mechanisms of Coherent Energy Transfer in Microtubules

6.1 The Electron Wavefunction in a Symmetric Double Well Potential

The electrostatic interior of the tubulin dimer may be considered as an infinite double well potential as discussed in Section 5.3.1 and 5.3.2 with a potential defined as,

$$\begin{aligned} V(x) &= +\infty && x \leq 0 \\ &= 0 && 0 < x < L_1 \\ &= V_0 && L_1 \leq x \leq L_2 \\ &= 0 && L_2 < x < L_3 \\ &= +\infty && x \geq L_3 \end{aligned} \qquad (6.1)$$

as pictured in Figure 6.1. To quantum mechanically investigate the properties of an electron confined within this potential the wavefunction, describing the behaviour of the confined electron wave and ultimately giving the electrons probability function, and the energy levels of the electron must be determined. The wavefunction of the electron in the above potential is defined as the eigenfunction $\psi(x)$ of the one-dimensional time-independent Schrödinger equation,

$$\frac{-\hbar^2}{2m_e}\frac{d^2}{dx^2}\psi(x)+V(x)\psi(x)=E\psi(x) \qquad (6.2)$$

where the corresponding eigenvalues E determine the specific energy levels of the particle, and m_e is the mass of the electron.

Following the work on infinite double square wells performed by Johnson in the 1980's the electron wavefunction bound in the potential described in Equation 6.1 is constructed from a linear combination of solutions given by the discontinuities of the potential [1].

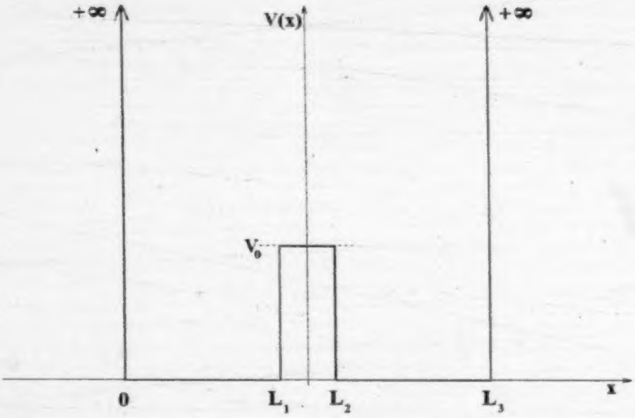

Figure 6.1: An infinite square double well potential, with total length of L_3, barrier width of L_2-L_1, and finite barrier height V_0.

Electrons bound within the double well structure must possess energies below the barrier height V_0. The wavefunctions $\psi(x)$ for electrons with energies below V_0 are given as,

$$\begin{aligned} \psi(x) &= 0 && x \le 0 \\ &= A\sin(kx) && 0 \le x \le L_1 \\ &= Be^{Kx} + Ce^{-Kx} && L_1 \le x \le L_2 \\ &= D\sin(k(x - L_3)) && L_2 \le x \le L_3 \\ &= 0 && x \ge L_3 \end{aligned} \tag{6.3}$$

where,

$$k = \frac{\sqrt{2m_e E}}{\hbar} \qquad K = \frac{\sqrt{2m_e(V - E)}}{\hbar} \tag{6.4}$$

and A, B, C, and D are coefficients to be determined.

Since the double well potential is symmetric under the interchange of x and $-x$, solutions of definite parity can be expected. For single solutions this results in wavefunctions extended over the entire well. However, as Gasiorowicz points out [19], if a superposition of an even state ψ_e of energy E_e, is taken with its nearest odd state ψ_o of energy E_o, such that,

$$\Psi(x) = \frac{\psi_e(x) - \alpha\psi_o(x)}{\sqrt{1+\alpha^2}} \tag{6.5}$$

and α is chosen to make the $\int_{-\infty}^{\frac{(L_1+L_2)}{2}} |\Psi(x)|^2 dx$ as small a possible, the electron can be considered localized as far as possible on the right hand side of the double well structure. If the superposition is allowed to evolve in time by multiplying the wavefunction by $e^{-iEt/\hbar}$, after a time t, the wavefunction can be written as,

$$\Psi(x,t) = e^{-iE_e t/\hbar}[\psi_e(x) + \alpha e^{-i(E_o-E_e)t/\hbar}\psi_o(x)]/\sqrt{1+\alpha^2} \tag{6.6}$$

indicating that the phase relationship between the two initial wavefunctions will vary. For the case where,

$$e^{-i(E_o-E_e)t/\hbar} = -1 \tag{6.7}$$

the electron is considered localized on the left hand side of the double well structure after a time t, indicating an oscillating behaviour for the electron. Thus, the frequency for oscillation can be determined as,

$$\omega = \frac{E_o - E_e}{\hbar} \tag{6.8}$$

which defines a period that is approximately equal to the tunneling time across the barrier between the two wells [19].

To solve for the energy eigenvalues, the continuity of the wavefunctions and their spatial derivatives at the discontinuities in the potential is required. As such the wavefunctions for $0 \leq x \leq L_1$, and $L_2 \leq x \leq L_3$, take on their given form so as to satisfy this condition at $x = 0$, and $x = L_3$. Enforcing this condition at $x = L_1$, and $x = L_2$ and solving yields three of the four coefficients,

$$\begin{aligned} \frac{B}{A} &= \frac{1}{2}e^{-KL_1}[\sin(kL_1) + \frac{k}{K}\cos(kL_1)] \\ \frac{C}{A} &= \frac{1}{2}e^{KL_1}[\sin(kL_1) - \frac{k}{K}\cos(kL_1)] \\ \frac{D}{A} &= -\cosh[K(L_2 - L_1)] - \frac{k}{K}\cot(kL_1)\sinh[K(L_2 - L_1)] \end{aligned} \tag{6.9}$$

where A can be found by the condition,

$$\int |\psi(x)|^2 \, dx = 1 \tag{6.10}$$

as well as a transcendental equation,

$$G(E) = \tanh[K(L_2 - L_1)][\frac{K^2}{k^2}\sin^2(kL_1) + \cos^2(kL_1)] + 2\frac{K}{k}\sin(kL_1)\cos(kL_1) \tag{6.11}$$

where $G(E) = 0$ yields the energy eigenvalue solutions to Equation 6.2.

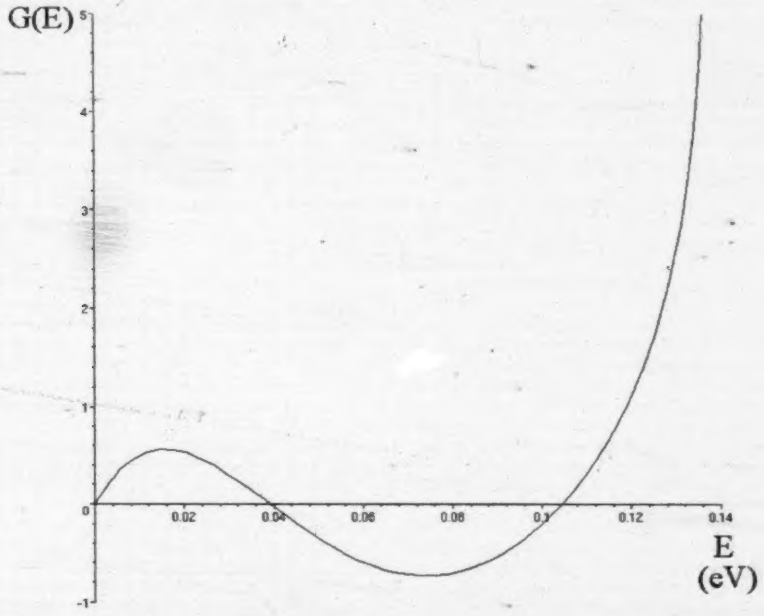

Figure 6.2: Plot of transcendental equation over energies below the potential barrier height to solve for the energy levels of an electron bound in a symmetric double well potential.

The solutions of Equation 6.11 are very difficult to solve algebraically. Thus, the energy eigenvalues were solved for numerically. As discussed in Section 5.3 the double well potential of the tubulin interior of Figure 5.3 possesses a barrier width of approximately 0.2 nm, a separation between the two wells of approximately 2 nm, and an overall length of 3.6 nm. Taking these values and applying it to the double well potential described in

Equation 6.1 yields L_1 = 1.7 nm, L_2 = 1.9 nm, and L_3 = 3.6 nm. As indicated previously by Hameroff and Tuszynski [2] the potential well depth V_0 in the tubulin dimer may range between 100-150 meV. Applying these values and plotting the transcendental equation G against energy E up to a value of the barrier height V_0 the possible energy levels of an electron bound within the double well structure were found. Figure 6.2 shows an example of such a plot.

Performing this analysis over the range of 100-150 meV, in 1 meV increments, showed that two bound states, a ground state and first excited state, existed for all given barrier heights 105 meV and above. Only states below the barrier height are considered, as those above the barrier height do not result in localization of the electron in the manner discussed above. For the minimum barrier height of 100 meV ground state and first excited state energy level values were found to be approximately 36 meV and 104 meV, respectively, with an energy difference between levels of 68 meV. At the other extreme, with a barrier height of 150 meV, approximate values of 40 meV and 104 meV were found for the ground and excited states, yielding an energy gap of 64 meV. Thus, the range of the gap between energy levels is given as,

$$64meV \le (E_1 - E_0) \le 68meV \tag{6.12}$$

where E_0 is the ground state energy, and E_1 is the energy of the first excited state. Values of E_0 and E_1 entered into Equation 6.3 result in an even wavefunction for the ground state ψ_0, and an odd wavefunction for the first excited state ψ_1. Thus, according to Equation 6.12 the period of oscillation $T = 2\pi/\omega$, ranges as,

$$60.8fs \le T \le 64.6fs \tag{6.13}$$

values comparable to those found in Section 5.5.2.

Taking the characteristic temperature of activation of the exciton to be,

$$T = \frac{(E_1 - E_0)}{k_B} \tag{6.14}$$

where kB is Boltzmann's constant, it is found that,

$$743K \le T \le 789K \tag{6.15}$$

This range is more than twice the physiological temperature of 310 K indicating that the exciton will not be easily excited by thermal fluctuations, and is more likely to be activated via other sources, such as exciton coupling, or phonon interactions.

6.2 Collective Excitations in Microtubules

6.2.1 The Phonon System

As discussed previously microtubules are aggregates of tubulin molecules that are polymerized into a cylindrical form. By considering the microtubule split between the 1st and 13th protofilament the lattice of tubulin dimers may be considered as a single layer of molecules (see Figure 6.3). Mechanisms of energy transfer in single layers of molecules, known as Scheibe aggregates, have been previously examined [3]. Scheibe aggregates are a class of molecular films that belong to the larger group of Langmuir-Blodgett films which are defined as one or more monolayers of an organic material, composed of polar molecules deposited from the surface of a liquid onto a solid by continually submerging and removing the solid substrate in the liquid. In the case of Scheibe aggregates the polar molecules are dye molecules composed of chromophores and fatty acids that form into a brick layer type arrangement.

By considering the microtubule as an aggregate layer in two dimensions the lattice vibrations in a sheet of tubulin dimers can be investigated. The Hamiltonian for a phonon system is given from Equation 2.9 as,

$$H_{ph} = \sum_k \hbar\omega_k (b_k^\dagger b_k + \frac{1}{2}) \tag{6.14}$$

where $\hbar\omega_k$ defines the phonon energy. Elastic vibrations in seamless microtubules considered as a two-dimensional planar lattice have been investigated previously [6]. It was found that for the canonical microtubule, a 3-start 13 protofilament microtubule corresponding to the MT-13A-6 lattice type discussed in section 5.2.1, the protofilament and dimer helical pathways possessed phonon frequencies of $\omega_{k,p} = 3.15 \times 10^{11}$ Hz, and $\omega_{k,h} = 4.8 \times 10^{10}$ Hz respectively. It can be estimated that the phonon energy in the microtubule system is,

$$\begin{aligned} \hbar\omega_{k,p} &\approx 0.207 meV \\ \hbar\omega_{k,h} &\approx 0.032 meV \end{aligned} \tag{6.15}$$

with a characteristic phonon time of,

$$\begin{aligned} \tau_{ph,p} &= \frac{1}{\omega_{k,p}} \approx 3.17 \times 10^{-12} s \\ \tau_{ph,h} &= \frac{1}{\omega_{k,h}} \approx 2.08 \times 10^{-11} s \end{aligned} \tag{6.16}$$

By rearranging Equations 2.6 and 2.8 it can be shown that the root mean square of the lattice fluctuations x_{rms} in the high temperature limit is given as [7],

$$\begin{aligned} x_{rms,p} &= \sqrt{\frac{4\pi\hbar}{m_{tub}\omega_{k,p}}}\left(\frac{T}{T_{ph,p}}\right)^{\frac{1}{2}} \approx 0.048\mathring{A} \times \left(\frac{T}{T_{ph,p}}\right)^{\frac{1}{2}} \\ x_{rms,h} &= \sqrt{\frac{4\pi\hbar}{m_{tub}\omega_{k,h}}}\left(\frac{T}{T_{ph,h}}\right)^{\frac{1}{2}} \approx 0.123\mathring{A} \times \left(\frac{T}{T_{ph,h}}\right)^{\frac{1}{2}} \end{aligned} \tag{6.17}$$

where m_{tub} is the mass of a tubulin dimer taken as 110 kD. The Debye temperature T_{ph} is the characteristic temperature at which all phonons become thermally active and is defined as [8],

$$\begin{aligned} T_{ph,p} &= \frac{\hbar\omega_{k,p}}{k_B} \approx 2.40K \\ T_{ph,h} &= \frac{\hbar\omega_{k,h}}{k_B} \approx 0.37K \end{aligned} \tag{6.18}$$

where k_B is Boltzmann's constant. Thus, at the physiologically relevant temperature of 310 K this corresponds to lattice fluctuations of approximately 0.55 Å and 3.6 Å along the protofilament and dimer helix, respectively. The Debye temperature can be seen to be much less than the physiologically relevant temperature, implying that the thermal environment may easily excite phonons in the microtubule system. Thus, thermal vibrations will most likely drown out energy supplied to the phonon system via other sources, such as excitons or other phonons, unless the system is somehow shielded from the environment.

6.2.2 The Exciton System

If there is only one electron bound within the double well potential then when it is excited from the ground state to the first excited state it will leave behind an empty state. As discussed in Section 2.3.2 this arrangement of an electron and hole is capable of forming an exciton. Thus, the second quantized Hamiltonian for a single exciton system,

$$H_{ex} = \hbar\Omega a^{\dagger} a \tag{6.19}$$

where $a^{\dagger}$ and a define the exciton creation and annihilation operators and $\hbar\Omega$ defines the energy difference between the ground and first excited states. As stated at the end of the previous section, for the double well system described by the tubulin dimer, values of $\hbar\Omega$

fall in the range 64 – 68 meV.

As discussed in [3] exciton energy transfer in Scheibe aggregates can be understood in terms of an energy hopping mechanism, which is governed by the interaction of molecular dipoles between dye molecules. That is, assuming that the exciton energy can be transferred between two molecules via a hopping mechanism the simplest second quantized Hamiltonian, as shown in Equation 2.18 takes the form,

$$H_{ex} = \hbar\Omega(a_1^\dagger a_1 + a_2^\dagger a_2) + J(a_1^\dagger a_2 + a_2^\dagger a_1) \tag{6.20}$$

where J is the hopping constant and should correspond to the dipole-dipole interaction energy, and the subscripts 1 and 2, on $a^\dagger$ and a, denote a central molecule and a neighboring molecule, respectively.

A transition dipole moment M is created when an electron makes a transition between its ground and first excited state [4], and may be given in one-dimension by,

$$M = < \psi_A \mid ey \mid \psi_B > \tag{6.21}$$

where e is the charge of an electron, y is the position operator, and ψ_A and ψ_B are the electron wavefunctions in the ground and first excited states respectively. Taking the wavefunction for the electrons described by Equation 6.3, and the energies for the ground and excited states defined by Equation 6.12 the transition dipole moment M was found to have an approximate magnitude of 1.2×10^{-28} Cm, or 36 Debye, over all ranges with the direction restricted to the y-direction.

The interaction J of two point dipoles in a dielectric medium of tubulin can be obtained from [5] as,

$$J = \frac{M_1 \cdot M_2 - 3(\hat{r} \cdot M_1)(\hat{r} \cdot M_2)}{4\pi\varepsilon\varepsilon_0 r^3} \tag{6.22}$$

where M_1 and M_2 are the dipole moments of molecule 1 and 2, respectively, ε is the dielectric constant of the medium, $r = \sqrt{x^2 + y^2}$ is the magnitude of the distance between molecule 1 and 2 with components along the x and y directions, and $\hat{r}$ is a unit vector pointing in the direction of $\vec{r}$. Considering each dimer posses the same dipole moment M that points only in the y-direction, for this one-dimensional case, Equation 6.22 may be simplified to,

$$J = \frac{M^2}{4\pi\varepsilon\varepsilon_0 r^5}(x^2 - 2y^2) \tag{6.23}$$

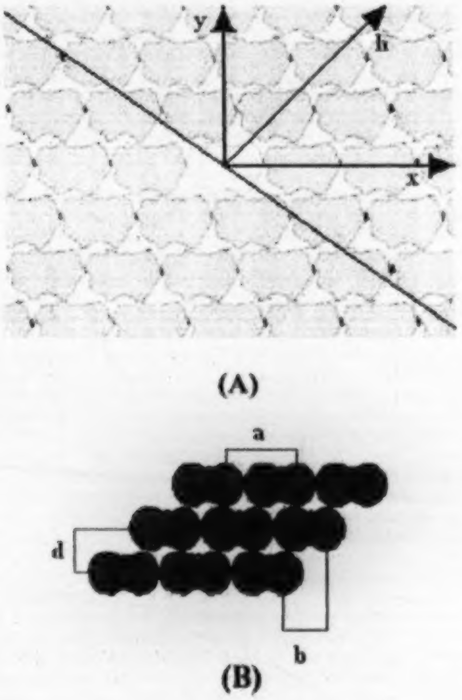

(A)

(B)

Figure 6.3: Diagram of tubulin neighborhood groups. (A) Symmetry around a central dimer, x protofilament direction, y microtubule circumference, and h dimer helix direction. (B) Distances between dimers where a = 8nm, b = 4.9nm and d = 5nm.

It can be seen from Figure 6.3(A) that a given neighborhood group contains *6N* dimers, where *N* determines the degree of separation from the central dimer. For nearest neighbors *N=1*, thus containing 6 dimers in the normal tilted hexagonal lattice neighborhood. For the neighborhood of next nearest neighbors *N=2*, yielding 12 dimers, and so on for increasing neighbor groups. It can also be seen from Figure 6.3(A) that the neighbors have symmetry about the central dimer. Due to this symmetry in the dimer neighborhoods a purely excitonic model yields a dispersion relation as follows from Equation 2.18,

$$\varepsilon_{\bar{k}} = \hbar\Omega + 2\sum_{i=1}^{N}\sum_{j=1}^{3i} J_{ij}\cos(\bar{k}\cdot\bar{r}_{ij}) \tag{6.24}$$

where i and j determine the neighborhood as mentioned above, J_{ij} is the dipole-dipole interaction energy between the central dimer dipole and a given neighbor dipole, and $\vec{r}_{ij}$ is the distance between dipoles. Expanding the dispersion energy around a minimum $\vec{k}$ value, $\vec{k}_{\min}$, yields,

$$\varepsilon_{\vec{k}} = \varepsilon_{\vec{k}_{\min}} + \sum_{i=1}^{N}\sum_{j=1}^{3i} \frac{J_{ij}}{2}(\vec{k}\cdot\vec{r}_{ij} - \vec{k}_{\min}\cdot\vec{r}_{ij})^2 + \dots \tag{6.25}$$

where the minimum energy $\varepsilon_{\vec{k}_{\min}}$ is given by

$$\varepsilon_{\vec{k}_{\min}} = \hbar\Omega + 2\sum_{i=1}^{N}\sum_{j=1}^{3i} J_{ij} \tag{6.26}$$

Unlike the Scheibe aggregate situation presented in [3], where the molecules of the monolayer are completely symmetrical around the x and y axis, the microtubule lattice structure does not provide a coordinate system in which the dipole contributions can be separated into two effective coupling constants in distinct directions. Due to the tilted hexagonal structure, and the direction of the dipole moment, there is skewed symmetry in the dipole couplings, thus the second term in Equation 6.25 may not be written in terms of an orthogonal axis.

Considering coupling only in the protofilament and dimer helix direction, the dispersion relations may be given as,

$$\begin{aligned} \varepsilon_{k_p} &= \hbar\Omega + \frac{2M^2}{4\pi\varepsilon\varepsilon_0 a^3}\sum_{i=1}^{N}\frac{1}{i^3}\cos(k_p a) \\ \varepsilon_{k_h} &= \hbar\Omega - \frac{2M^2(2d^2 - b)}{4\pi\varepsilon\varepsilon_0 (b^2+d^2)^{5/2}}\sum_{i=1}^{N}\frac{1}{i^3}\cos(k_h(b^2+d^2)^{1/2}) \end{aligned} \tag{6.27}$$

where the second term gives the dipole-dipole coupling to the N^{th} nearest neighbors, $a = 8$ nm, $b = 4.8$ nm and $d = 5$ nm. As the coefficient is necessarily positive in both cases the dispersion energy takes on a minimum when $k_p = k_{pmin} = \pi/a$, and for $k_h = k_{hmin} = 0$ yielding values of,

$$\begin{aligned} \varepsilon_{k_{pmin}} &= \hbar\Omega - \frac{2M^2}{4\pi\varepsilon\varepsilon_0 a^3}\sum_{i=1}^{N}\frac{1}{i^3} \\ \varepsilon_{k_{hmin}} &= \hbar\Omega - \frac{2M^2(2d^2 - b^2)}{4\pi\varepsilon\varepsilon_0 (b^2+d^2)^{5/2}}\sum_{i=1}^{N}\frac{1}{i^3} \end{aligned} \tag{6.28}$$

Expanding Equation 6.27 around this minimum energy up to orders of k^2 yields,

$$\begin{aligned} \varepsilon_{k_p} &= \varepsilon_{k_{p\min}} + J_p a^2 (k_p - \frac{\pi}{a})^2 + \ldots \\ \varepsilon_{k_h} &= \varepsilon_{k_{h\min}} + J_h (b^2 + d^2)(k_h - \frac{\pi}{(b^2+d^2)^{1/2}})^2 + \ldots \end{aligned} \tag{6.29}$$

where,

$$\begin{aligned} J_p &= \frac{M^2}{4\pi\varepsilon\varepsilon_0 a^3} \sum_{i=1}^{N} \frac{1}{i^3} \\ J_h &= \frac{M^2(2d^2 - b^2)}{4\pi\varepsilon\varepsilon_0 (b^2 + d^2)^{5/2}} \sum_{i=1}^{N} \frac{1}{i^3} \end{aligned} \tag{6.30}$$

Taking the extreme case of an infinitely long microtubule, N → ∞, for the protofilament case gives,

$$\begin{aligned} \varepsilon_{k_{p\min}} &= \hbar\Omega - \frac{2M^2}{4\pi\varepsilon\varepsilon_0 a^3}(1.2020569\ldots) \\ J_p &= \frac{M^2}{4\pi\varepsilon\varepsilon_0 a^3}(1.2020569\ldots) \end{aligned} \tag{6.31}$$

with the infinite sum value obtained from [9, 10]. As discussed in section 3.3.2 a typical lower end length of a microtubule is approximately 200 nm, corresponding to 12 dimers on either end of the central dimer. The sum of inverse cubes drops off rapidly with a sum to $N = 12$ yielding approximately 1.19, a value in good agreement with the infinite sum. Thus, since microtubules range in length from the lower end value of approximately 200 nm to values on the order of micrometers, the infinite sum is taken as an acceptable approximation.

One turn around the microtubule for the helical case corresponds to N = 6 dimers on both sides of the central dimer. A sum of inverse cubes up to N = 6 yields,

$$\begin{aligned} \varepsilon_{k_{h\min}} &= \hbar\Omega - \frac{2M^2(2d^2 - b^2)}{4\pi\varepsilon\varepsilon_0 (b^2 + d^2)^{5/2}}(1.1785729\ldots) \\ J_p &= \frac{M^2(2d^2 - b^2)}{4\pi\varepsilon\varepsilon_0 (b^2 + d^2)^{5/2}}(1.1785729\ldots) \end{aligned} \tag{6.32}$$

Taking the dielectric constant to range between 2 and 10, as discussed in section 5.4.1 yields a minimum energy range and coupling value in the protofilament direction of,

$$\begin{gathered} \hbar\Omega - 1.90meV \leq \varepsilon_{k_{p,min}} \leq \hbar\Omega - 0.38meV \\ 0.19meV \leq J_p \leq 0.95meV \\ \\ \hbar\Omega - 1.47meV \leq \varepsilon_{k_{h,min}} \leq \hbar\Omega - 0.29meV \\ 0.15meV \leq J_h \leq 0.74meV \end{gathered} \tag{6.33}$$

The characteristic time for exciton coupling is defined as,

$$\tau_{ex} = \frac{\hbar}{2J} \tag{6.34}$$

thus yielding a range of,

$$\begin{gathered} 3.46 \times 10^{-13}s \leq \tau_{ex,p} \leq 1.73 \times 10^{-12}s \\ 4.45 \times 10^{-13}s \leq \tau_{ex,h} \leq 2.19 \times 10^{-12}s \end{gathered} \tag{6.35}$$

The correlation between two exciton sites is given by the expression [3],

$$\begin{aligned} \Gamma(x) &= \int_{-\infty}^{\infty} a_k^{\dagger} a_k e^{-ikx} dk \\ &= e^{\frac{-x^2}{2x_{corr}^2}} \end{aligned} \tag{6.36}$$

where the creation and annihilation operators for the exciton are given by Equation 2.20, and the correlation length x_{corr} is defined as,

$$x_{corr} = |\vec{r}| \left(\frac{T_{ex}}{T} \right)^{1/2} \tag{6.37}$$

The characteristic temperature for exciton coupling T_{ex} is defined as [3],

$$T_{ex} = \frac{2J}{k_B} \tag{6.38}$$

This gives a range of,

$$\begin{gathered} 4.41K \leq T_{ex,p} \leq 22.09K \\ 3.42K \leq T_{ex,h} \leq 17.14K \end{gathered} \tag{6.39}$$

over the described parameters, and results in correlation lengths of,

$$\begin{aligned} 0.95nm \le x_{corr,p} \le 2.14nm \\ 0.74nm \le x_{corr,h} \le 1.65nm \end{aligned} \tag{6.40}$$

As in the phonon case the temperature of the microtubule environment is well above this characteristic temperature indicating that the thermal environment is likely to overwhelm the coupling between excitons removing any transmission of energy.

6.3 Discussion of Results

The exciton characteristic temperature given at the end of section 6.1 is above the temperature of the environment indicating that excitons will not be easily disrupted by thermal fluctuations. However, as stated at the end of section 6.2.1 and 6.2.2 the phonon and exciton coupling characteristic temperatures are well below the temperature of the microtubule thermal environment. This means that the vibrations caused by the thermal energy of the surrounding medium are more than sufficient to overwhelm both phonon and exciton coupling energy transfer in the microtubule lattice, and any chance of forming a coherent excitation is likely to be destroyed. It has been stated that the inside of a cell is too "warm and wet" to support quantum coherence [11-13]. However, there have been replies to this line of reasoning stating that mechanisms exist to shield a microtubule from the environment, thus allowing coherent quantum states to exist.

One such suggested mode of isolation is from actin gel states that are purported to solidify around microtubules thus shielding them from thermal effects [14, 16]. Condensed ion clouds that are attracted to the microtubule due to its large negative surface charge, known as Debye screening has been suggested as another form of shielding [14]. Similar to this idea is shielding to due the existence of ordered water surrounding the microtubule [14, 15]. Spectroscopic studies of resonant intermolecular transfer of vibrational energy in liquid water have shown that energy is transferred rapidly along water molecules before it dissipates [18], thus providing a mechanism for shielding the microtubule from thermal energy. Other suggested mechanisms to avoid thermal decoherence include coherent pumping of the system via the environment. This was previously discussed under the notion of biological coherence in section 2.3.3. When a system is strongly coupled to its environment via given degrees of freedom, it may lock out other degrees of freedom enabling coherent superpositions and entanglement to persist [17]. This locking out is described via a quantum Zeno effect, in which an unstable state, if observed continuously, will never decay since every measurement causes the wavefunction to reduce to a pure eigenstate thus allowing unfavorable states to persist. This effect was not taken into account in the above analysis, yet since it has been shown that thermal vibrations of the environment easily excite phonons and the exciton coupling in the model, a coherent pumping mechanism in the environment can be understood to result in coherent collective excitations. However, to date there is no known experimental evidence to show such a mechanism in relation to the microtubule.

While the stated mechanisms seem plausible, the degree of isolation required for the model discussed above is very high. The characteristic temperature scale of both phonons and exciton coupling in the proposed model range from a maximum of 30 K down to a few tenths of a degree. Thus, for any coherent state to exist in the given model the isolation would need to be almost absolute. Currently the mechanisms of isolation are only theoretical propositions, and to date there is no known experimental evidence quantifying the effect of the above mechanisms on microtubules.

Assuming such a mechanism exists, in whatever form it may take, then the existence of coherent excitations, in the form of excitons and phonons as described in the model above, is feasible. The energy and characteristic timescales of action for exciton coupling and phonons, along both the protofilament and helical directions, are in close relation indicating a strong possibility of coupling between the two types of excitation.

References

[1] E. A. Johnson, and H. T. Williams, *Quantum solutions for a symmetric double square well*, American Journal of Physics, Vol. 50, pp.239-243, (March 1982)

[2] S. R. Hameroff, and J. A. Tuszynski, *Search for quantum and classical modes of information processing in microtubules: implications for "the living state"*, Bioenergetic Organization in Living Systems, Eds. Franco Musmeci and Mae-Wan Ho, (World Scientific, Singapore 2003)

[3] J. A. Tuszynski, M. F. Jørgensen, and D. Möbius, *Mechanisms of exciton energy transfer in Scheibe aggregates*, Physical Review E; Vol. 59, No. 4, pp. 4374-4382, (April 1999)

[4] V. Czikklely, H. D. Forsterling, and H. Kuhn, *Extended Dipole Model for Aggregates of Dye Molecules*, Chemical Physics Letters, Vol. 6, No. 3, pp. 207-210, (August 1, 1970)

[5] J. D. Jackson, Classical Electrodynamics, 3rd Edition, (John Wiley and Sons, Inc., New York, 1999), p. 151

[6] S. Portet, J. A. Tuszynski, C. W. V. Hogue, and J. M. Dixon, *Elastic vibrations in seamless microtubules*, European Biophysics Journal, Vol. 34, pp. 912-920, (2005)

[7] E. A. Bartnik, and K. J. Blinowska, *Stability of quantum capture in Langmuir-Blodgett monolayers against positional disorder*, Physics Letters A, Vol. 169, pp. 46-50, (1992)

[8] M. P. Marder, Condensed Matter Physics, (John Wiley and Sons, Inc., New York, 2000)

[9] J. Schoutens, *Dipole-dipole interactions in microtubules*, Journal of Biological Physics, Vol. 31, pp. 35-55, (2005)

[10] L. B. W. Jolley, Summation of Series, 2nd Revision , (Dover Publications,New York, 1961)

[11] M. Tegmark, *Importance of quantum decoherence in brain processes*, Physical Review E, Vol. 61, p. 4194, (2000)

[12] C. Seife, *Cold Numbers Unmake the Quantum Mind*, Science Vol. 287, No. 5454, p.791, (February 4, 2000)

[13] C. Koch, and K. Hepp, *Quantum mechanics in the brain*, Nature 440, p. 611, (March 30, 2006)

[14] S. Hameroff, *Consciousness, Neurobiology and Quantum Mechanics: The Case for a Connection*, in The Emerging Physics of Consciousness, edited by J. A. Tuszynski, (Springer-Verlag, New York, 2006)

[15] A. Mershin, H. Sanabria, J. H. Miller, D. Nawarathna, E. M. C. Skoulakis, N. E. Mavromatos, A. A. Kolomenski, H. A. Schuessler, R. F. Luduena, and D. V. Nanopoulos, *Towards Experimental Tests of Quantum Effects in Cytoskeletal Proteins*, in The Emerging Physics of Consciousness, edited by J. A. Tuszynski, (Springer-Verlag, New York, 2006)

[16] S. Hameroff, A. Nip, M. Porter, and J. A. Tuszynski, *Conduction pathways in microtubules, biological quantum computation, and consciousness*, Biosystems, Vol. 64, No. 1-3, pp. 149-168, (January 2002)

[17] M. Nielson, and I. L. Chuang, Quantum Computation and Quantum Information, (Cambridge University Press, Cambridge, 2001)

[18] S. Woutersen, and H. J. Bakker, *Resonant intermolecular transfer of vibrational energy in liquid water*, Nature, Vol. 402, pp. 507-509, (December 2, 1999)

[19] S. Gasiorowicz, Quantum Physics, Second Edition, (John Wiley and Sons Inc., New York, 1996)

Conclusion

This report aims at investigating the information processing capabilities of microtubules at relevant temperatures within the body, and the relation of such capabilities to possible explanations for the phenomena of consciousness. The phenomena of consciousness are a new area of study for the physical sciences. Chapter 1 of this report examined consciousness from the viewpoint of the physical sciences. In terms of physical science consciousness is defined as "the condition of being aware of one's surroundings and one's own existence" and is taken to be a function of the material brain. Defining consciousness as a function of the material brain provides the physical sciences with an arena of investigation. The classical view of consciousness is explained as resulting from increasing complexity in the neuronal network of the brain, thus being an emergent phenomenon. It is pointed out that several of the features of consciousness cannot be understood from this classical standpoint, such as: the nature of subjective experience, the binding problem, its non-computable aspects, the notion of free will, and the rudimentary consciousness of less complex organisms.

In light of these objections to the classical view the aspects of quantum theory are examined and several quantum theories of consciousness are discussed. In contrast to the deterministic theories of emergence, quantum theories of consciousness were outlined illustrating several of the advantages of such approaches to understanding consciousness, such as non-locality explaining the lack of a specific center of consciousness, lack of determinism allowing for free will and non-computability, and the sense of unity as a result of coherence. Arguments in support of quantum theories of consciousness are weighed against those raised in opposition to such an explanation. Specifically those arguments concerning the implication of microtubule information processing as a key component to cognitive brain functions are examined in light of three main criticisms.

The first criticism objects that there appears to be no special quantum mechanical properties needed to explain psychological and neurological phenomena, and that the relevance of quantum effects to the structure and function of the brain does not necessitate their involvement in explaining consciousness. The use of quantum theories to investigate living systems is not a new concept. Chapter 2 outlined the connection between standard quantum based theories of solids and the working of biomolecular polymers. The chapter provided the basic formalisms used to describe biopolymers from a quantum perspective, namely phonons and the lattice properties of non-rigid crystals, excitons and conductivity, and the interaction between them. Several quantum based descriptions of biological phenomena are outlined during this discussion including an explanation of enzyme processes via semiconduction and proton tunneling, quantum-mechanical manipulation of proteins in the eye and explanation of functions of the eye via semiconduction, as well as semiconduction and electronic quantum coherence in photosynthesis, with a specific quantum mechanical explanation of anesthetic gas via London forces given in relation to consciousness. The material focuses on biosystems in general and therefore does not focus specifically on explanations of neurological and psychological phenomena, however the breadth of material, both experimental and theoretical, explaining biological processes via quantum processes supports the quantum approach to understanding brain function, at least from a molecular viewpoint.

The second criticism notes that the empirical evidence linking how the activity of a single synapse, including its constituent organelles, enters into the dynamics of neural assemblies is lacking thus the relevance of quantum processes in mental phenomena is merely a claim. In reply, the structure and biophysical functions of microtubules, specifically those functions related to signaling, conduction and cellular transport, and possible mechanisms for microtubules to influence brain cell firing are discussed in Chapter 3. As well the lack of definitive parameters of the conductive properties of microtubules, and its effect on the predictions of theoretical models is discussed. In response to the second criticism the significant headway in the investigation of microtubule conductivity is reported. Novel experimental designs that have been employed including electrical contact to single molecules and electroorientation were discussed showing that the electrical nature of microtubules is an active field of research. The evidence obtained from these investigations indicates that microtubules are likely conductive in nature, yet precise values for inclusion within theoretical models are still needed. The difficulty in obtaining accurate measurements of conductivity has been illustrated by an analysis of the electroorientation method of Minoura and Muto, which showed that even with very refined measurements small changes in experimental variables results in appreciable differences in the values obtained. As well the difficulty in segregating the conductivity into an intrinsic microtubule conductivity and a conductivity due to the effect of ion cloud condensation has been discussed.

In regards to microtubules affecting the functioning of neural dynamics, Chapter 4 provides an overview of the cytoskeleton as an information processing device. Previous models of microtubules as information processing devices are outlined along with an assessment of their reliability. From the models of microtubules as cellular automata, ferroelectric lattices, and quantum Hopfield networks, it was shown that microtubules do possess capabilities for information processing, information storage, and signal transfer. The functioning of microtubules within neurons and their effects on neuronal firing patterns, and thus the overall functioning of the brain, are also discussed. Based on the discussion of the experimental evidence linking MAP2, and kinesin to learning and memory, as well as the theoretical predictions of the computational ability of the dendritic cytoskeleton a specific functional role for microtubules in neurons is proposed that differs from their well-characterized structural significance. The role of microtubules within the neurons is outlined as follows:

1) Synaptic transmission signals arrive at the postsynaptic density causing ionic waves to move along associated actin filaments.
2) These waves propagate along MAP2 via the movement of counter ions from the actin filaments to microtubules.
3) These waves in turn affect the conformation states of the C-termini on the microtubule.
4) The change in C-termini states affects the kinesin based movement along microtubules as well as the MAP2 connections along the microtubule affecting memory and learning.
5) The change in MAP2 connections then alters the electronic information processing within microtubules that may give rise to a conscious event.
6) These changes in MAP2 connection also affect connections with other microtubules.
7) The wave may then propagate along the new connections to other actin filaments that in turn affect ion channels and neuron signaling.

The above scheme elucidates the way in which external stimuli affect our learning and memory as well as our conscious perception, for example by eliciting changes in MAP2 patterns affecting information processing. However, with a mechanism to explain how the environment affects microtubule function, the key question now becomes how does the electronic information processing in microtubules associated with consciousness affect the external system thus accounting for concepts such as conscious free will, the so-called mind-body problem?

The final major criticism indicates that decoherence arising from the thermal environment within the brain can destroy any quantum information processing effects within microtubules. While theoretical predictions of Hagan et. al., and Rosa et. al.

indicate that this may not be so, it has been shown that direct experimental evidence of quantum effects within microtubules is required. The investigative aims of this thesis report were to theoretically evaluate information processing and quantum coherence in microtubules at physiologically relevant temperature. From the cellular automata modeling of a microtubule based on the electrostatic potential of tubulin presented in Chapter 5, it was determined that under assumed conditions microtubules are capable of information processing on an electrical level at physiological temperature. The model used a typical microtubule configuration of 13 protofilaments with its constituent tubulin proteins packed into a seven-member neighborhood in a tilted hexagon configuration known as an A-Lattice. The interior of the tubulin protein was taken to contain a region of two areas of positive charge separated by a barrier of negative charge and was based on electrostatic maps of the protein interior. The interior arrangement constituted a double well potential structure within which a mobile electron was used to determine the states of an individual tubulin dimer. Dynamics of the system were determined by the minimization of the overall energy associated with electrostatic interactions between neighboring electrons as well as thermal effects. The model allowed transitions for electrons with sufficient energy to overcome the potential barrier in which the new configuration lowers the system's energy, or if the configuration raises the system's energy with a finite probability. Quantum mechanically the model allowed the electron to tunnel through the potential barrier allowing transitions for which the system's energy is lowered even if the electron does not possess the necessary energy to overcome the potential barrier. The emergence of self-organizing static, oscillating or propagating patterns determined the system's capability to process information. The information processing capability was shown to be dependent on the method of updating, thus requiring a synchronous global clocking mechanism within the cell. Ionic wave propagation, from either condensed counter ions surrounding the microtubule, or via nerve impulses, was suggested as a possible clocking mechanism. However, while the information processing capability of microtubules was shown to be robust in the presence of physiologically relevant temperature it relied heavily on the electric properties of the tubulin dimer, which remains an area under active investigation. The model predicted information processing capabilities for a tubulin dielectric constant of 7.8 or greater. While this value is larger than the typical protein range of 2-4, experimental evidence has yielded tubulin dielectric constants of 10 or less. The information processing capability is also highly reliant on the depth of the potential well, but as stated this property is not yet experimentally determined.

The collective excitation model in Chapter 6 was used to investigate coherent quantum excitations in microtubules. The model was based on the dipole-dipole interaction of excitons formed from the transition of electrons between ground and excited states in a double well structure based on the tubulin electrostatic map coupled to the microtubule lattice. Using previous studies on the elastic properties of microtubules phonon energies, and characteristic times and temperatures in the protofilament and dimer helix direction were determined. The electron transition dipole, and energy levels were determined via solving for the ground and first excited state wavefunctions for an electron in an infinite double well structure. The energy difference between the ground and first excited state was taken as the exciton energy. With the dipole magnitude and direction the dipole coupling values were estimated. The microtubule lattice was taken as an aggregate of tubulin dimers. Due to the tilted hexagonal structure, and the transition dipole pointing in the direction of the microtubule circumference, one-dimensional coupling between dimers in the protofilament and dimer helix directions were considered. Expanding the energy dispersion relation around the minimum dispersion energy yielded the dipole-dipole coupling constants. From these values characteristic times and temperatures were determined. It was found that the temperature of activation for excitons was well above physiological temperature. This indicated that excitons are not easily excited by the thermal environment, but rather rely on other mechanisms of excitiation such as coupling to other excitons, or phonons. However, it was found that the exciton couling and phonon temperatures of activation were well below the temperature of the microtubule environment. These values were below 30 K indicating that thermal vibrations of the environment are more than sufficient to excite phonons and excitons removing any form of coherent collective excitation. Phonon and exciton coupling energies and characteristic times were shown to be on comparable scales with energies in the range of meV and times on the order of 10^{-12}-10^{-13} s indicating a strong possibility for coupling between the two excitations in the absence of thermal effects. Mechanisms to isolate microtubules from their environment, such as layers of ordered water or counter ions, and coherent pumping mechanisms, have been suggested, however they remain theoretical in nature with no experimental evidence verifying their effect on microtubules.

Appendix – QCAMM Code

The following is the code used to create the cellular automata simulation described in Chapter 5. The program was created on a Mac OS X version 10.4.10 with 1.83 GHz Intel Core Duo processor, and 512 MB 667 MHz RAM using Xcode version 2.2.1. The program was written in the C language and compiled with the GNU Compiler Collection that is standard on the machine described.

QCAMM.C

```
/*QCAMM Code written in 2005-2007 at the University of Alberta for the purpose of investigating
information processing in microtubules. Qcamm.c and all related functions were written by Travis
Craddock during this time period except for ranmar.c and ranmar.h which were obtained from public
sources*/

#include <math.h>
#include <stdio.h>
#include <time.h>

#define bolt 0.08617385         /*Boltzmann constant in meV/K*/
#define IJ 31328
#define KL 30081


main()
{
        FILE* in_file;     /*Input file*/
        FILE* image;       /*PPM Image Output file*/

        /*Declare variables*/

        double e_diff; /*energy difference value*/
        double enerdiff(int, int, int[6], double); /*function to calculate energy difference on A6 lattice*/

        double energy; /*energy value of centre electron*/
        double enercalc(int, int[6], double); /*function prototype to calculate energy value on A6 lattice*/

        double force; /*force value on the central dipole moment*/
double for_calc(int, int[6]); /*function prototype to calculate force value on A6 lattice*/

double num, num1, num2;  /*random numbers*/
double ranmar();  /*function prototype to pseudo-randomly a value of zero or one*/

double probabil; /*probability of electron to tunnel*/
double probcalc(double, double); /*function prototype to calculate tunneling probability*/

double potdepth; /*depth of the electron's potential well*/

double thresh; /*threshold to determine extent which mobile electron is affected by neighbours*/

double T;     /*temperature of the system*/

double dc;  /*tubulin dielectric constant*/

double update;   /*updating rule; 0 - synchronous, 1 - random asynchronous*/

double tempprob; /*probability of electron changing positions due to temperature*/

int centinit, centfin;  /*initial and final positions of centre dimer electron*/

int position[13][100]; /* electron positions in microtubule lattice, 0 - left well, 1 - right well */

int newposit[13][100]; /*new positions of electrons as positions are updated during a timestep*/

int holdposit[13][100][500];

int ROAposit[13][100]; /*track of updated dimers in Random Order Asynchronous Updating*/

int neighpos[6];  /*array of electron positions for a given neighbourhood on A6 lattice*/

int i,j,k,l,m,n,a,b,c,u,v,w,x,y,z;  /*index variables*/

double weight;  /* the weighting between alpha and beta states, and percentage value*/

int signal;  /*signal sent on microtubule; 0 - no signal, 1 - constant minus end, random fed plus end*/

int scenario; /*scenario type to be used in calculations; 0 - classical, 1 - quantum*/

int rule;    /*rule type to be used in determining system dynamics; 0 - energy, 1 - force*/

int initial;   /*initial seeding of the microtubule lattice; 0 - random, 1 - strip, 2 checkered*/

int timestep;        /*number of timesteps in simulation*/

int now, now_usec; /*times in seconds and milliseconds to seed RNG*/

int seed1, seed2;  /*seeds for RNG*/

char buffer[80];
```

```
float red, green, blue;

/*Open input file*/
in_file = fopen("input.dat","r");

/*Seed Random Number Generator*/
now = time(NULL);
now_usec = now*1000;
seed1 = (now_usec - KL * (now_usec / KL));
seed2 = (now - IJ * (now / IJ));
rmarin2(seed1, seed2);

/*Read in input values*/

fscanf(in_file, "%d", &rule);
if(rule == 0)
        fscanf(in_file, "%d", &scenario);
else
        scenario = 0;
fscanf(in_file, "%d", &initial);
fscanf(in_file, "%lf", &update);
fscanf(in_file, "%lf", &weight);
fscanf(in_file, "%d", &signal);
if(rule == 0){
        fscanf(in_file, "%lf", &T);
        fscanf(in_file, "%lf", &potdepth);
}else
        fscanf(in_file, "%lf", &thresh);
fscanf(in_file, "%lf", &dc);
fscanf(in_file, "%d", &timestep);

/*Initialize place holding array*/
for(i = 0; i < 13; i++)
{
        for(j = 0; j < 100; j++)
        {
                newposit[i][j] = 0;
        }
}

/*Initialize states*/
if(initial == 0)      /*weighted random seeded states*/
{
        for(i = 0; i < 13; i++)
        {
                for(j = 0; j < 100; j++)
                {
                        num = ranmar();
                        if(num < (weight/100))
                                position[i][j] = 1;
                        else
                                position[i][j] = 0;
                }
            }
        }
        else if(initial == 1)
        {
            k = 0;
            for(j = 0; j < 100; j++)
            {
                for(i = 0; i < 13; i++)
                {
                    if(k == 0)
                        position[i][j] = 0;
                    else
                        position[i][j] = 1;
                }
                if(k == 0)
                    k = 1;
                else
                    k = 0;
            }
        }

        /*Timesteps of progression For Synchrouns updating*/
        if(update == 0)
        {
            for(k = 0; k < timestep; k++)
            {
                if(signal == 1)
                {
                    for(l = 0; l < 13; l++)
                    {
                        num = ranmar();
                        if(num < 0.5)
                            position[l][99] = 1;
                        else
                            position[l][99] = 0;
                        position[l][0] = 1;
                    }
                }

                /*Create PPM image file of electron positions at timestep k*/
                sprintf (buffer, "slab-%09d.ppm", k);
                image = fopen (buffer, "w");
                fprintf (image, "P6\n%d %d\n255\n", 228, 33);

                for(i = 0; i < 2280; i++) /*header bar*/
                {
                    fprintf (image, "%c%c%c", (int)(99), (int)(99), (int)(99));
                }

                for(i = 0; i < 13; i++)
                {
```

```
        for(m = 20; m > i ; m = m-1) /*spacing for MT slant*/
        {
                fprintf(image, "%c%c%c", (int)(99), (int)(99), (int)(99));
        }

        for(j = 0; j < 100; j++)
        {

                if(position[i][j] == 1)
                {
                        red = 0.0;
                        green = 0.0;
                        blue = 0.0;
                }
                else
                {
                        red = 1.0;
                        green = 1.0;
                        blue = 1.0;
                }
                fprintf (image, "%c%c%c", (int)(red*255.0), (int)(green*255.0),
                (int)(blue*255.0));
                fprintf (image, "%c%c%c", (int)(red*255.0), (int)(green*255.0),
                (int)(blue*255.0));
        }

        for(m = 0; m < i+8; m = m+1) /*spacing for MT slant*/
        {
                fprintf(image, "%c%c%c", (int)(99), (int)(99), (int)(99));
        }
}

for(i = 0; i < 2280; i++) /*footer bar*/
{
        fprintf (image, "%c%c%c", (int)(99), (int)(99), (int)(99));
}

fclose(image);

/*Select dimer and neighbourhood, check energy difference, move centre electron to least
energy configuration*/
for(i = 0; i < 13; i++)
{
        for(j = 0; j < 100; j++)
        {
                /*Set boundary conditions*/
                a = i-1;
                b = i;
                c = i+1;
                u = j-1;
                v = j;
                w = j+1;
```

```
x = j+1;
y = j;
z = j-1;

/*wrapping of protofilaments to form microtubule type A*/
if(a < 0)
{
        a = 12;
        u = u + 8;
        v = v + 8;
}

if(c > 12)
{
        c = 0;
        x = x - 8;
        y = y - 8;
}

/*torroidal boundary conditions*/
if(u < 0)
        u = u + 100;
if(u > 99)
        u = u - 100;
if(v > 99)
        v = v - 100;
if(w > 99)
        w = w – 100;
if(x > 99)
        x = x - 100;
if(x < 0)
        x = x + 100;
if(y < 0)
        y = y + 100;
if(z < 0)
        z = z + 100;

/*Set neighbour positions for center dimer position i,j*/
neighpos[0] = position[a][u];  /*N0 position*/
neighpos[1] = position[a][v];  /*N1 position*/
neighpos[2] = position[b][w];  /*N2 position*/
neighpos[3] = position[c][x];  /*N3 position*/
neighpos[4] = position[c][y];  /*N4 position*/
neighpos[5] = position[b][z];  /*N5 position*/

/*Set initial and final center dimer electron position to calculate energy
change*/
centinit = position[i][j];

if(centinit == 0)
        centfin = 1;
else
```

```
        centfin = 0;

/*Check energy difference for changing position of centre dimer electron, and
change position if new position lowers the energy*/
e_diff = enerdiff(centinit, centfin, neighpos, dc);
tempprob = exp(-e_diff/(bolt*T));

/*Perform update according to classical scenario*/
if(scenario == 0)
{
        energy = enercalc(centinit, neighpos, dc);
        force = for_calc(centinit, neighpos);

        if(rule == 0)
        {
                if((e_diff <= 0) && (energy > potdepth))
                        newposit[i][j] = centfin;
                else if((e_diff > 0) && (energy > potdepth))
                {
                        if(T != 0)
                        {
                                num = ranmar();
                                if(num < tempprob)
                                        newposit[i][j] = centfin;
                                else
                                        newposit[i][j] = centinit;
                        }
                }
                else
                        newposit[i][j] = centinit;
        }

        if(rule == 1)
        {
                if(force > (thresh/1000))
                        newposit[i][j] = 1;
                else if(force < -(thresh/1000))
                        newposit[i][j] = 0;
                else
                        newposit[i][j] = position[i][j];
        }
}

/*Perform update according to quantum scenario*/
if(scenario == 1)
{
        energy = enercalc(centinit, neighpos, dc);
        if((e_diff <= 0) && (energy > potdepth))
                newposit[i][j] = centfin;
        else if((e_diff > 0) && (energy > potdepth))
        {
                if(T != 0)
```

```
                        {
                            num = ranmar();
                            if(num < tempprob)
                                newposit[i][j] = centfin;
                        }
                        else
                            newposit[i][j] = centinit;
                    }
                    else if((e_diff <= 0) && (energy <= potdepth))
                    {
                        num = ranmar();
                        probabil = probcalc(potdepth,energy);
                        if(num < probabil)
                            newposit[i][j] = centfin;
                        else
                            newposit[i][j] = centinit;
                    }
                    else if((e_diff > 0) && (energy <= potdepth))
                    {
                        num = ranmar();
                        probabil = probcalc(potdepth,energy)*tempprob;
                        if(num < probabil)
                            newposit[i][j] = centfin;
                        else
                            newposit[i][j] = centinit;
                    }
                    else
                        newposit[i][j] = centinit;
                }
            }
        }

        /*Update array of electron positions*/
        for(i = 0; i < 13; i++)
        {
            for(j = 0; j < 100; j++)
            {
                holdposit[i][j][k] = position[i][j];
                position[i][j] = newposit[i][j];
            }
        }

        for(i = 0; i < 6; i++)
        {
            neighpos[i] = 0;
        }
    }

}

/*Timesteps of Progression for Asynchronous Updates*/
else
```

```
{
    for(k = 0; k < timestep; k++)
    {
        /*Signal*/
        if(signal == 1)
        {
            for(l = 0; l < 13; l++)
            {
                num = ranmar();
                if(num < 0.5)
                    position[l][99] = 1;
                else
                    position[l][99] = 0;
                position[l][0] = 1;
            }
        }

        /*Create PPM image file of electron positions at timestep k*/
        sprintf (buffer, "slab-%09d.ppm", k);
        image = fopen (buffer, "w");
        fprintf (image, "P6\n%d %d\n255\n", 228, 33);

        for(i = 0; i < 2280; i++) /*header bar*/
        {
            fprintf (image, "%c%c%c", (int)(99), (int)(99), (int)(99));
        }

        for(i = 0; i < 13; i++)
        {
            for(m = 20; m > i ; m = m-1) /*spacing for MT slant*/
            {
                fprintf(image, "%c%c%c", (int)(99), (int)(99), (int)(99));
            }

            for(j = 0; j < 100; j++)
            {

                if(position[i][j] == 1)
                {
                    red = 0.0;
                    green = 0.0;
                    blue = 0.0;
                }
                else
                {
                    red = 1.0;
                    green = 1.0;
                    blue = 1.0;
                }
                fprintf (image, "%c%c%c", (int)(red*255.0), (int)(green*255.0),
                (int)(blue*255.0));
                fprintf (image, "%c%c%c", (int)(red*255.0), (int)(green*255.0),
        (int)(blue*255.0));
    }

    for(m = 0; m < i+8; m = m+1) /*spacing for MT slant*/
    {
        fprintf(image, "%c%c%c", (int)(99), (int)(99), (int)(99));
    }
}

for(i = 0; i < 2280; i++) /*footer bar*/
{
    fprintf (image, "%c%c%c", (int)(99), (int)(99), (int)(99));
}

fclose(image);

/*Initialize array to keep track of which dimers have updated in a given timestep*/
for(i = 0; i < 13; i++)
{
    for(j = 0; j < 100; j++)
    {
        ROAposit[i][j] = 0;
    }
}

/*Select dimer and neighbourhood at random, check energy difference, move centre
electron to least energy configuration*/
for(m = 0; m < 1300; m++)
{
    /*Choose a dimer at random from dimers that have not been chosen before*/
    do
    {
        num1 = ranmar()*1300;
        l = (int)(num1+0.5);


        if((l >= 0) && (l < 100))
        {
            i = 0;
            j = l;
        }
        else if((l >= 100) && (l < 200))
        {
            i = 1;
            j = l - 100;
        }
        else if((l >= 200) && (l < 300))
        {
            i = 2;
            j = l - 200;
        }
        else if((l >= 300) && (l < 400))
```

```
{
        i = 3;
        j = l - 300;
}
else if((l >= 400) && (l < 500))
{
        i = 4;
        j = l - 400;
}
else if((l >= 500) && (l < 600))
{
        i = 5;
        j = l - 500;
}
else if((l >= 600) && (l < 700))
{
        i = 6;
        j = l - 600;
}
else if((l >= 700) && (l < 800))
{
        i = 7;
        j = l - 700;
}
else if((l >= 800) && (l < 900))
{
        i = 8;
        j = l - 800;
}
else if((l >= 900) && (l < 1000))
{
        i = 9;
        j = l - 900;
}
else if((l >= 1000) && (l < 1100))
{
        i = 10;
        j = l - 1000;
}
else if((l >= 1100) && (l < 1200))
{
        i = 11;
        j = l - 1100;
}
else if((l >= 1200) && (l < 1300))
{
        i = 12;
        j = l - 1200;
}

if(ROAposit[i][j] == 1)
        n = 1;
        else
                n = 0;
}while (n == 1);

/*Set boundary conditions*/
a = i-1;
b = i;
c = i+1;
u = j-1;
v = j;
w = j+1;
x = j+1;
y = j;
z = j-1;

/*wrapping of protofilaments to form microtubule type A*/
if(a < 0)
{
        a = 12;
        u = u + 8;
        v = v + 8;
}

if(c > 12)
{
        c = 0;
        x = x - 8;
        y = y - 8;
}

/*torroidal boundary conditions*/
if(u < 0)
        u = u + 100;

if(u > 99)
        u = u - 100;

if(v > 99)
        v = v - 100;

if(w > 99)
        w = w - 100;

if(x > 99)
        x = x - 100;

if(x < 0)
        x = x + 100;

if(y < 0)
        y = y + 100;
```

```
if(z < 0)
        z = z + 100;

/*Set neighbour positions for center dimer position i,j*/
neighpos[0] = position[a][u];  /*N0 position*/
neighpos[1] = position[a][v];  /*N1 position*/
neighpos[2] = position[b][w];  /*N2 position*/
neighpos[3] = position[c][x];  /*N3 position*/
neighpos[4] = position[c][y];  /*N4 position*/
neighpos[5] = position[b][z];  /*N5 position*/

/*Set initial and final center dimer electron position to calculate energy change*/
centinit = position[i][j];

if(centinit == 0)
        centfin = 1;
else
        centfin = 0;

/*Check energy difference for changing position of centre dimer electron, and
change position if new position lowers the energy*/
e_diff = enerdiff(centinit, centfin, neighpos, dc);
tempprob = exp(-e_diff/(bolt*T));

/*Perform update according to classical scenario*/
if(scenario == 0)
{
        energy = enercalc(centinit, neighpos, dc);
        force = for_calc(centinit, neighpos);

        if(rule == 0)
        {
                if((e_diff <= 0) && (energy > potdepth))
                        newposit[i][j] = centfin;
                else if((e_diff > 0) && (energy > potdepth))
                {
                        if(T != 0)
                        {
                                num = ranmar();
                                if(num < tempprob)
                                        newposit[i][j] = centfin;
                                else
                                        newposit[i][j] = centinit;
                        }
                }
                else
                        newposit[i][j] = centinit;
        }

        if(rule == 1)
        {
                if(force > (thresh/1000))
```

```
                        newposit[i][j] = 1;
                else if(force < -(thresh/1000))
                        newposit[i][j] = 0;
                else
                        newposit[i][j] = position[i][j];
        }
}

/*Perform update according to quantum scenario*/
if(scenario == 1)
{
        energy = enercalc(centinit, neighpos, dc);
        if((e_diff <= 0) && (energy > potdepth))
                newposit[i][j] = centfin;
        else if((e_diff > 0) && (energy > potdepth))
        {
                if(T != 0)
                {
                        num = ranmar();
                        if(num < tempprob)
                                newposit[i][j] = centfin;
                }
                else
                        newposit[i][j] = centinit;
        }
        else if((e_diff <= 0) && (energy <= potdepth))
        {
                num = ranmar();
                probabil = probcalc(potdepth,energy);
                if(num < probabil)
                        newposit[i][j] = centfin;
                else
                        newposit[i][j] = centinit;
        }
        else if((e_diff > 0) && (energy <= potdepth))
        {
                num = ranmar();
                probabil = probcalc(potdepth,energy)*tempprob;
                if(num < probabil)
                        newposit[i][j] = centfin;
                else
                        newposit[i][j] = centinit;
        }
        else
                newposit[i][j] = centinit;
}

/*Update array of electron positions*/

position[i][j] = newposit[i][j];
```

```
                        for(i = 0; i < 6; i++)
                        {
                                neighpos[i] = 0;
                        }
                }
        }
    }
}
```

ENERCALC.C

```
/*enercalc.c --- Function to calculate the energy of the electron in the centre dimer. Use gcc enercalc.c -lm
to compile*/

#include <math.h>
#include <stdio.h>

double enercalc(int centinit, int neighpos[6], double dc)
{
        /*Declare variables*/
        double distance[2][6][2];           /*array of distance values for all electron configurations*/
        double distenr6(int, int, int);     /*calculates distance of centre electron to neighbor electron*/
        double energy;                      /*Coulomb energy*/
        double C;                           /*Constant in Coulomb energy calculation*/
        int posit;                          /*variable  to hold specific neighbour positions*/
        int i, j, k;                        /*index variables*/

        /*Calculate Constant*/
        C = 1439.9602/dc;                   /* C = e^2/(4*pi*epsilon*epsilon-0)
                                            e - 1.602176462*10^(-19) C
                                            pi - 3.14159265
                                            epsilon - 8.854187817*10^(-12) C/N.m
                                            epsilon-0 - dc */

        /*Read in Distances (units nanometers) for electron separations from Distance Calculation Function*/
        for(i = 0; i < 6; i++)
        {
                for(j = 0; j < 2; j++)
                {
                        for(k = 0; k < 2; k++)
                        {
                                distance[j][i][k] = distenr6(j, i, k);
                        }
                }
        }

        /*Calculate energy of centre dimer electron*/
        energy = 0;
        for(i = 0; i < 6; i++)
        {
                posit = neighpos[i];
                energy = energy + C*(1/distance[centinit][i][posit]);
        }

        return(energy);
}
```

ENERDIFF.C

```
/*enerdiff.c --- Function to calculate the energy difference when a switch of the centre dimer
electron is made.  Use gcc enerdiff.c -lm to compile*/

#include <math.h>
#include <stdio.h>

double enerdiff(int centinit, int centfin, int neighpos[6], double dc)
{
        /*Declare variables*/
        double distance[2][6][2];           /*array of distance values for all electron configurations*/
        double distenr6(int, int, int);     /* calculates distance of centre electron to neighbour electron*/
        double enerdiff;                    /*Coulomb energy difference between final and initial state*/
        double C;                           /*Constant in Coulomb energy calculation*/
        int posit;                          /*variable  to hold specific neighbour positions*/
        int i, j, k;                        /*index variables*/

        /*Calculate constant*/
        C = 1439.9602/dc;                   /* C = e^2/(4*pi*epsilon*epsilon-0)
                                            e - 1.602176462*10^(-19) C
                                            pi - 3.14159265
                                            epsilon - 8.854187817*10^(-12) C/N.m
                                            epsilon-0 - dc*/

        /*Read in Distances (units nanometers) for electron separations from Distance Calculation Function*/
        for(i = 0; i < 6; i++)
        {
                for(j = 0; j < 2; j++)
                {
                        for(k = 0; k < 2; k++)
                        {
                                distance[j][i][k] = distenr6(j, i, k);
                        }
                }
        }

        /*Calculate energy difference when centre dimer electron is moved from intial to final position*/
        enerdiff = 0;
        for(i = 0; i < 6; i++)
        {
                posit = neighpos[i];
                enerdiff = enerdiff + C*(1/distance[centfin][i][posit] - 1/distance[centinit][i][posit]);
        }
        return(enerdiff);
}
```

FOR_CALC.C

```
/*for_calc.c --- Function to calculate the force on the tubulin dipole in the centre dimer.  Use gcc enercalc.c
-lm to compile*/

#include <math.h>
#include <stdio.h>

double for_calc(int centinit, int neighpos[6], double dc)
{
        /*Declare variables*/
        double distance[2][6][2];               /*array of distance values for all electron configurations*/
        double distfor6(int, int, int);         /*calculates distance from centre electron to neighbor electron*/
        double force;                           /*Coulomb force*/
        double r;                               /*distance value between dipoles*/
        int posit;                              /*variable  to hold specific neighbour positions*/
        int i, j, k;                            /*index variables*/

        /*Calculate constant*/
        C = 1439.9602/dc;                       /* C = e^2/(4*pi*epsilon*epsilon-0)
                                                e - 1.602176462*10^(-19) C
                                                pi - 3.14159265
                                                epsilon - 8.854187817*10^(-12) C/N.m
                                                epsilon-0 - dc*/

        /*Read in Distances (units nanometers) for electron separations from Distance Calculation Function*/
        for(i = 0; i < 6; i++)
        {
                for(j = 0; j < 2; j++)
                {
                        for(k = 0; k < 2; k++)
                        {
                                distance[j][i][k] = distfor6(j, i, k);
                        }
                }
        }

    /*Calculate force of centre dimer electron*/
    force = 0;
    for(i = 0; i < 6; i++)
    {
        posit = neighpos[i];
        if(i == 5)
                force = force + 1/(distance[centinit][i][posit]*distance[centinit][i][posit]);
        else if(i == 2)
                force = force - 1/(distance[centinit][i][posit]*distance[centinit][i][posit]);
        else
        {
```

```
                    r = sqrt(25+(distance[centinit][i][posit]*distance[centinit][i][posit]));
                    force = force + distance[centinit][i][posit]/r/r/r;
            }
    }

    return(force);

}
```

DISTENR6.C

```
/* distenr6.c --- Function to calculate the separation distance between the centre dimer electron
and neighbour dimer electrons for all configurations for energy calculations of A6 lattice.
Use gcc distenr6.c -lm to compile*/

#include <math.h>
#include <stdio.h>

double distenr6(int cent_val, int neighb, int neighval)
{
  /*Declare variables*/

   double well_off;                   /*potential well offset from centre*/
   double fil_sep;                    /*protofilament separation measured from centre to centre*/
   double tub_sep;                    /*tublin dimer separation measured from centre to centre*/
   double mon_sep;                    /*tubulin monomer separation from centre alpha to centre beta*/
   double prot_off;                   /*protofilament offset from dimer center to adjacent dimer centre*/
   double distance[2][6][2];          /*distance between centre dimer electrons and neighbour electrons
                                      first value centre electron location 0 - left, 1 - right
                                      second value neighbour dimer location  0-5 - N0-N5
                                      third value neighbour electron location 0 - left, 1 - right*/

   /*Set variable values*/
   well_off = 1.0;                    /*all values in nanometers (10^(-9)metres)*/
   fil_sep = 5.0;
   tub_sep = 8.0;
   mon_sep = 4.0;
   prot_off = 3.1;

   /*Determine distance from centre dimer wells to neighbour wells. Neighbour configuration
              N0 N1
            N5 C N2
             N4 N3
   Two wells (L-left, R-Right) in centre dimer with two wells in each neighbour dimer with six
   neighbours = 24 configurations*/

   distance[0][0][0] = sqrt(prot_off*prot_off + fil_sep*fil_sep);  /*CL-N0L*/
   distance[0][0][1] = sqrt(prot_off*prot_off + (fil_sep + 2*well_off)*(fil_sep + 2*well_off));  /*CL-N0R*/
   distance[1][0][0] = sqrt(prot_off*prot_off + (fil_sep - 2*well_off)*(fil_sep - 2*well_off));  /*CR-N0L*/
   distance[1][0][1] = sqrt(prot_off*prot_off + fil_sep*fil_sep);  /*CR-N0R*/
   distance[0][1][0] = sqrt((tub_sep - prot_off)*(tub_sep - prot_off) + fil_sep*fil_sep);  /*CL-N1L*/
  distance[0][1][1] = sqrt((tub_sep - prot_off)*(tub_sep - prot_off) + (fil_sep + 2*well_off)*(fil_sep +
  2*well_off)); /*CL-N1R*/
  distance[1][1][0] = sqrt((tub_sep - prot_off)*(tub_sep - prot_off) + (fil_sep - 2*well_off)*(fil_sep -
  2*well_off)); /*CR-N1L*/
  distance[1][1][1] = sqrt((tub_sep - prot_off)*(tub_sep - prot_off) + fil_sep*fil_sep);  /*CR-N1R*/
  distance[0][2][0] = tub_sep;  /*CL-N2L*/
  distance[0][2][1] = sqrt(tub_sep*tub_sep + (2*well_off)*(2*well_off));  /*CL-N2R*/
  distance[1][2][0] = sqrt(tub_sep*tub_sep + (2*well_off)*(2*well_off));  /*CR-N2L*/;
  distance[1][2][1] = tub_sep;  /*CR-N2R*/
  distance[0][3][0] = sqrt(prot_off*prot_off + fil_sep*fil_sep);  /*CL-N3L*/
  distance[0][3][1] = sqrt(prot_off*prot_off + (fil_sep - 2*well_off)*(fil_sep - 2*well_off)); /*CL-N3R*/
  distance[1][3][0] = sqrt(prot_off*prot_off + (fil_sep + 2*well_off)*(fil_sep + 2*well_off)); /*CR-N3L*/
  distance[1][3][1] = sqrt(prot_off*prot_off + fil_sep*fil_sep);  /*CR-N3R*/
  distance[0][4][0] = sqrt((tub_sep - prot_off)*(tub_sep - prot_off) + fil_sep*fil_sep); /*CL-N4L*/
  distance[0][4][1] = sqrt((tub_sep - prot_off)*(tub_sep - prot_off) + (fil_sep - 2*well_off)*(fil_sep –
  2*well_off)); /*CL-N4R*/
  distance[1][4][0] = sqrt((tub_sep - prot_off)*(tub_sep - prot_off) + (fil_sep + 2*well_off)*(fil_sep +
  2*well_off)); /*CR-N4L*/
  distance[1][4][1] = sqrt((tub_sep - prot_off)*(tub_sep - prot_off) + fil_sep*fil_sep); /*CR-N4R*/
  distance[0][5][0] = tub_sep;  /*CL-N5L*/
  distance[0][5][1] = sqrt(tub_sep*tub_sep + (2*well_off)*(2*well_off));  /*CL-N5R*/
  distance[1][5][0] = sqrt(tub_sep*tub_sep + (2*well_off)*(2*well_off));  /*CR-N5L*/
  distance[1][5][1] = tub_sep;  /*CR-N5R*/
  return(distance[cent_val][neighb][neighval]);
}
```

DISTFOR6.C

```
/* distfor6.c — Function to calculate the separation distance between the centre dimer electron
and neighbour dimer electrons for all configurations for force calculations on A6 lattice.
Use gcc distfor6.c -lm to compile*/

#include <math.h>
#include <stdio.h>

double distfor6(int cent_val, int neighb, int neighval)
{
  /*Declare variables*/

  double distance[2][6][2];      /*distance between centre dimer electrons and neighbour electrons
                                 first value centre electron location 0 - left, 1 - right
                                 second value neighbour dimer location  0-5 - N0-N5
                                 third value neighbour electron location 0 - left, 1 - right*/

   /*Set distance from centre dimer wells to neighbour wells.  See Hameroff, Rasmussen and Mansson, or
  Smith, Hameroff and Watt for values.  Neighbour configuration
            N0 N1
          N5 C N2
           N4 N3
  Two wells (L-left, R-Right) in centre dimer with two wells in each neighbour dimer with six
neighbours = 24 configurations*/

 distance[0][0][0] = 3.1;  /*CL-N0L*/
 distance[0][0][1] = -0.9;  /*CL-N0R*/
 distance[1][0][0] = 7.1;  /*CR-N0L*/
 distance[1][0][1] = 3.1;  /*CR-N0R*/
 distance[0][1][0] = -4.9;  /*CL-N1L*/
 distance[0][1][1] = -8.9; /*CL-N1R*/
 distance[1][1][0] = -0.9; /*CR-N1L*/
 distance[1][1][1] = -4.9;  /*CR-N1R*/
 distance[0][2][0] = -8;  /*CL-N2L*/
 distance[0][2][1] = -12;  /*CL-N2R*/
 distance[1][2][0] = -4;  /*CR-N2L*/;
 distance[1][2][1] = -8;  /*CR-N2R*/
 distance[0][3][0] = -3.1;  /*CL-N3L*/
 distance[0][3][1] = -7.1; /*CL-N3R*/
 distance[1][3][0] = 0.9; /*CR-N3L*/
 distance[1][3][1] = -3.1;  /*CR-N3R*/
 distance[0][4][0] = 4.9; /*CL-N4L*/
 distance[0][4][1] = 0.9; /*CL-N4R*/
 distance[1][4][0] = 8.9; /*CR-N4L*/
 distance[1][4][1] = 4.9; /*CR-N4R*/
 distance[0][5][0] = 8;  /*CL-N5L*/
 distance[0][5][1] = 4;  /*CL-N5R*/
 distance[1][5][0] = 12;  /*CR-N5L*/
 distance[1][5][1] = 8;  /*CR-N5R*/

 return(distance[cent_val][neighb][neighval]);
}
```

PROBCALC.C

```
/*probcalc.c --- Function to calculate the probability of the electron tunnelling through the potential barrier.
Use gcc probcalc.c -lm to compile*/

#include <math.h>
#include <stdio.h>

/*Define constants*/
#define me 0.000000000005678                /*electron rest mass divided by c^2 in eV*/
#define c 299792458                         /*speed of light in vacuum in m/s*/
#define hbar 0.0000000000000006582122       /*planck's constant/2*PI in eV/s*/

double probcalc(double potdepth, double energy)
{
        /*Declare variables*/
        double barrier;               /*half width of the potential barrier*/
        double probabil;              /*calculated probability of electron to tunnel*/
        double Vo;                    /*barrier height*/
        double E;                     /*electron energy*/
        /*Define values*/
        barrier = 0.0000000001;         /*value given in metres*/
        Vo = potdepth/1000;             /*potential barrier in eV*/
        E = energy/1000;                /*particle energy in eV*/

        /*Calculate Probability - probability for tunneling given by exp(-2*A*well_sep) approximated
        calculation of electron tunneling through square potential barrier of length well_sep where */
        probabil = exp(-4*barrier/hbar*sqrt(2*me*(Vo-E)));

        return(probabil);

}
```

RANMAR.C

```
/*ranmar.c --- Function to generate a Gaussian random number between 0 and 1. Orginally described in G.
Marsaglia, A. Zaman and W.-W Tsang, Stat. Prob. Lett 9 (1990) p 35. Use gcc ranmar.c -lm with
compile*/

#include <math.h>

double u[98], ccc, cd, cm;
int i97, j97;

void rmarin(void)
{
        int i, j, k, l, ii, jj, m;
        double s, t;
        int ij=1802,kl=9373;
        i = (ij/177)%177 + 2;
        j = ij%177 + 2;
        k = (kl/169)%178 + 1;
        l = kl%169;

      for (ii=1; ii<=97; ii++)
      {
            s = 0.0;
            t = 0.5;
            for (jj=1; jj<=24; jj++)
            {
                  m = (((i*j)%179)*k) % 179;
                  i = j;
                  j = k;
                  k = m;
                  l = (53*l + 1) % 169;
                  if ((l*m)%64 >= 32) s += t;
                  t *= 0.5;
            }
            u[ii] = s;
```

```
    }
    ccc = 362436.0 / 16777216.0;
    cd = 7654321.0 / 16777216.0;
    cm = 16777213.0 / 16777216.0;
    i97 = 97;
    j97 = 33;
}

void rmarin2(int ij, int kl)
{
     int i, j, k, l, ii, jj, m;
     double s, t;
     i = (ij/177)%177 + 2;
     j = ij%177 + 2;
     k = (kl/169)%178 + 1;
     l = kl%169;

     for (ii=1; ii<=97; ii++)
     {
          s = 0.0;
          t = 0.5;
          for (jj=1; jj<=24; jj++)
          {
               m = (((i*j)%179)*k) % 179;
               i = j;
               j = k;
               k = m;
               l = (53*l + 1) % 169;
               if ((l*m)%64 >= 32) s += t;
               t *= 0.5;
          }
          u[ii] = s;
    }
    ccc = 362436.0 / 16777216.0;
    cd = 7654321.0 / 16777216.0;
    cm = 16777213.0 / 16777216.0;
    i97 = 97;
    j97 = 33;
}

double ranmar(void)
{
     double uni;
     uni = u[i97] - u[j97];
     if (uni < 0.0) uni += 1.0;
     u[i97] = uni;
     i97--;
     if (i97==0) i97 = 97;
     j97--;
     if (j97==0) j97 = 97;
     ccc -= cd;
     if (ccc<0.0) ccc += cm;
```

```
        uni -= ccc;
        if (uni<0.0) uni += 1.0;
        return(uni);
}

/* ---------------------------------------------------------------- */
/*        Pseudo Random function  -> U[a,b]                        */
/* ---------------------------------------------------------------- */
double Unif(double a, double b)
{
        return( a + (b-a) *  ranmar() );
}

/* ---------------------------------------------------------------- */
/*        Integrer Pseudo Random function  -> U[a,b]               */
/* includes  extremum points a and b.                              */
/* ---------------------------------------------------------------- */
int IUnif(int a, int b)
{
        return( (int) floor(a + (b-a+1) *  ranmar()) );
}

#define zero 0.00000
#define  one 1.00000
#define  two 2.00000

/* ================================================================        */
/* Returna a normally distributed deviate with mean "med"                   */
/* and unit variance = sigma^2                                              */
/*                  N[m, sigma^2]                                           */
/* ================================================================        */
double normal(double med, double sigma)
{
        static int iset = 0;
        static double gset;
        double fac,rsq,v1,v2;

        if (iset == 0)
        {
                do
                {
                        v1 = two * ranmar() - one;
                        v2 = two * ranmar() - one;
                        rsq = v1 * v1 + v2 * v2 ;
                }
                while (rsq >= one || rsq == zero);
                fac = sqrt(-two * log(rsq) / rsq);
                gset = v1 * fac;
                iset = 1;
                return( med + sigma * v2 * fac );
        }
        else
        {
                iset = 0;
                return( med + sigma * gset );
        }
}

#undef zero
#undef one
#undef two
```

RANMAR.H

```
/* NOTE: The seed variables can have values between:      0 <= IJ <= 31328
C                                                         0 <= KL <= 30081
C The random number sequences created by these two seeds are of sufficient
C length to complete an entire calculation with. For example, if sveral
C different groups are working on different parts of the same calculation,
C each group could be assigned its own IJ seed. This would leave each group
C with 30000 choices for the second seed. That is to say, this random
C number generator can create 900 million different subsequences -- with
C each subsequence having a length of approximately 10^30.
C
C Use IJ = 1802 & KL = 9373 to test the random number generator. The
C subroutine RANMAR should be used to generate 20000 random numbers.
C Then display the next six random numbers generated multiplied by 4096*4096
C If the random number generator is working properly, the random numbers
C should be:
C         6533892.0  14220222.0  7275067.0
C         6172232.0  8354498.0   10633180.0
*/

#define RANMAR_IJ_MAX  31328
#define RANMAR_KL_MAX  30081

void rmarin(void);
void rmarin2(int, int);

double ranmar(void);
double Unif(double, double);
int IUnif(int, int);
double normal(double, double);
```

INPUT.DAT

A Sample input file for the QCAMM program using energy dynamics as used in Chapter 5.

```
0         rule
1         scenario
```

```
0       initial
1       update
1       weight
0       signal
300     temperature
130     potential depth
8.41    dielectric constant
3000    timesteps
```

A Sample input file for the QCAMM program using force dynamics to test against the Hameroff simulations described in Chapter 4.

```
0       rule
0       initial
0       update
10      weight
0       signal
0.9     threshold
8.41    dielectric constant
3000    timesteps
```